Doctoral Thesis

Reactive transport and adsorption-desorption processes of fluoride in a granitic soil

（花崗岩質土壌中のフッ化物の反応性輸送および吸脱着プロセス）

Sakambari Padhi

サカンバリ　パデイ

Abstract of the Dissertation

Fluoride contamination of groundwater is a serious environmental concern. The source of fluoride in groundwater can be natural or anthropogenic. While interaction of groundwater with the fluoride bearing minerals is ascribed to be the major controlling factor for fluoride contamination of groundwater, leachable fluoride from soil can be a potential source of fluoride to the shallow groundwater under suitable conditions.

In this research, first, areas with fluoride contamination of groundwater in India (e.g. Rangareddy, Telengana) and Japan (Nishinomiya, Japan) were selected and investigated to understand the behavior of fluoride in groundwater and soil system. Granitic soils from Nakatsugawa (Japan) and Tsukuba (Japan) were also investigated to understand the geochemical factors responsible for fluoride mobilization in the soil system. The leachable fluoride in Rangareddy, India is comparatively high (1.2-30 mg/kg) and corresponds to the occurrence of dissolved fluoride in groundwater in the respective area (2.0-2.3 mg/l). Fluoride in groundwater and soil leachate is negligible in Nakatsugawa (Japan) and Tsukuba (Japan). In Nishinomiya (Japan), soil leachable fluoride is in lower range although shallow groundwater is contaminated with fluoride. Soil pH, mineral constituents and infiltrating solutions were found to be the controlling factors in addition to the environmental factors for the amount of soil leachable fluoride.

Next, the processes of fluoride removal by calcite were investigated by laboratory batch kinetic and equilibrium experiments and surface complexation modeling. Fluoride adsorption decreased with increase in pH. Fluoride adsorption was described by the formation of two surface complexes, $>CaF^0$ and $>CO_3FCa^0$. The mechanism of fluoride sorption was found to be adsorption at low fluoride concentrations whereas precipitation plays a role at higher fluoride concentration and lower pH.

The mechanism of fluoride sorption on a granitic soil from Tsukuba was further studied through a series of batch kinetic and equilibrium experiments, surface complexation modeling and FTIR spectroscopy. Fluoride sorption was pH dependent, increase in sorption with decreasing pH. Sorption was influenced by electrolyte

i

concentration and surface area. Fluoride induced Al release was observed with decreasing release of Al with increase in pH. Ionic strength affects Al release by decreasing Al release. The observed temporal behavior was best explained by second order kinetic model, suggesting chemisorption processes. A surface complexation model was developed by considering fluoride sorption to a generic surface site. The equilibrium surface complexation constants were optimized with a nonlinear optimization program PEST in combination with PHREEQC. The forward modeling results reveals that including dissolved Al and Al-F complex sorption better explains the data. The mechanism of fluoride sorption in a complex soil assemblage was explained to be ion exchange, surface adsorption and Al-F complex sorption.

Finally, fluoride transport processes in a granitic soil were investigated by laboratory column experiment and numerical modeling during fluoride sorption and desorption. Fluoride sorption in the column was high. Fluoride desorption was comparatively fast, and slow after 10 pore volumes of flushing with long tailing. A geochemical model considering the liner Kd model and fluoride sorption in soil by surface complexation were developed in PHREEQC framework and used to explain fluoride transport during sorption and desorption in the column. The linear Kd model could not explain the data (especially, the tailing). The model including fluoride sorption by surface complexation could better explain the data. Effect of flow interruption on the fluoride concentration in the effluent is negligible, suggesting that equilibrium conditions can be assumed for this study. The results from a two domain model does not vary much from that of the single domain model, which shows that in the experimental conditions, mass transfer to the immobile zones may not be important as that of considering fluoride sorption by surface processes.

In conclusion, fluoride transport processes in soil should be studied in order evaluate contribution of soil leachable fluoride to fluoride contamination of shallow groundwater. The long tailing during desorption should be considered while implementing remediation technologies. Fluoride induced Al release is another factor to be looked in to, especially at industrial sites with high fluoride contamination.

Acknowledgements

I would like to dedicate this work to my parents for their unconditional love, support, believe and guidance, spiritual teachings and for everything that inspired me to achieve my goals in my professional and personal life.

Finally, thank you God for your kind blessings on me and my family.

Table of contents

List of Figures

xv

List of Tables

Nomenclatures

Symbols

C_d: capacitance density (F m^{-2})

S: surface area (m^2 g^{-1})

a: suspension density (g L^{-1})

F: Faraday constant (C mol^{-1})

R: molar gas constant (J mol^{-1} K^{-1})

T: absolute temperature (K)

D: dielectric constant of water

I: ionic strength (mol)

C: solute concentration (ML^{-3})

x: distance (L)

t: time (T)

v_x: average linear velocity in the x direction (LT^{-1})

D_L: coefficient of longitudinal hydrodynamic dispersion (L^2/T)

q_e: sorbed concentration (MM^{-1})

K_d: distribution coefficient (L^{3}M^{-1})

R: Retardation factor

$q_m,\ b$: Langmuir constants

$K,\ N$: Freundlich constants

E : measured electrode potential (mV)

E_o: reference potential (a constant) (mV)

C_e : Equilibrium fluoride concentration (mg l^{-1}) in solution

K_E : Dubinin- Radushkevick parameter

q_t : amount of fluoride on soil (mg g^{-1}) at time t

k_1 : first-order rate constant (min^{-1})

k_2 : pseudo-second-order rate constant (g mg^{-1} min^{-1})

R_L: adsorption intensity

Greek letters

σ_0: surface charge density (mol L^{-1})

ψ_o: surface potential (V)

ε_0 : premittivity of vacuum

θ: volumetric water content (L^{3}L^{-3})

ρ_b: dry soil bulk density (ML^{-3})

α: mass transfer coefficient in the mobile- immobile model (T^{-1})

β: fraction of mobile water in the mobile- immobile model

α_k: first-order kinetic rate coefficient (T^{-1})

ϵ^0 : Polanyi potential

Chapter 1: General Introduction

1.1. Background

Extensive contamination of groundwater with fluoride is a serious environmental concern due to its possible effect on contamination of drinking water resources and natural ecosystems. While fluoride is desired for strong teeth and bone, excessive intake (exceeding the WHO guideline value of 1.5 mg/l in drinking water (WHO, 2004)) results in serious health risks (Ayoob and Gupta, 2006). Presently, defluoridation is the most adapted method to provide safe drinking water to the society. Fluoride in groundwater can be due to natural or anthropogenic sources. In addition to groundwater, soil fluoride contamination due to natural or anthropogenic sources is also reported (Scanlon et al., 2009; Wang et al., 2002; Arnesen and Krogstad, 1998). The soluble fluoride can leach from the fluoride contaminated soil and contaminate the shallow groundwater under suitable conditions. A schematic figure depicting possible source of fluoride contamination in groundwater is shown in Figure 1.1.
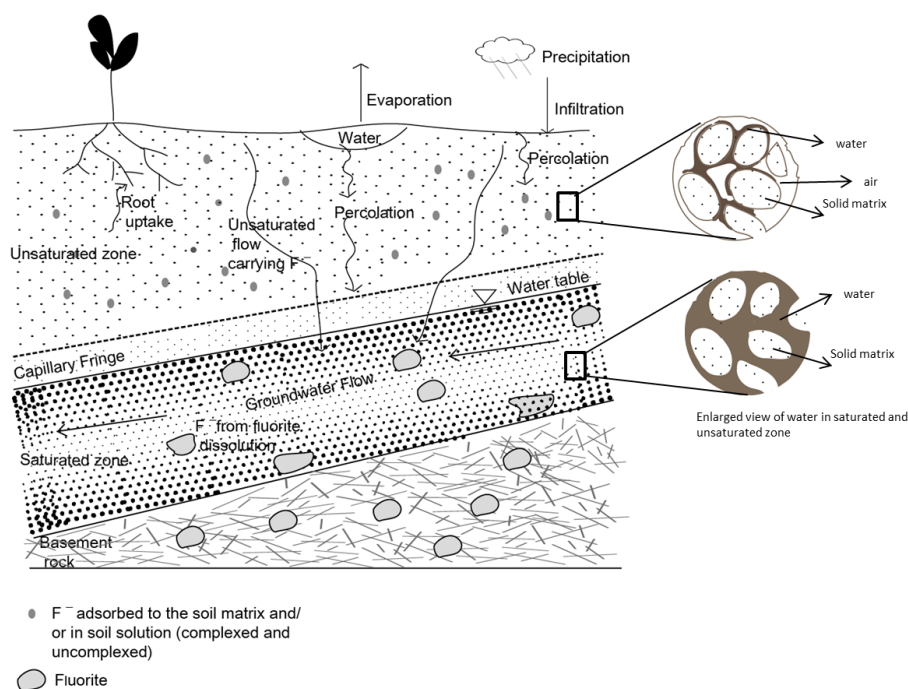
Figure 1.1. Schematic diagram showing possible sources of groundwater fluoride contamination.

Few studies have been conducted for fluoride leaching from soil. One such study by Scanlon et al., (2009) in natural ecosystems, rain-fed areas and irrigated systems in Australia and USA reveals that leachable fluoride in soil is about 10 mg/kg, extending up to a depth of more than 10 m in rain fed area and about 30 m in natural ecosystems. The authors concluded that fluoride will not reach the water table and contaminate the groundwater because the water table is deep.
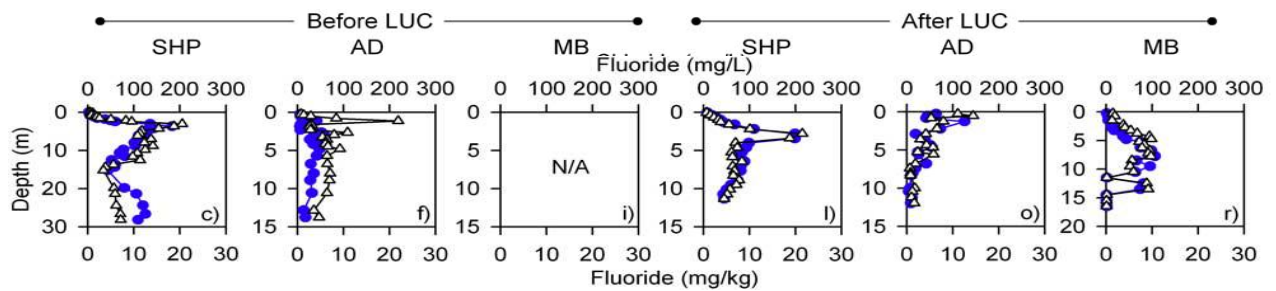
Figure 1.2. Representative fluoride profiles in (c,f,i) natural ecosystems and (l and r): rain-fed and (o): irrigated agricultural ecosystems. Values are shown for mg/L (triangles) and mg/kg (circles). LUC, land use change; SHP, Southern High Plains; AD, Amargosa Desert; MB, Murray Basin (after Scanlon et al., 2009).

Similarly, Lognathan et al. (2001) concluded that fluoride will not leach to the groundwater in the New Zealand pasture soil. However, a good correlation is found between soil leachable fluoride and groundwater fluoride contamination (Wang et al., 2002; Saxena and Rani, 2012).

Nevertheless, unravelling the mechanism of fluoride immobilization processes and its transport behavior in subsurface is necessary to understand the possible contribution of soil leachable fluoride to groundwater, and thus to decipher effective strategies to prevent further groundwater contamination from the contaminated soil sources. The transport of solutes in porous media is subjected to a variety of physical and chemical non-equilibrium processes, and the fate of a contaminant depends on the geochemical reactions at mineral-water interface in addition to the transport processes. Hence, this study aims to investigate the reactive transport of fluoride in a saturated column by column experiments and solute transport modeling at laboratory scale.

1.2. Literature Survey

1.2.1. *Fluoride in groundwater*

Fluoride is a minor element representing about 0.3g/kg by weight of the Earth's crust and exists as fluorides in number of minerals (WHO, 2004). Excess fluoride in groundwater is reported from more than 35 countries in the world (Ayoob et al., 2008). Figure 1.3 shows the map of countries with groundwater fluoride contamination, prepared by UNICEF. In many of the Asian and African countries, fluoride levels in water are high. The reported maximum dissolved fluoride ion levels in groundwater, for example, are: Rajasthan, India (69.7 mg/l), Kuitan, China (21.5 mg/l), Tanzania (12 mg/l), South Africa (13 mg/l) (Ayoob et al., 2008), and Kenya (55 mg/l) (Gitonga et al., 1984). In short, many millions of people are exposed to toxic concentrations of fluoride well above the usual upper limit set by many public health authorities around the world such as: 1.5 mg/l (WHO, 2004; BIS, 1991), 0.8 mg/l (DWQS, 2010), and so on.

On a local scale, considerable amount of fluoride can be introduced to the environment by anthropogenic sources such as, application of phosphate containing fertilizer and from aluminum smelters (Arnesen and Krogstad, 1998). However, in general, fluoride concentration in groundwater is mainly governed by geogenic processes (Edmunds and Smedley, 2005; Ayoob and Gupta, 2006) where groundwater becomes contaminated in contact with fluoride bearing minerals such as fluorite,
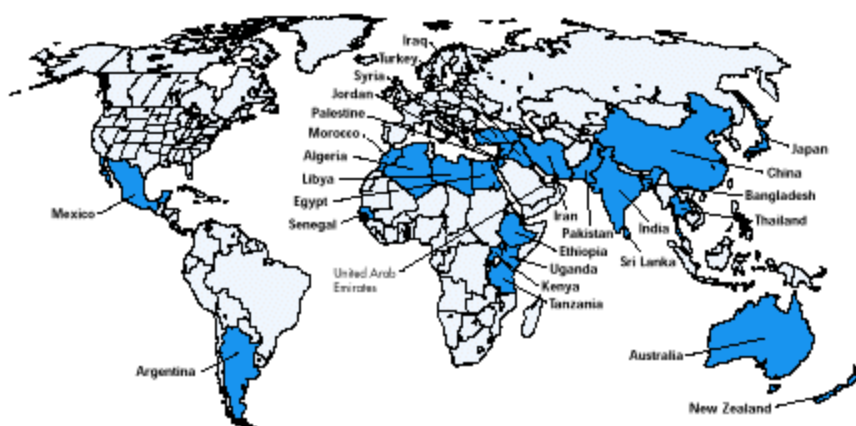
Countries with endemic fluorosis due to excess fluoride in drinking water

Figure 1.3: World map showing F contamination affected countries Source: UNICEF (http://www.nofluoride.com/Unicef_fluor.cfm)

fluoroapatite, biotite, topaz, and their corresponding host rocks such as granite and basalt by the dissolution of these minerals (Edmunds and Smedley, 2005; Apambire et al., 1997).

Fluorite (CaF_2) is found to be the predominant mineral that controls the dissolved fluoride concentration in groundwater (Edmunds and Smedley, 2005; Handa, 1975), and fluoride release depends mainly upon geochemical environment. For example, low calcium concentration associated with high pH promotes the dissolution of fluorite (Handa, 1975). Hence, these conditions are often associated with high fluoride groundwater regions in a sodium bicarbonate dominated system. Hydrological properties (e.g., residence time) as well as climatic conditions (e.g., evapotranspiration, precipitation) also influence fluoride concentration in groundwater (Edmunds and Smedley, 2005; Jacks et al., 2005).

In granitic aquifers, dissolution of fluoride can be the possible reason for presence of fluoride in groundwater. The hydrolysis of alumino-silicate minerals in the hard rock aquifers produces bicarbonate ion, which can enhance fluorite (CaF_2) dissolution by precipitating $CaCO_3$ as defined by the following reactions:

$$CaF_2 + 2HCO_3^- \rightarrow CaCO_3 + 2F^- + H_2O + CO_2 \qquad (1.1)$$
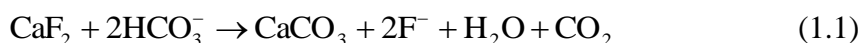
In the presence of excessive sodium bicarbonates in groundwater, the amount of dissolved fluoride will be elevated and can be expressed as:

$$CaF_2 + 2NaHCO_3 \rightarrow CaCO_3 + 2Na^+ + 2F^- + H_2O + CO_2 \qquad (1.2)$$

(Handa, 1975).

Also, a handful of research are found on the possibility of fluoride leaching from the soil and contaminating groundwater (Zhu et al., 2009).

1.2.2. *Effect of fluoride consumption*

Fluoride can enter human body through a variety of sources, e.g., water, food, air, medicaments and cosmetics, though drinking water is the major contributor of daily fluoride intake (Meenakshi et al., 2004). Although it is evidenced that fluoride is beneficial for prevention of dental caries, the essentiality has not been demonstrated unequivocally (WHO, 2011). In fact, adverse effects of the long-term ingestion of fluoride (>1.5 mg/l) is well documented (Ayoob and Gupta, 2006). Dental and skeletal

4

fluorosis are the most common health effects of fluoride consumption. Besides this, excessive consumption of fluoride may affect various organ systems, including the immune system, circulatory system, the liver and kidney, the reproductive system, the brain and the skin (Meenakshi and Maheswari, 2006; Liu et al., 2008). Animals are also equally affected as that of human beings by drinking fluoride rich water. In addition, irrigation with high fluoride water is found to adversely affect the various physiological features of plants including decreased plant growth, chlorosis, etc. (Dey et al., 2012; Elloumi et al., 2005).

Because of the adverse effects of fluoride consumption on human health, considerable amount of researches have been dedicated for the removal of fluoride from groundwater using various techniques, e.g., adsorption, ion exchange, precipitation–coagulation, membrane separation, electrolytic defluoridation, electrodialysis, etc., using different materials. The details of these processes are reviewed by Meenakshi and Maheswari (2006).

1.2.3. Fluoride in soil

Presence of fluorine in soil is related to the weathering of primary minerals such as fluorapatite, cryolite, fluorite, and topaz. Industries such as aluminum smelters also contaminate the soil (Arnesen and Krogstad, 1998). Air borne pollution by direct adsorption of gases such as hydrogen fluoride or silicon tetrafluoride is also observed. Figure 1.4 shows a schematic diagram interlinking the possible sources of fluoride in the ecosystem.

The average fluorine content of most soils throughout the world has been reported to be 329 ppm (Kabata- Pendias et al., 1992). Sandy soils in humid climates are found to possess the lowest fluorine in general whereas higher fluorine concentrations are found in heavy clay soils and soils from weathered mafic rocks (Fuge and Andrews, 1988). Clay soils are often associated with high amount of sorbed fluoride because fluoride has a strong affinity for aluminum (Al) compounds including (hydro)oxides, and hence, the amount of sorbed fluoride in soil is highly correlated with amorphous Al and Fe oxide content and crystalline Al content (Peek and Volk, 1985) and poorly ordered amorphous Al oxides (Omueti and Jones, 1977). The potential for
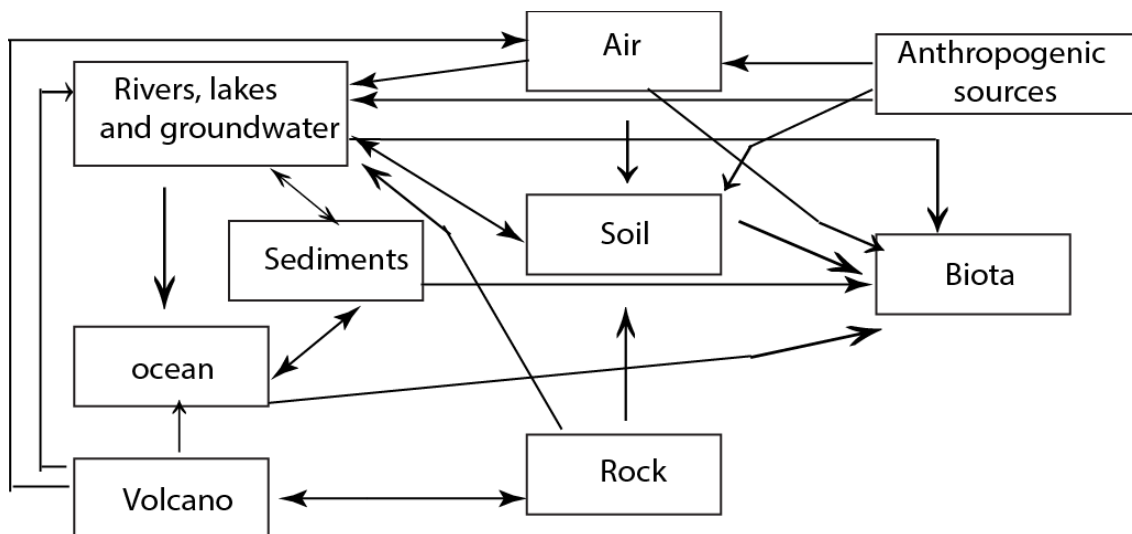
Figure 1.4: Schematic diagram showing fluoride in the geo-environment.

soil contamination from natural and anthropogenic sources lead many researchers in different countries to study the soil fluorine behavior, e.g., (1) Norway (Arnesen and Krogstad 1998), (2) India (Madhavan and Subranian, 2002; Padhi and Muralidharan, 2012; Chaudhary et al.,2009; Saxena and Rani 2012) among others, (3) China (Zhu et al., 2007; Wang et al., 2002; Zhu et al., 2009), (4) Spain (Gago et al., 2002), (5) Srilanka (Jayawardene et al., 2012), (6) Ghana (Abugri and Pelig-Ba, 2011), and (7) USA (Scanlon et al., 2009).

Soil fluoride contamination is recently of growing concern because of the following reasons: (1) high fluoride levels are found in crops grown over fluoride contaminated soils or irrigated with fluoride rich water, and fluoride enters the food chain of human beings through these crops (Susheela, 2003; Gautam et al., 2010; Amalraj and Pius, 2013), (2) grazing animals are affected by consuming fluoride contaminated soil (Cronin et al., 2003), (3) high levels of soluble fluoride in soil may leach and contaminate shallow groundwater under suitable conditions (Wang et al., 2002; Pickering, 1985), and (4) fluoride contamination induces aluminum release from soil, which is another potential toxic element (Polomski et al., 1982).

High levels of soluble fluoride in soil may leach and contaminate the shallow groundwater under the following conditions, i.e., acidic and alkaline soils (Wang et al., 2002; Wenzel and Blum, 1992; Pickering, 1985; Arnesen and Krogstad, 1998), coarse

6

textured soil (Wang et al., 2002), alkaline sandy loam (Chaudhary et al., 2009), presence of relatively thick B horizon (Arnesen and Krogstad,1998), and higher degree of weathering and higher clay content (Wang et al., 2002, Zhu et al., 2007; Omueti and Zones, 1977). On the contrary, the study by Lognathan et al.(2001) showed that in most of the New Zealand pastoral soils, fluoride applied to soils as fertilizer may not move down the soil profile nor pollute groundwater. Similarly, the leaching experiments of fluoride in sandy soils by Murray (1983) showed that 94.9 to 98.4% of applied fluoride was retained in the soil column, and Murray (1983) concluded that little fluoride would be leached to groundwater. Barrow (1986) also found that fluoride was strongly adsorbed to soil. Thus, the contribution of adsorbed fluoride in soil to groundwater contamination is still controversial, which urges to study the dynamic distribution of fluoride in the porous media.

1.2.4. Mechanism of fluoride sorption in soil

The factors that affect the retention and release of fluorine in soil are, Al, Fe oxides, Calcium (Ca), organic matter, and pH (Murray, 1984). Du et al. (2011) investigated the mechanism of fluoride sorption on different clay minerals under varying geochemical conditions and initial fluoride concentrations and found that the mechanism of fluoride sorption is heavily dependent on the solution pH and fluoride concentration. Harrington et al. (2003) studied the behavior of fluoride facilitated Al release from soils controlled by difference in soil mineralogy, morphology and soil solution chemistry. Acidic and alkaline soils with low Al and Fe (hydro)oxides favor fluoride leaching from the soil matrix (Wang et al., 2002). Also, non-specifically bound fluoride has the higher tendency to be released easily and contaminate groundwater/surface water bodies or may enhance plant fluoride uptake. Hence, understanding the mechanism of fluoride sorption in soil is highly necessary.

The mechanism of fluoride sorption in soil can be due to surface complexation, electrostatic attraction or chemical reactions including ion exchange and/or precipitation, depending on the adsorbent characteristics and solution pH among other parameters (Ayoob et al., 2008; Harrington et al., 2003). In soil, fluoride is mainly bound to clay minerals, aluminum and iron hydro(oxides) (Peek and Volk, 1985). Subsurface

materials with significant clay content may bind fluoride by an ion exchange process, but fluoride is also bound strongly at the edge sites of these minerals by surface complex formation (e.g., kaolinite) (Weerasooriya et al., 1998). Thus, adsorption by complexation with hydroxyl sites on oxide mineral surfaces and edges of clay minerals might play an important role for fluoride retention in soil. A considerable amount of research has investigated the uptake of fluoride by various common minerals using a variety of macroscopic and spectroscopic techniques (Du et al., 2011; Cochiara, 2009). Fluoride is found to be strongly retained via the formation of inner-sphere adsorption complexes, e.g., on Al-oxides (Hao and Huang, 1986) and kaolinite (Weerasooriya et al. 1998 and 1999) over a range of pH and ionic strength. Different models that can be used to predict the mechanism of fluoride sorption on soil are discussed below.

1.2.4.1. Isotherm models

An adsorption isotherm describes the relation between the equilibrium concentration of the adsorptive and the quantity of adsorbate on the surface (Sparks, 2003). The most commonly used isotherms to describe contaminant sorption on different materials include Langmuir, Freundlich, Redlich-Peterson, and Dubinin-Radushkevick equations (Mahramanlioglu et al., 2002). Detailed information on adsorption, i.e., monolayer/multilayer adsorption, interaction between the adsorbed species, and homogeneous/heterogeneous pore distribution can be obtained from the best fit of these isotherms (Sparks, 2003). In addition, the thermodynamic parameters such as Gibb's free energy change, enthalpy of adsorption, and entropy change can be estimated from the isotherm, which can help to understand the nature and mechanism of sorption reactions under equilibrium conditions (Romero-Gonzalez et al., 2005).

The equilibrium- based isotherm models are widely applied to describe cation and anion sorption on soil and synthesized materials. Researches are also dedicated to demonstrate sorption of fluoride on laterite (Sarkar et al., 2006), kaolinite and bentonite (Kau et al., 1998), iron oxides (Mohapatra et al., 2011), alumina cement granules (Ayoob et al., 2008), activated alumina (Ghorai and Pant, 2005), and many more by using isotherm models.

1.2.4.2. Surface complexation modeling

Adsorption reactions can be described by various models. Empirical models, e.g., the distribution coefficient, the Freundlich adsorption isotherm, and the Langmuir adsorption isotherm, provide descriptions of macroscopic data without theoretical basis and do not definitely prove a reaction mechanism (Sparks, 2003). Surface complexation models (SCM) are chemical models based on molecular descriptions of the electric double layer using equilibrium-derived adsorption data and calculate value of thermodynamic data mathematically (Sparks, 2003). SCMs are advanced from the so-called isotherm models in that, they consider surface charge resulting from protonation and dissociation reactions as well as surface complexation reactions of reactive surface hydroxyl groups at mineral surfaces (Goldberg, 1992). These models have been highly successful in describing the sorption of metal ions by hydrous metal oxide surfaces. A number of SCMs have been proposed and applied to successfully describe adsorption of several different ions onto a wide range of adsorbents over an extensive set of aqueous solution conditions (Dzombak and Morel, 1990; Goldberg, 1998). Some of the studies referred here are for application of SCM for anion sorption, e.g., fluoride sorption to kaolinite (Weerasooriya et al., 1998), fluoride, bromide and iodide sorption on kaolinite (Weerasooriya and Wickramarathna, 1999), arsenate and arsenite sorption to iron oxide minerals (Dixit and Hering, 2003) and to calcite (So et al., 2008), phosphate adsorption to calcite (So et al., 2011), sulphate and selenite adsorption on iron oxides (Fukushi and Sverjensky, 2007).

Surface complexes can exist in two types of structural configurations, outer-sphere and inner-sphere surface complexes. Outer-sphere surface complexes involve electrostatic coulombic interactions. The process is usually rapid and reversible and occurs on surfaces of opposite charge to the adsorbate. Whereas, inner-sphere surface complexes involve ionic or covalent bonding. The process is relatively slower and irreversible and can occur on a surface regardless of the charge (Sparks, 2003). The commonly used SCMs are the constant capacitance model (Stumm et al., 1980) (CCM), the generalized two layer model (Dzombak and Morel, 1990), and the triple layer model (Davis et al., 1978). The basic difference in these models is the description on the electric double layer.

A thorough discussion on the SCMs and their application for protonation-dissociation reactions, metal ion adsorption and inorganic anion adsorption on oxides, clay minerals and soils can be found in Goldberg (1992). Fluoride sorption to different adsorbents by surface complexation has been studied, e.g., kaolinite (Weerasooriya et al., 1998), alumina (Hao and Huang, 1986), and alumina, bauxite and laterite (Craig et al., 2015). However, SCMs have not been widely applied to study fluoride adsorption on natural materials. Hence, the intrinsic acidic constants, speciation, and spectroscopic data are scarce for fluoride sorption to natural materials. Also, the application of SCMs to natural sediments of varying mixtures of minerals is difficult because of the presence of secondary minerals and organic coatings (Davis et al., 2004).

A descriptive explanation of the CCM and the generalized two layer model, which will be used in this study, is given below (Goldberg, 1992).

The constant capacitance model:

The assumptions made in a CCM are: (i) all surface complexes are inner-sphere complexes; (ii) no surface complexes are formed with ions from the background electrolyte; (iii) one plane of charge represents the surface; (iv) the relationship between surface charge density, σ_o, and surface potential, ψ_o, (where o represents the surface plane), is

$$\sigma_0 = \frac{C_d S a}{F} \psi_0 \qquad (1.3)$$

where C_d: capacitance density (F m^{-2}), S: surface area (m^2 g^{-1}), a:suspension density (g L^{-1}), F: Faraday constant (C mol^{-1}), σ_0: has units of mol L^{-1}, ψ_o: has units of V. The structure of the surface-solution interface for the constant capacitance model is shown in Figure 1.5 (Westall, 1986).
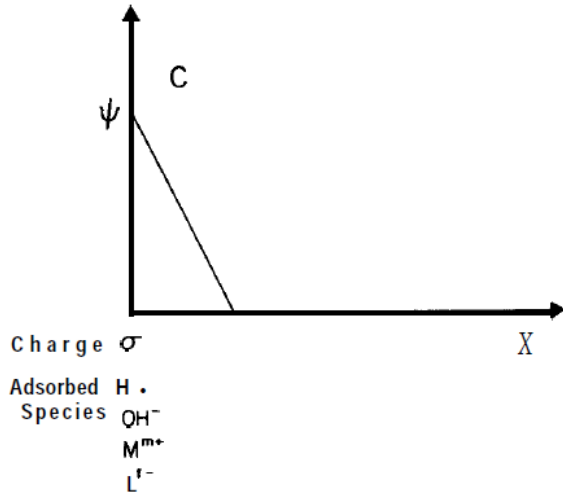
Figure 1.5. Structure of the surface-solution interface for the constant capacitance model (after Westall, 1986).

The equations representing the surface complexation reactions in a CCM are:
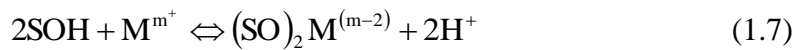
$$SOH + H^+ \Leftrightarrow SOH_2^+ \tag{1.4}$$

$$SOH \Leftrightarrow SO^- + H^+ \tag{1.5}$$

$$SOH + M^{m^+} \Leftrightarrow SOM^{(m-1)} + H^+ \tag{1.6}$$

$$2SOH + M^{m^+} \Leftrightarrow (SO)_2 M^{(m-2)} + 2H^+ \tag{1.7}$$

$$SOH + L^{l^-} \Leftrightarrow SL^{(l-1)^-} + OH^- \tag{1.8}$$

$$2SOH + L^{l^-} \Leftrightarrow S_2 L^{(l-2)^-} + 2OH^- \tag{1.9}$$

here, SOH represents surface functional group, M is a metal ion of charge m^+, and L is a ligand of charge l^-.

The intrinsic equilibrium constants describing the surface complexation reactions can be defined as:

$$K_+(int) = \frac{[SOH_2^+]}{[SOH][H^+]} \exp[F\psi_0 / RT] \tag{1.10}$$

$$K_-(int) = \frac{[SO^-][H^+]}{[SOH]} \exp[-F\psi_0 / RT] \tag{1.11}$$

11

$$K_M^1(int) = \frac{[SOM^{(m-1)}][H^+]}{[SOH][M^{m^+}]} \exp[(m-1)F\psi_0/RT] \qquad (1.12)$$

$$K_M^2(int) = \frac{[(SO)_2M^{(m-2)}][H^+]^2}{[SOH]^2[M^{m^+}]} \exp[(m-2)F\psi_0/RT] \qquad (1.13)$$

$$K_L^1(int) = \frac{[SL^{(1-1)^-}][OH^-]}{[SOH][L^{1^-}]} \exp[-(1-1)F\psi_0/RT] \qquad (1.14)$$

$$K_L^2(int) = \frac{[S_2L^{(1-2)^-}][OH^-]^2}{[SOH]^2[L^{1^-}]} \exp[-(1-2)F\psi_0/RT] \qquad (1.15)$$

where R: molar gas constant (J mol^{-1} K^{-1}), *int*: intrinsic, T: absolute temperature (K), square brackets: concentrations (mol L^{-1}).

The mass balance and charge balance of the surface functional group, SOH, is in accordance with the surface complexes formed.

The generalized two-layer model

The generalized two-layer model was developed by Dzombak and Morel (1990) as an expansion of the diffuse layer model proposed by Stumm and coworkers (Stumm et al., 1970; Huang and Stumm, 1973). This model considers that the oxide-water interface consists of a surface layer for specifically sorbed ions and a diffuse layer of counter-ions in solution. The diffuse layer commences at the d-plane and extends into the solution phase. The model assumes that: (i) all surface complexes are inner-sphere complexes; (ii) no surface complexes are formed with ions in the background electrolyte; (iii) two planes of charge represent the surface; (iv) the relationships between surface charges and surface could be written as (Sposito, 1984):

$$\Psi_a = \Psi_d \qquad (1.16)$$

$$\sigma_d = -\frac{Sa}{F}(8\varepsilon_0 DRTI)^{1/2} \sinh\left(\frac{F\Psi_d}{2RT}\right) \qquad (1.17)$$

where ε_0 : premittivity of vacuum, D: dielectric constant of water, I: ionic strength
The surface-solution interface in the generalized two-layer model could be represented by Figure 1.6.
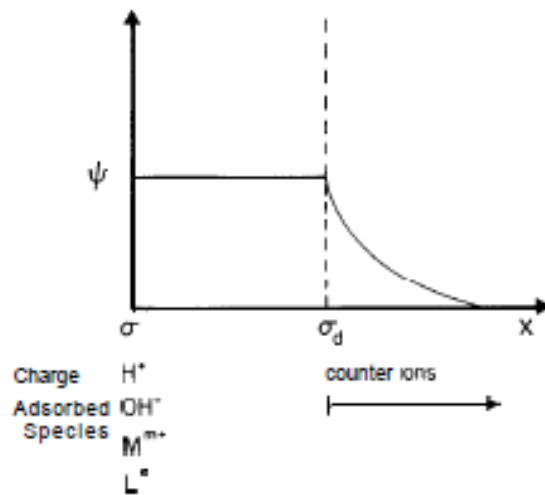
Figure 1.6. Structure of the surface-solution interface for the diffuse layer model (after Dzombak and Morel, 1990).

The surface reactions in the generalized two-layer model could be represented as:
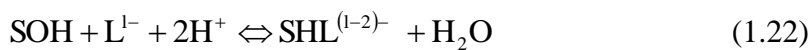
$$SOH + H^+ \Leftrightarrow SOH_2^+ \tag{1.18}$$

$$SOH \Leftrightarrow SO^- + H^+ \tag{1.19}$$

$$SOH + M^{m+} \Leftrightarrow SOM^{(m-1)} + H^+ \tag{1.20}$$

$$SOH + L^{l-} + H^+ \Leftrightarrow SL^{(l-1)-} + H_2O \tag{1.21}$$

$$SOH + L^{l-} + 2H^+ \Leftrightarrow SHL^{(l-2)-} + H_2O \tag{1.22}$$

here, SOH represents surface functional group, M is a metal ion of charge m^+, and L is a ligand of charge l^-. Equations 1.18 and 1.19 represents protonation and deprotonation at the surface respectively. Metal ion adsorption is represented by equation 1.20 and can be considered to occur in two types of sites: strong sites with high affinity and weak sites with low affinity. Ligand exchange is represented by equations 1.21 and 1.22 and it is not necessary to specify two sets of binding sites.

The intrinsic conditional equilibrium constants for reactions 1.18 to 1.22 in the generalized two-layer model are defined by the following reactions 1.23 to 1.27 respectively: The equations for the intrinsic conditional equilibrium constants for the metal adsorption to strong and weak sites are similar.

13

$$K_+(int) = \frac{[SOH_2^+]}{[SOH][H^+]} \exp[F\psi_0 / RT] \qquad (1.23)$$

$$K_-(int) = \frac{[SO^-][H^+]}{[SOH]} \exp[-F\psi_0 / RT] \qquad (1.24)$$

$$K_M^1(int) = \frac{[SOM^{(m-1)}][H^+]}{[SOH][M^{m+}]} \exp[(m-1)F\psi_0 / RT] \qquad (1.25)$$

$$K_L^1(int) = \frac{[SL^{(l-1)-}]}{[SOH][L^{l-}][H^+]} \exp[-(l-1)F\psi_0 / RT] \qquad (1.26)$$

$$K_L^2(int) = \frac{[SHL^{(l-2)-}]}{[SOH][L^{l-}][H^+]^2} \exp[-(l-2)F\psi_0 / RT] \qquad (1.27)$$

where F: Faraday constant (C mol^{-1}), R: molar gas constant (J mol^{-1} K^{-1}), int: intrinsic, T: absolute temperature (K), square brackets: concentrations (mol L^{-1}).

The mass balance for the surface functional group, SOH could be written as:

$$[SOH]_T = [SOH] + [SOH_2^+] + [SO^-] + [SOM^{(m-1)}] + [SL^{(l-1)-}] + [SHL^{(l-2)-}] \quad (1.28)$$

The charge balance expression is:

$$\sigma_d = [SOH_2^+] - [SO^-] + (m-1)[SOM^{(m-1)}] - (l-1)[SL^{(l-1)-}] - (l-2)[SHL^{(l-2)-}] \quad (1.29)$$

where σ_d is the surface charge (mol L^{-1}).

1.2.5. *Contaminant transport in soil*

During the past several decades, we are increasingly experiencing the contamination of soil, surface water and groundwater due to natural contaminants, waste disposals, leakage of industrial and municipal wastes, use of fertilizers, etc. After releasing contaminants to the subsurface, contaminants interact with soil matrix and groundwater. The major hydrological processes of interaction are advection, dispersion and diffusion, and decay in the case of radioactive contaminants whereas the chemical processes include aqueous complexation, reduction/oxidation, sorption (surface complexation (adsorption) or ion exchange), and precipitation/dissolution.

Transport of a reactive contaminant in groundwater systems could be affected by physical non-equilibrium processes (e.g., soil heterogeneity, preferential flow, and

kinetic diffusion) or chemical non-equilibrium processes (e.g., caused by kinetic sorption or transformation reactions) (Brusseau et al., 1997). Local equilibrium conditions are only valid when solute transport occurs in a homogeneous porous medium and sorption is linear, reversible, and not kinetically limited (Brusseau et al., 1989). Consequently, the fluoride retention processes in the soil matrix should be studied under non-equilibrium conditions to correctly assess the fate and transport of it in the soil system.

Solute transport in subsurface can be described by a set of partial differential equations and the chemical reactions are described by a set of nonlinear algebraic equations. There are large number of specialized numerical models to simulate different processes and for different applications, depending on the objective (e.g., Simunek and van Genuchten, 2006).

Here, the more generalized transport models and the models with increasing complexity for contaminant transport in the subsurface are discussed.

1.2.5.1. Generalized transport model for contaminant transport in subsurface

The advection-dispersion equation for one dimensional flow in a homogenous, isotropic porous medium without sorption and degradation can be expressed as (Fetter, 1999):

$$\frac{\partial C}{\partial t} = D_L \frac{\partial^2 C}{\partial x^2} - v_x \frac{\partial C}{\partial x} \qquad (1.30)$$

where, C: solute concentration (ML^{-3}), x: distance (L), t: time (T), v_x: average linear velocity in the x direction (LT^{-1}) and D_L: coefficient of longitudinal hydrodynamic dispersion (L^2/T).

The advection- dispersion equation (equation 1.30) can be used for transport of inert, non-adsorbing solutes during steady-state water flow. Whereas, contaminant sorption can be included in the model, expressed as follows (van Genuchten and Wagenet, 1989):

$$\theta \frac{\partial C}{\partial t} + \rho_b \frac{\partial q_e}{\partial t} = \theta D_L \frac{\partial^2 C}{\partial x^2} - \theta v_x \frac{\partial C}{\partial x} \qquad (1.31)$$

where, θ: volumetric water content ($L^3 L^{-3}$), ρ_b: dry soil bulk density (ML^{-3}) q_e: sorbed concentration (MM^{-1}).

This equation can be used for both equilibrium and kinetic sorption processes. In the case of linear sorption, which is the simplest form of adsorption, the relation between the sorbed concentration and solute concentration in solution concentration can be defined as:

$$q_e = K_d C \qquad (1.32)$$

where K_d is an empirical distribution coefficient ($L^3 M^{-1}$). The term retardation factor (R) can be defined as

$$R = 1 + \frac{\rho_b K_d}{\theta} \qquad (1.33)$$

When the sorption of contaminant is non-linear, the retardation factor is not constant, rather it changes as a function of concentration. In that case, the most commonly used Langmuir and Freundlich non-linear sorption models can be used as (Fetter, 1999):

Langmuir isotherm: $\quad q_e = \dfrac{q_m b C}{1 + bC} \qquad (1.34)$

where, q_m and b are constants for the Langmuir isotherm, and

Freundlich isotherm: $\quad q_e = K C^N \qquad (1.35)$

where, K and N are constants for the Freundlich isotherm.

1.2.5.2. Nonequilibrium transport

Equilibrium solute transport models often fail to describe experimental data (e.g., Simunek and van Genuchten, 2006). A large number of non-equilibrium models have been provided and applied to describe the transport of contaminants (Nielsen et al., 1986; Brusseau, 1999) which resulted in better description of observed laboratory and field data.

Physical Nonequilibrium

Physical nonequilibrium (PNE) arises because of non-uniformity of the flow field and is generally represented by the mobile/immobile model (van Genuchten and Wierenga, 1976). The model is represented schematically as shown in Figure 1.7. This model assumes that the liquid phase can be partitioned into distinct mobile (flowing)

and immobile (stagnant) zones, and transport in the mobile zone is governed by the advection–dispersion equation while solute exchange between mobile and immobile zones occurs by diffusive mass transfer, described with a first-order rate equation.

Mobile Water

Immobile Water

Soil region adjacent to mobile water

Stagnant soil region
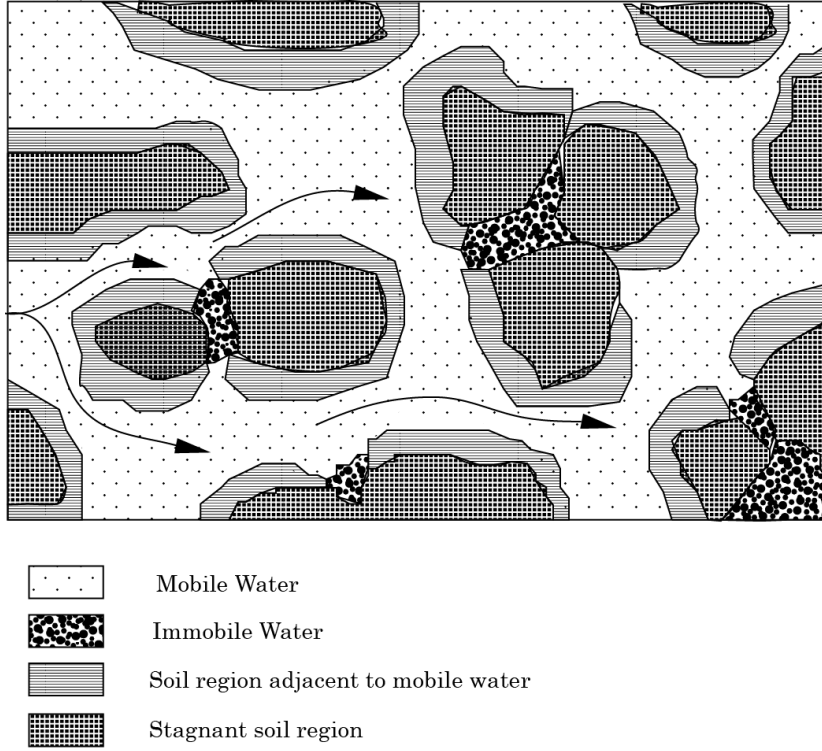
Figure 1.7. Schematic diagram representing the conceptual model of the saturated zone consisting of mobile and immobile zones in soil matrix. Flow lines in the mobile zone are also shown.

The model is defined as:

$$\theta_m \frac{\partial C_m}{\partial t} + \theta_{im} \frac{\partial C_{im}}{\partial t} + \rho_b \frac{\partial s}{\partial t} = \theta_m D_m \frac{\partial^2 C_m}{\partial x^2} - \theta_m v_m \frac{\partial C_m}{\partial x} \tag{1.36}$$

$$\theta_{im} \frac{\partial C_{im}}{\partial t} + \rho_b \frac{\partial s_{im}}{\partial t} = \alpha(C_m - C_{im}) \tag{1.37}$$

The conditions that hold for these equations are:

$$\theta_m + \theta_{im} = \theta, \quad \theta_m v_m = \theta_V, \quad \theta_m D_m = \theta D, \quad s_m + s_{im} = s \tag{1.38}$$

17

where, the subscripts *m* and *im* refer to the mobile and immobile regions respectively, *s* is the solid phase concentration of solute from either the mobile or immobile region per mass of dry soil (MM^{-1}), α is a coefficient for mass transfer between mobile and immobile region (T^{-1}).

Chemical non-equilibrium

Rate limited chemical reactions at an interface results in chemical non-equilibrium (Sparks, 2003). Consequently, models describing chemical non-equilibrium only affect the concentration of solutes that interact with an interface. The simplest of the models assumes first order linear kinetics, and is written as follows:

$$\frac{\partial q_e}{\partial t} = \alpha_k (K_d C - q_e) \qquad (1.39)$$

where α_k: first-order kinetic rate coefficient (T^{-1}).

However, these one-site models did not significantly improve the model predictions to analyze laboratory column experiments (Simunek and van Genuchten, 2006). Hence, this model is extended to the two-site model, which assumes sorption on one fraction to be instantaneous, while sorption on the remaining sites is considered to be time-dependent. A combined physical and chemical nonequilibrium transport model is developed and applied to colloid transport by Leij and Bradford (2009).

1.2.6. *Summary for literature search results*

From the intensive literature survey, the following research outputs are obtained.

Fluoride in the environment*:*

- Fluoride contamination of soil and groundwater is a major environmental issue. The health hazards of consuming fluoride rich water in any form are numerous.
- The source of fluoride in groundwater could be geogenic or anthropogenic. The geogenic fluoride source in groundwater is generally attributed to water-rock interaction.
- Although fluoride is known to be strongly retained by soil, in highly polluted areas, fluoride from soil can leach and pollute the groundwater and surface water sources.

Mechanism of fluoride sorption in soil:

- The retention and release of fluoride in soil depends on the abundance of clay minerals in soil, structure of the soil matrix, geochemical processes at the mineral-water interface, climate, etc.
- Many equilibrium and kinetic models have been used to explain fluoride sorption behavior in mineral surfaces, moreover, surface complexation model better explains the quantification of the mineral surface.

Fluoride transport:

- The simple advection dispersion equation may not be able to explain the reactive contaminant transport behavior.
- Physical and chemical non-equilibrium is needed to be considered to explain contaminant transport in a heterogenous system.

1.3. Objectives

Based on previous research results and the importance of fluoride in the geo-environment, it can be understood that mobility of fluoride in soil can have significant effect on shallow groundwater fluoride contamination and fluoride uptake by plants. Fluoride mobility in soil also affects the mobility and availability of aluminum for plant uptake, which is another potentially toxic element (Gago et al., 2002). Numerous studies have been conducted to find the fluoride sorption/desorption processes by clay minerals and composites. However, only handful research has been conducted to understand fluoride sorption mechanism in the soil system (e.g., Craig et al., 2015 studied fluoride sorption on laterite).

In addition, dynamic behavior of fluoride in subsurface is also important, especially reactive transport processes are needed to be properly modeled to simulate how chemical agents move through subsurface systems (Steefel et al., 2005). Many models are proposed to explain reactive transport of contaminant by considering the aqueous and surface chemistry of the contaminant and the soil/sediment, e.g., Liu et al. (2009) discussed uranium (U(VI)) transport by developing a model to consider U(VI) aqueous and surface chemistry. Considering fluoride transport in the subsurface, Johannes et al. (1996) studied fluoride transport in a sand-goethite column, Usunoff et

al. (2009) studied fluoride transport in a quartz-sand packed column, and Begin et al. (2003) studied fluoride transport in a unsaturated soil. Nonetheless, all these studies considered pure mineral phases for fluoride transport (Johannes et al., 1996; Usunoff et al., 2009) or fluoride transport was described by linear sorption (Begin et al., 2003). Since reactive transport in the subsurface is highly non-linear, the goal of this study is set to understand the non-linear fluoride transport behavior in the subsurface from laboratory experiment and numerical modeling.

The overall objectives of this dissertation are set to be:

1) To identify the mechanism of fluoride sorption/desorption in a granitic soil under wide range of pH and solid/solution ratio and validating the results with spectroscopic studies,

2) To develop a fluoride reactive transport model describing the physical and chemical non-equilibrium processes observed in laboratory scale and

3) To discuss the impact of leachable soil fluoride on the geo-environment

1.4. Methodology followed

The methodology followed in this thesis to meet the objective is shown in terms of a flow chart diagram (Figure 1.8). First, related research were understood to get an overall idea about the current state of art of fluoride transport research. Next, field survey were conducted in groundwater fluoride contaminated areas of India and Japan and also in Tsukuba, Japan, where groundwater is not fluoride contaminated.

Next step includes understanding fluoride sorption behavior in the original soil. Since understanding the sorption behavior of fluoride is complicated in complex soil system, calcite was chosen first to understand the fluoride sorption behaviors and also to understand the applicability of surface complexation processes. Next, fluoride sorption processes were evaluated in a granitic soil with sorption isotherm and surface complexation modeling.

Finally, fluoride transport behavior in a saturated column were investigated by column experiment and numerical modeling.
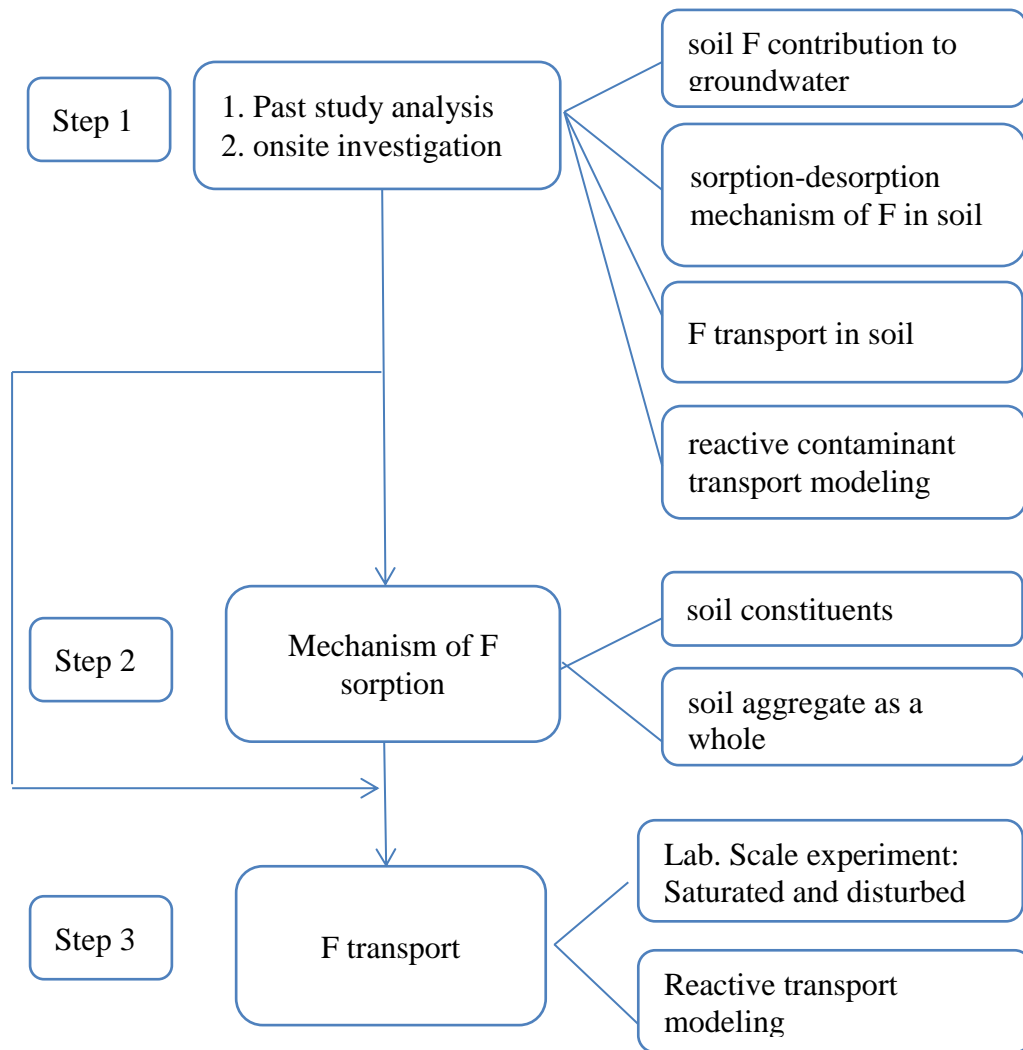
Figure 1.8. Flow diagram showing the methodology followed for investigating fluoride sorption processes in this thesis

1.5. Organization of the dissertation

This dissertation contains six chapters.

Chapter 1 contains the general introduction, understanding from previous studies related to the state and toxicity of fluoride in groundwater and soil, equilibrium and kinetic models that can explain mechanism of fluoride sorption in soil, geochemical solute transport models and the objective of this research.

Chapter 2 is dedicated to a brief description of the analytical methods followed in this thesis and field observations for possible fluoride contamination of groundwater from soil in granitic terrains.

Chapter 3 describes the mechanism of fluoride sorption to calcite from batch experiments and surface complexation modeling with a developed set of intrinsic surface complexation constants for fluoride sorption on the calcite surface.

Chapter 4 contains the details of pH dependent fluoride removal by a granitic soil from Tsukuba, Japan, from batch experiments, surface copmplexation modeling, and spectroscopic studies. In the modeling approach, the general composite approach (Davis et al., 1998) is tested to find the suitability of the method in order to explain fluoride sorption in soil. FTIR spectroscopy is used to characterize the local structure of fluoride in the soil sample before and after sorption.

Chapter 5 describes the fluoride transport processes in a granitic soil column during sorption and desorption. Fluoride sorption and release are described with surface complexation constants optimized for soil. A combined physical and chemical non-equilibrium model is used to describe fluoride transport.

Chapter 6 summarizes the key findings from this research, environmental implications and recommendations for future research.

Chapter 2: Analytical Methods and Field observations

2.1. Analytical methods

This section contains the details of the analytical procedures used in this thesis for estimating physico-chemical parameter of water/soil leachate and soil analysis for physical, chemical, mineralogical and spectroscopic properties.

2.1.1. Water /soil leachate analysis

2.1.1.1. pH and electrical conductivity

pH was measured using an Horiba 9625-10D pH electrode connected to an Horiba D54 pHCond meter. Multipoint calibrations were done using pH 4, 7 and 10 commercial buffers (Kanto Chemicals). Electrical conductivity was measured using a Horiba 9382-10D conductivity electrode connected to the Horiba D 54 pHCond meter.

2.1.1.2. Major ion

Major cation (Ca^{2+}, Mg^{2+}, Na^+ and K^+) concentration and major anion (Cl^-, NO_3^-, SO_4^{2-} and F^-) concentration in the solution were measured using ion chromatography (IC) (Dionex DX120 IC) with Dionex IonPac Column, CS12A, 4×250 mm, and Dionex IonPac Column, AS12A, 4×250 mm, respectively. The eluent used for cation analysis is 0.02M methane sulphonic acid at a flow rate of 1.0 ml/min and that for anion analysis is 2.7mM Na_2CO_3 and 0.3mM $NaHCO_3$ at a flow rate of 1.5 ml/min.

2.1.1.3. Fluoride

The analytical methods for fluoride measurement in solution used in this thesis are: Ion Selective Electrode (ISE) method, IC method and colorimetric method. The details of these methods are described below.

2.1.1.3.1. Fluoride ISE

ISE method for fluoride analysis is widely used because these electrodes are relatively inexpensive, simple to use and have an extremely wide concentration range. Also, with careful use, and frequent calibration, an accuracy of $\pm$ 2 or 3% precision

levels can be achieved.

The Fluoride ISE method utilizes a fluoride selective membrane, which is typically a lanthanum fluoride crystal. When this membrane comes in contact with a solution containing fluoride ions, a potential develops across the membrane. This potential is then measured against an constant reference potential with a standard pH/mV meter. The potential depends on the level of free fluoride ions in the solution as described by a Nernstian equation as follows (equation 2.1):

$$E = E_0 - \frac{RT}{F} \ln[F^-] \qquad\qquad (2.1)$$

where: E : measured electrode potential (V), E_o: reference potential (a constant) (V), R: the gas constant (J mol^{-1} K^{-1}), T: the absolute temperature (K), F: the Faraday constant (C mol^{-1}) and $[F^-]$: the activity of fluoride in solution. The activity, $[F^-]$, represents the effective concentration of free fluoride ions in the solution.

This method is sensitive to solution pH. At low pH, the results could be underpredicted whereas, at high pH, the results could be overpredicted because of the formation of hydrofluoric acid and response of hydroxide ion to the ISE at respective pH. Hence, to adjust the pH to an optimum value of 5.0-5.5 and to provide constant ionic strength, a Total Ionic Strength Adjustment Buffer (TISAB) solution is typically added to both samples and standards.

The TISAB used in this study was prepared by adding 58.0 g of NaCl, 4.0 g of CDTA, 57.5 ml of acetic acid and sufficient amount of NaOH to 1.0L of solution so that the final pH is in the range of 5 to 5.5. A fluoride ISE (model 6561-10C, Horiba Ltd.) was used with a Horiba D53 pH/ORP/Ion meter to measure fluoride concentrations. The fluoride ISE was calibrated with known standard fluoride solutions until a slope of 56±2mV was achieved. Equal volume of TISAB was added to standards and solutions for calibration and fluoride measurement.

2.1.1.3.2. SPADNS method (colorimetric method)

Fluoride determination by SPADNS method is accepted by the US EPA and is equivalent to EPA's method 340.1 for drinking water and wastewater. Fluoride is colorless and it will not absorb any light wave in the UV-VIS range. In Hach SPADNS method, fluoride ions reacts with a red zirconium dye solution to form a colorless

complex, the concentration being approximate in proportion to the concentration of fluoride in water. The amount of fluoride concentration is determined by absorbance at 580 nm proportional to the bleached red color.

A DR/ 890 (Hach, USA) portable colorimeter with a fluoride detection limit of 0.05 mg/l was used in this study with SPADNS solution (Hach, USA).

2.1.1.3.3. IC method

IC method for fluoride determination is approved by USEPA (Method 300.0). The IC method for determining major anions using Dionex IonPac Column, AS12A, 4×250 mm with Na_2CO_3 and $NaHCO_3$ eluent can measure only the free fluoride, but, fluoride tends to be in complex form with Al^{3+}, Fe^{2+}, Fe^{3+}, and Ca^{2+} in presence of these ions under favorable pH conditions.

Dionex (ThermoScientific) developed a method for fluoride analysis by IC in presence of complexing ions without adding de-complexing agents. In this method, a KOH eluent was used. The total dissolved fluoride concentration in the solution can be calculated which includes all dissolved F species (e.g., F^-, HF, $AlF_n^{(3-n)}$) in the sample, which can be explained as follows:

For example, in the presence of aluminum, fluoride exists as:

$$Al^{3+} + F^- \rightarrow AlF^{2+} \tag{2.2}$$

$$Al^{2+} + 2F^- \rightarrow AlF_2^+ \tag{2.3}$$

In the presence of hydroxide ion during the IC analysis (because KOH was used as an eluent), the hydroxide ion can act as a competing ion, binding to aluminum, freeing fluoride (Lin et al., 2009):

$$Al^{3+} + 4OH^- \rightarrow Al(OH)_4^- \tag{2.4}$$

The column designed to be used with a KOH eluent is Dionex IonPac Column, AS18, 4×250 mm. This column is used in this study in IC (Dionex DX120) with an eluent of 23mM KOH and a flow rate of 1.0 ml/min.

2.1.1.4. Total elemental concentration

Total elemental concentration of Ca, Mg, Na, K, Al, and Fe were analyzed by an Inductively Coupled Plasma Mass Spectrometer (ICP-MS).

2.1.2. Soil analysis

2.1.2.1. Sample drying

The sample was dried in the oven at 106ºC for 24 hours, hereafter referred as oven dried sample, and the sample was dried at 30 ℃ - 35 ℃ in an oven for 3-7 days, hereafter referred to as air dry samples (Burt, 2004).

2.1.2.2. Grain size distribution

The oven dried sample was subjected to sieve analysis by using a nested column of sieves, with sieve diameter ranging from 2000µm to 75µm. A size distribution curve was generated by plotting sieve size vs % fine passing the sieve.

2.1.2.3. Soil particle density

Pycnometer was used to determine the particle density of soil by calculating the volume of the weighed soil accurately.

2.1.2.4. Elemental analysis

X-Ray Fluoroscence spectroscopy was used to quantify major oxides in the bulk soil by a wavelength dispersive Rigaku ZSX Primus II XRF spectrometer.

2.1.2.5. Mineralogy

The mineralogical compositions of the bulk (<2mm) sample was identified by X-ray powder diffraction (XRD). The sample was prepared by grinding by hand in mortar and pestle and then loaded to the specially designed sample cells. The sample was then analyzed with a Philips X'Pert diffractometer with graphite-monochromated Cu Kα radiation (40mV and 50 mA) with a scanning speed of 2°/min. The XRD pattern obtained was then viewed and the minerals were identified by matching to reference mineral patterns.

2.1.2.6. Clay mineral analysis

The clay fraction of the bulk sample was separated by adding a dispersant (sodium hexa meta phosphate) to the soil suspension and then allowing the suspension

to settle. The clay sample was then analyzed for clay minerals by XRD with a scanning speed of 1°/min. XRD pattern of the ethylene glycol-solvated clay sample was also collected in order to identify any expandable clay mineral.

2.1.2.7. *Spectroscopic analysis*

Fourier Transform Infrared (FTIR) Spectroscopy was used in this study. In order to obtain FTIR spectra, KBr pressed-disc technique was used for preparing the solid sample. About 0.7 mg of air dried sample was dispersed in 150 mg of KBr and the pellets were prepared. The infrared spectra were recorded on a Jasco FT/IR-670 Plus spectrometer in the region 4000-400 cm^{-1}.

2.1.2.8. *Surface area and pore size distribution*

The NOVA 2200e surface area and pore size analyzer (Quantachrome) was used to obtain the nitrogen adsorption/desorption isotherms for the bulk soil (oven dried) at standard 77 K in order to estimate the pore size and surface area of the sample. The applied relative pressure (p/p_0) ranged from 0.01 to 0.997. The soil samples were dried and degassed by using nitrogen gas as a carrier gas before the measurement. The Barrett–Joyner–Halenda (BJH) method was used to evaluate the pore size distribution from the adsorption isotherm. The Brunauer–Emmett–Tellers (BET) multilayer adsorption theory was used to deduce the internal specific area of pores. These methods were comprehensively discussed by Gregg and Sing (1982).

2.1.2.9. *Soil pH and EC*

Soil (<2mm, oven dried) pH was measured with a Sentix 81 pH electrode combined with a inoLab pH 7310 pH meter in 1:2 deionized water (pHw) and in 1:2 0.01M $CaCl_2$ (pHCaCl$_2$) suspension whereas, EC was measured only in 1:2 deionized water.

2.1.2.10. *Leachable ions*

Soil samples (<2mm, oven dried) were mixed with MilliQ water (Millipore), stirred for 15 mins and left overnight. The supernatant liquid was filtered with 0.45µm

syringe filter. Part of the filtrate was acidified to pH <2 with conc. nitric acid for cation and total elemental analysis. Both acidified and unacidified samples were refrigerated and analyzed for respective leachable ions by one of the methods described above in section 2.1.

2.1.2.11. *Total Al and Fe*

Total Al and Fe concentrations in the soil were measured by acid digestion following the USEPA method 3050B. This method dissolves the elements that could be environmentally available. In this method, the sample was digested with repeated addition of nitric acid and hydrogen peroxide (H_2O_2), the resultant digestate is diluted to a final volume of 100 ml and then analyzed by ICP-MS.

2.1.2.12. *Exchangeable Al*

Exchangeable Al in the soil was extracted from the soil sample (<2mm, oven dried) with 1.0N KCl (1:10). The supernatant liquid was filtered with 0.45μm syringe filter and acidified to pH <2 with conc. nitric acid for exchangeable Al analysis by ICP-MS.

2.1.2.13. *Total fluorine*

Total fluoride content in soil was estimated through NaOH fusion method as described by McQuaker and Gurney (1977). This method involves fusion of soil samples with 16 N NaOH at 600 °C, adjusting pH to 8–9, filtering and diluting to 100 ml volume and analyzing for fluoride by ISE (section 2.1.1.3.1). Total fluorine in some of the samples was also measured by X-Ray Fluoroscence spectroscopy.

2.1.2.14. *Soil Organic carbon*

Total soil organic carbon was analyzed by the dry combustion method using a CN corder.

2.2. Field Observations

Onsite investigations are necessary to provide objective data in support of the impact and process evaluation. Field investigations were conducted in India and Japan to access fluoride behavior in the soil-water system.

2.2.1. Onsite investigation for fluoride behavior in the soil-water system in India

India is one of the worst affected countries in terms of groundwater fluoride contamination (Handa, 1975). Andhra Pradesh, India, is one of the states in India, which is rippling under extreme groundwater fluoride contamination (Padhi and Muralidharan, 2012). The role of water harvesting tanks in Anantapur district, Andhra Pradesh, was studied by Padhi and Muralidharan (2012), and it was found that the soil leachable fluoride could play an important role in those areas. Hence, few of the water harvesting tanks, and one percolation tank, along with groundwater and surface water were studied to understand the fluoride vicious cycle in the Rangareddy district of Andhra Pradesh, India because this area is already known to be fluorosis endemic (Figure 2.1).

The geology of this area is mainly comprised of granitic and gnessic rocks. The soil types are mainly sandy loams or sandy clay and are red in color. The annual rainfall ranges from 516 mm in 2011 to 1110 mm in 2010 (CGWB, 2013). The major source of water for both domestic and agricultural use is groundwater. Water demand for irrigation is partly fulfilled by manmade water harvesting tanks. These tanks are much older and accumulate silt and clay with time.

Soil and surface water samples were collected from some of these tanks (Yacharam Percolation tank, Nalvelly tank, and Ibrahimpatnum tank) and groundwater samples from nearby areas in order to understand if fluoride leaching from these soils can contaminate the shallow groundwater.

Soil samples from three tanks up to a depth of 80 cm are collected and analyzed for volumetric water content, soil pH, electrical conductivity, water leachable fluoride, total fluorine, major oxides, trace elements, and mineralogy following standard procedure (Section 2.1.2). Surface water samples from three tanks are collected. Two groundwater samples were also collected. The samples were analyzed for

29

physico-chemical parameters, following standard procedures of sample analysis (Section 2.1.1).
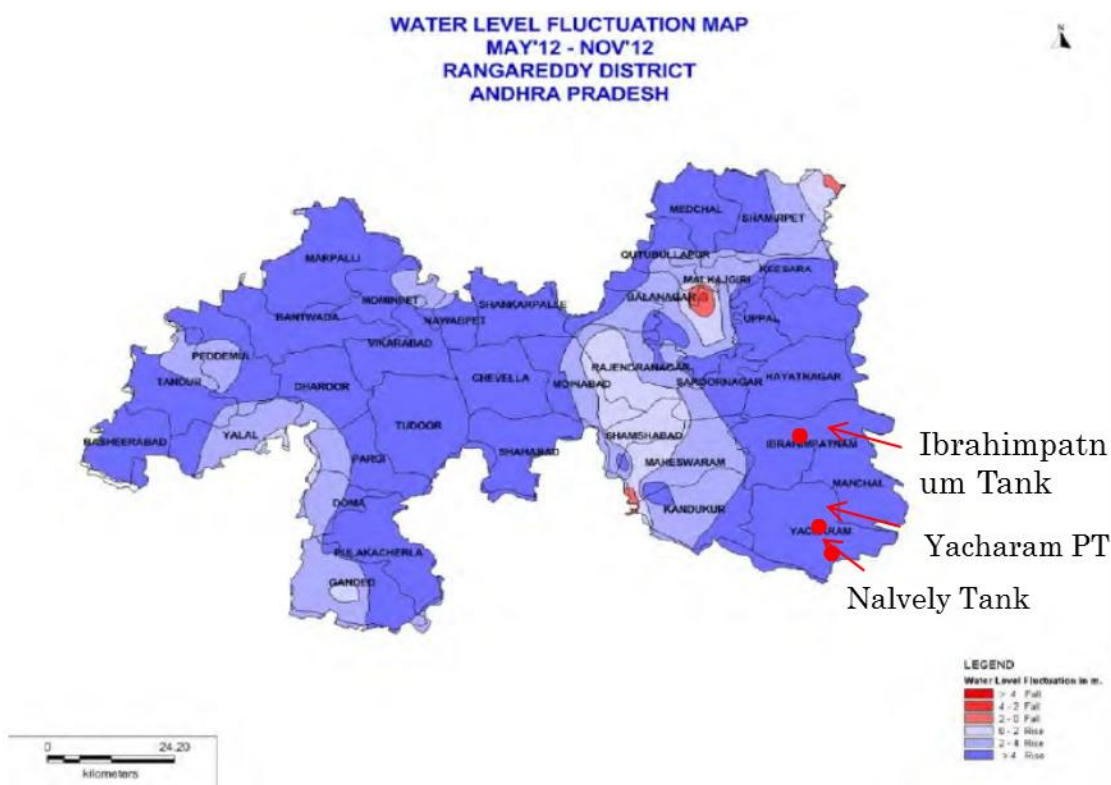
Figure 2.1: The water level fluctuation map for the year 2012, produced by CGWB, India (CGWB, 2012), showing locations of the tanks from where groundwater, surface water and soil samples were collected.

Figure 2.2 shows the soil pH (Figure 2.2(a)) and leachable fluoride (Figure 2.2(b)) for all the samples. The Yacharam samples are acidic to neutral in nature with small leachable fluoride whereas the Nalvelly and Ibrahimpatnum tanks were with high leachable fluoride and the soil were alkaline in nature.

The total fluorine contents of soil in all the three tanks are comparable (Table 2.1) whereas the leachable fluoride in the Nalvelly and Ibrahimpatnum tank were high. The alkaline nature of the tanks (soils S2 and S3, Table 2.1) might be responsible for high leachable fluoride concentration in these soils.
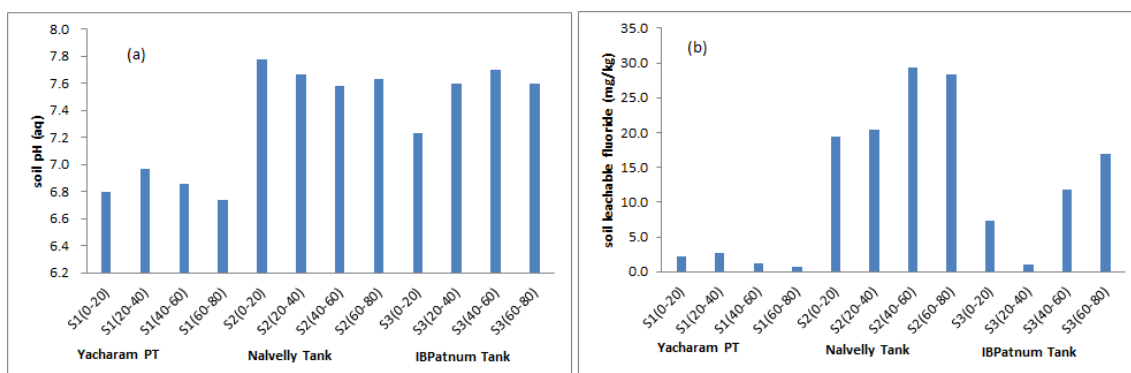
Figure 2.2: Soil analysis results. (a) soil pH with 1:1 deionized water and (b) leachable fluoride from soil.

Table 2.1: XRF elemental analysis results of Rangareddy soil samples

S.no.	[*]Site Name	SiO_2 (%)	Al_2O_3 (%)	Fe_2O_3 (%)	MgO (%)	CaO (%)	Na_2O (%)	K_2O (%)	Total fluorine(ppm)
1	S1(0-80)	53.6-54.2	5.3-5.5	3.1-3.5	2.27	1.6-1.7	1.6	9.3-9.6	884-1032
2	S2(0-80)	51.6-53.7	5.7-6.1	3.3-3.6	3.1-3.5	2.1-3.6	1.2-1.3	7.5-7.7	887-1153
3	S3(0-87)	54-58.8	6.3-7.0	3.7-4.1	3.4-3.9	3.2-3.9	0.9-1.0	6.3-6.9	830-1075

[*]Numbers in bracket indicate depth of soil sampling

2.2.2. *Onsite investigation for fluoride behavior in the soil-water system in Japan*

Groundwater fluoride contamination is reported in many parts of Japan, e.g., in Mizunami, Gifu (Abdelgawad et al., 2009), Nishinomiya, Hyogo (Sumikawa, 1990; Otsuka and Terrakado, 2003; Tsurumaki and Sakuramoto, 1985), and Kinki (Adachi et al., 1991). In Nakatsugawa, Japan, fluoride is proposed to be the carrier for rare earth minerals in soil (Murakami and Ishihara, 2008). However, fluoride mobility in soil was not understood in these fluoride contaminated areas. Hence, groundwater and soil samples from Nishinomiya and Nakatsugawa, Japan, were studied in order to understand the fluoride mobility in soil and factors affecting the retention and release of fluoride in soil.

Groundwater and soil samples (from outcrops) were collected from Naegi (Nakatsugawa), Gifu. Groundwater samples were also collected from Nishinomiya, Japan. The major rock types in the studied area in Naegi are younger Ryoke granites and

31

sedimentary rocks. The granites are sporadically overlain by the Quarternary clay sediments, which are derived from the reworked sediments of the weathered Naegi granites (Murakami and Ishihara, 2008). The clay rich layers have considerable amount of halloysite and kaolinite with minor quartz and lignite (Murakami and Ishihara, 2008). The results of soil and groundwater analysis are listed in Table 2.2 and are compared to that of the results in Rangareddy district, India and other fluoride contaminated areas.

Table 2.2: Study results from field survey

Env./geological parameters Region/Country	Geology	Avg. rainfall (mm/a)	Fluorine bearing minerals in soil	Total fluorine in soil (mg/kg)	Soil leachable fluoride (mg/kg)	Fluoride in groundwater (mg/l)	Reference
RR district, south India	Granites, gneisses	~783	-	830-1032	1.2-30	2.0-2.3	This study
Nishinomiya, Japan	Granites	~1456	-	-	0.3-5.4	2.08-2.4	This study
Nakatsugawa, Japan	Granites/ Clay sediments	~1830	Biotite, kaolinite	Not analyzed	not detected	-	This study
Anantapur District, India	Granites, gneisses	~560	Pink granites	200-460	8-15	2.6-6.5	Padhi and Muralidharan (2012)
Guangdong, China	Granites, limestone	~1336	Fe, Al rich soil	78-3130	-	Not analyzed	Zhu et al.,2007
Guangdong, China	-	~1500	-	186-387	0.7-2.7	Not analyzed	Fung et al., 1999
Hebei,China	Alluvial plain	~500	Biotite, hornblende and clay minerals	300-460	5.7-11.3	0.2-5.6	Jianhui, 1997
Tsukuba, Japan	Granites		Clay minerals	----	0.06	Not detected	This study

The results show interesting findings that in areas with heavy rainfall, the leachable fluoride is negligible where as in arid/semi-arid areas, the leachable fluoride is rather high suggesting the possible secondary enrichment of fluoride in the soil.

Groundwater in Tsukuba was found to be not fluoride contaminated. In spite of that, groundwater and soil samples from Tsukuba were collected and studied for possible fluoride sorption behavior in soil and leachability of fluoride from this soil because fluoride contamination of groundwater is often correlated to granitic terrains.

[1]Chapter 3: Surface complexation modeling of fluoride sorption onto calcite

3.1.Introduction

Calcite is an important constituent in geochemical systems such as arid land soils, subsurface materials, and aquifer sediments as well as coal combustion fly ash. Calcite has been treated not to be a major contributor to sorption (Neal et al., 1987; Borr'ero et al., 1988) although studies with natural materials containing calcite have implicated calcite as an important sorbent for cations and anions (Dudley etal., 1988; Goldberg and Glaudiberg, 1988a, 1988b). Furthermore, the interaction of fluoride with calcite can be important due to the fact that many water bodies with high fluoride contamination are found to be in equilibrium or saturated with respect to calcite (Handa, 1975). In addition, calcite and limestone have been used for fluoride removal from drinking water and waste water (Turner et al., 2005; Reardon and Wang, 2000). Therefore, it is necessary to better understand the mechanism of fluoride sorption on calcite.

A considerable amount of research has investigated the mechanism of fluoride removal by calcite using a variety of macroscopic and spectroscopic techniques. For example, fluorite (CaF_2) precipitation was considered to be the main mechanism for fluoride removal by calcite (Pickering, 1985; Reardon and Wang, 2000; Farrah et al., 1985; Yang et al., 1999) whereas Fan et al. (2003) found that fluoride uptake by calcite occurred by surface adsorption. Turner et al. (2005) extended the work by Fan et al. (2003) using crushed limestone and by considering high fluoride concentration where fluorite precipitation is known to occur, and concluded that fluoride was removed by a combination of surface adsorption and precipitation. Similarly, Nasr et al. (2014), in the presence of acetic acid, found that at low initial fluoride concentration (5 mg/l), fluoride was mainly removed by adsorption at calcite surface whereas at high fluoride concentration (50 mg/l), fluorite precipitation occurred. Calcite is found to adsorb divalent metals (Zachara, 1991), arsenate and arsenite (So etal., 2008) and phosphate

---

[1] Part of this Chapter is published in Journal of Environmental Chemical Engineering

(So et al., 2011), and the extent of adsorption depends on the solution chemistry in the corresponding studies.

The objective of the study in this chapter is to further investigate and elucidate the mechanism of fluoride sorption on calcite through a series of batch experiments. The initial fluoride concentration used in this study is equal to or below 7.5 mg/l, which is the equilibrium fluoride concentration considering fluorite dissolution to pure water and within the range of fluoride concentration observed naturally in groundwater except for a few areas where fluoride concentrations are quite high (Amini et al., 2008). For comparison, we also tested high fluoride concentration (10 mg/l). The sorption of fluoride on solid calcite ($CaCO_3(s)$) in equilibrium $CaCO_3$ (aq) suspensions was investigated in this study because little is known regarding the surface reaction of this ion on $CaCO_3$ (s). The surface complexation model (SCM) developed by Pokrovsky and Schott (2002) for calcite is extended to model the adsorption of fluoride in this study.

3.2. Theoretical background of fluoride removal by calcite from aqueous phase

3.2.1. *Fluorite precipitation*

Fluorite precipitation in a solution can occur when the solubility limit of fluorite is reached. The equilibrium fluoride concentration in pure water is 7.5 mg/l considering an equilibrium constant of fluorite (log $K_{fluorite}$) of -10.5 (at standard temperature and pressure), which is based on the thermodynamic database of Visual Minteq 3.0 (Gustafsson, 2012). A broad range of fluorite solubility, i.e., log $K_{fluorite}$ values ranging from -8.27 to -11.23, was reported from experimental measurements at 25 °C and 1atm pressure condition (Nordstrom and Jenne, 1977). Mineral saturation in aqueous solution in the Visual Minteq 3.0 is determined by saturation index (SI = log (IAP/K_{sp}); where IAP is the ion activity product and K_{sp} is the solubility constant) of the mineral. SIs are approximate indicators of equilibrium because of the uncertainty in the analytical measurements and in the thermodynamic constants used to calculate the equilibrium constants. The equilibrium formation constants for reactions relevant to the calcite-F^--Ca^{2+}-CO_3^{2-}-H^+ system used in this study were taken from the default database of Visual Minteq 3.0 (Gustafsson, 2012) (Table 3.1).

Table 3.1: **Equilibrium formation constants for reactions relevant to the calcite-F⁻- Ca²⁺- CO₃²⁻ - H⁺ system at 25ºC based on the thermodynamic database of Visual Minteq 3.0.**

Equilibrium reactions	logK
$H_2O = H^+ + OH^-$	-13.997
$Ca^{2+} + CO_3^{2-} + H^+ = CaHCO_3^+$	11.434
$Ca^{2+} + H_2O = CaOH^+ + H^+$	-12.697
$Ca^{2+} + CO_3^{2-} = CaCO_3 (aq)$	3.22
$CO_3^{2-} + 2H^+ = H_2CO_3 (aq)$	16.681
$CO_3^{2-} + H^+ = HCO3^-$	10.329
$Ca^{2+} + 2NO_3^- = Ca(NO_3)_2$	-4.5
$Ca^{2+} + NO_3^- = CaNO_3^+$	0.5
$K^+ + NO_3^- = K(NO_3) (aq)$	-0.19
$K^+ + H_2O = KOH (aq)$	-13.757
$H^+ + F^- = HF (aq)$	3.18
$H^+ + 2F^+ = HF_2^-$	3.78
$Ca^{2+} + F^+ = CaF^+$	1.14

The equilibrium fluoride concentration in a calcite-fluorite system depends on the Ca^{2+} concentration and pH of the solution which is explained by the following equations:

$$CaCO_{3(s)} + H^+ + 2F^- \Leftrightarrow CaF_{2(s)} + HCO_3^- \qquad (3.1)$$
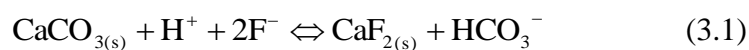
$$K_{cal.fluor} = \frac{^a\text{HCO}_3^-}{^a\text{H}^+ \times (^a\text{F}^-)^2} \qquad (3.2)$$

where $K_{cal.fluor}$ is the equilibrium constant for the calcite-fluorite system, $^a HCO_3^-$, $^a H^+$, and $^a F^-$ are the activities of HCO_3^-, H^+, and F^- in solution, respectively.

3.2.2. Adsorption of fluoride at calcite surface

Previous studies on fluoride removal by calcite in a system under the condition that fluorite precipitation should not occur showed that a considerable amount of fluoride was removed by calcite (Turner et al., 2005; Fan et al., 2003). Thus, adsorption of fluoride should be considered in addition to fluorite precipitation when the mechanism of fluoride removal by calcite is inferred.

Surface charge of calcite was believed to be influenced by HCO_3^-, OH^-, $CaOH^+$, and $CaHCO_3^+$ by some researchers (Somasundaran and Agar, 1967). While, the potential determining ions (PDIs) on the calcite surface are considered to be only Ca^{2+} and CO_3^{2-} with pCa = 4.4 (Foxall et al., 1979) (where pCa = -log[Ca]), which was further confirmed by steaming potential measurement (Thompson and Pownall, 1981). A pCa of 4.4 means that the surface exhibits positive charge at Ca concentrations above this value and negative charge at Ca concentrations below this value. Hence, calcite will have predominantly positive charge below pH 9.0 in saturated calcium carbonate solutions in contact with atmospheric $CO_2(g)$.

SCMs were widely used to investigate cation and anion adsorption at the metal oxides and calcite surfaces (So et al., 2008, 2011; Pokrovsky et al., 2004), and there exist different models, e.g., non-electrostatic, diffuse layer, constant capacitance, triple layer, and so on (Goldberg, 1992). A SCM explaining surface charge and dissolution kinetics of calcite was proposed by van Cappellen et al. (1993), which was further evaluated and refined by Pokrovsky et al. (2000) and Pokrovsky and Schott (2002). Successful applications of the refined model were found in literatures (So et al., 2008, 2011; Pokrovsky et al., 2004). Based on surface sensitive spectroscopic techniques, surface titration and electrokinetic study, SCMs for calcite dissolution were postulated which assumed two surface sites at calcite surface (van Cappellen et al., 1993), i.e., >Ca and >CO_3 with a 1:1 stoichiometry and each with a site density of 8.22 µmol/m^2

(Lakshtanov and Stipp, 2007). When exposed to aqueous solution, the species to be formed at the >Ca and >CO$_3$ sites are as follows: >CaOH$_2^+$, >CaOH^0, >CaO$^-$, >CaHCO$_3^0$, >CaCO$_3^-$, >CO$_3$Ca$^+$, >CO$_3$H^0, and >CO$_3^-$ (Pokrovsky et al., 2000). The reactions for the formation of these species along with the equilibrium formation constants were listed in Table 3.3.

Fluoride adsorption to both >Ca and >CO$_3$ sites was considered in this study. This was supported by the fact that fluoride sorption was found to occur on the entire calcite surface as observed by atomic force microscopy (Turner et al., 2005). Here, fluoride sorption at the >Ca and >CO$_3$ sites of calcite surface was set to be represented by the following reactions:

$$> CaCO_3^- + F^- = >CaF^0 + CO_3^{2-} \qquad (3.3),$$

$$> CO_3H^0 \quad + Ca^{2+} + F^- = >CO_3FCa^0 + H^+ \qquad (3.4)$$
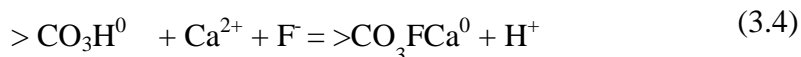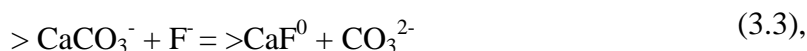
here, the choice of the reactions related to fluoride surface complexation formation was based on the analogy between aqueous and surface complex formation (reaction 3.3) and to explain pH dependency of our observed data (reaction 3.4). The details are discussed in the subsequent section (Section 3.4.4.2).

3.3. Materials and experimental procedures

3.3.1. Materials

All chemicals used in the experiments were reagent grade and used without further purification. Milli-Q water was used to prepare the solutions. Fluoride solutions were prepared by dissolving appropriate amount of analytical grade NaF (Wako Pure Chemicals Industries, Ltd.). The solution was diluted to get the desired fluoride concentration. Reagent-grade calcite (CaCO$_3$) was used throughout the study. The XRD patterns collected by a X-ray diffractometer using Cu Kβ radiation operated at 40 kV and 20 mA confirmed it to be pure calcite. The specific surface area was determined using a five-point N$_2$-BET method (NOVA station B) for the two lots of calcite used in this study, and was 0.199 m^2/g for the smaller fraction (180 µm) and 0.138 m^2/g for the larger fraction (700 µm), respectively.

3.3.2. Calcite equilibrated solutions

Calcite-equilibrated solutions at pH 6 were prepared following Plummer and Wigley (1976). Approximately 20 g/L of calcite (180 µm) was added to Milli-Q water in glass bottles. The solution was constantly stirred with a magnetic stirrer to keep all the particles in suspension. The solution temperature was kept constant at approximately 25°C. Commercial grade CO_2 was bubbled through the solution by controlling CO_2 pressure at 1 atm for a period of more than 24 hours until equilibrium is reached. pH and electrical conductivity of the solution were measured at regular intervals to ascertain the attainment of equilibrium. After equilibrium was reached, alkalinity and Ca^{2+} concentration of the solution were measured and were compared to the speciation results for calcite equilibrium solution calculated by Visual Minteq 3.0 (Gustafsson, 2012). The solution was then filtered and stored for use in batch experiments. The solutions at pH 7, 8, and 9 were prepared by adding 1M NaOH to the calcite equilibrated solution at pH 6. Solution at pH 5 was prepared by adding 0.2M H_2SO_4 to the calcite equilibrated solution at pH 6.

3.3.3. Analytical methods

The pH of the solutions was measured using a pH meter (D 54, Horiba Ltd.), calibrated using commercial solutions with pH 4.0, 7.0, and 10.0. Fluoride was measured with a fluoride ion selective electrode (ISE) (model 6561-10C, Horiba Ltd.). The fluoride ISE was calibrated with known standard fluoride solutions. Total Ionic Strength Adjustment Buffer (TISAB) was prepared by adding 58.0 g of NaCl, 4.0 g of CDTA, 57.5 ml of acetic acid and sufficient amount of NaOH to 1.0L of solution so that the final pH is in the range of 5 to 5.5. Equal volume of TISAB was added to solutions for fluoride measurement. Calcium concentrations in the calcite equilibrated solutions and solutions from selected sorption experiments were measured using ion chromatography.

3.3.4. Kinetic experiments

Firstly, kinetic experiments were conducted to quantify the dynamics of fluoride uptake by calcite and to select appropriate reaction times to be used for subsequent

equilibrium sorption experiments. No calcite equilibrated solution was used in these experiments. 0.25 g of calcite was put into 100 ml bottles, and 50 ml of 5 mg/l and 10 mg/l fluoride solutions were poured to these bottles. The experiments were conducted at ambient pH and the ionic strength of the solution was not controlled. For the first 1 hour, samples were collected at 10 minutes interval, then, samples were collected at 30 minutes interval for a total period of 12 hours. The samples were filtered with 0.45 μm filter paper and the fluoride concentration was measured. The amount of fluoride sorbed/precipitated was determined by mass calculation.

3.3.5. Batch experiments

A series of batch experiments was performed in clean, acid-washed, 100 ml polycarbonate screw-top bottles. Calcite equilibrated solutions were used in all the batch fluoride sorption experiments. Calcite, at solid-to-liquid ratios of 20 g/l was added to each bottle by measuring its mass using an analytical balance with an accuracy of 0.001 g. By considering a high solid to liquid ratio and exceeding the solubility limit of calcite, we can assume a constant surface area throughout the experiments. Aliquots of 50 mg/l fluoride solution were added to the batch test bottles to give the required final fluoride concentration ranging from 0.0 (blank) to 10 mg/l. The ionic strength of the solution was kept constant for each batch test at 0.07 M by adding 2.5M KNO_3 solution to the bottles. The bottles were then capped to avoid CO_2 exchange, thereby replicating the closed system conditions with respect to CO_2. The solutions were then agitated in a shaker water bath at 25°C at 180 rotations per minute for 12 hours because the results of sorption kinetic experiment suggested that equilibrium was reached within 12 hours (section 3.4.1). After the experiment, pH and EC of the solution were measured. The solution was filtered using 0.45 μm filter paper, and the fluoride concentration in the filtrate was measured by an fluoride ISE. Dissolved Ca^{2+} concentration in the filtrate was also measured in some selected samples.

3.3.6. Isotherms for fluoride removal

For obtaining data for isotherms, calcite equilibrated solutions with varying pH from 5 to 9 were used. The initial fluoride concentration was in between 2.5 and 10 mg/l

and the sorption period was 12 hours. The effect of grain size on fluoride removal was determined by varying calcite grain size from 180 μm to 700 μm for initial fluoride concentration of 5 mg/l. Also, the effect of ionic strength on fluoride uptake was tested at different ionic strengths of 0.05, 0.07 and 0.1M by adding appropriate amount of KNO_3 at an initial fluoride concentration of 5 mg/l.

3.4.Results and discussion

3.4.1. *Kinetics of fluoride removal by calcite*

During the early stage of the batch kinetic experiments, fluoride in solution was removed rapidly, then, the rate of removal was decreased, and the amount of removed fluoride remained constant in the case of the initial fluoride concentration of 10 mg/l (Figure 3.1). This temporal pattern of fluoride removal in our study was similar with the previous studies by Turner et al.(2005) and Fan et al.(2003), for fluoride sorption on calcite. In our experimental conditions, equilibrium was reached within 5 hours. Turner et al. (2005) reported a longer equilibrium time with a solution pH of 10. Their initial fluoride concentration and solid concentration were much higher than our study. An equilibrium time of 60 minutes was reported by Fan et al. (2003).

3.4.2. *Effect of the surface area*

Variation of fluoride removal as a function of calcite surface area with an initial fluoride concentration of 5 mg/l was shown in Figure 3.2. The amount of fluoride removed decreased with an increase in calcite grain size from 180 μm to 700μm because of the decrease of the surface area for sorption, which is expected considering fluoride removal by sorption. Turner et al. (2005) also observed decreased fluoride removal with increase in calcite grain size although the tested fluoride concentrations were high (700 mg/l and 2090 mg/l) and no calcite equilibrated solution was used in the experiments.
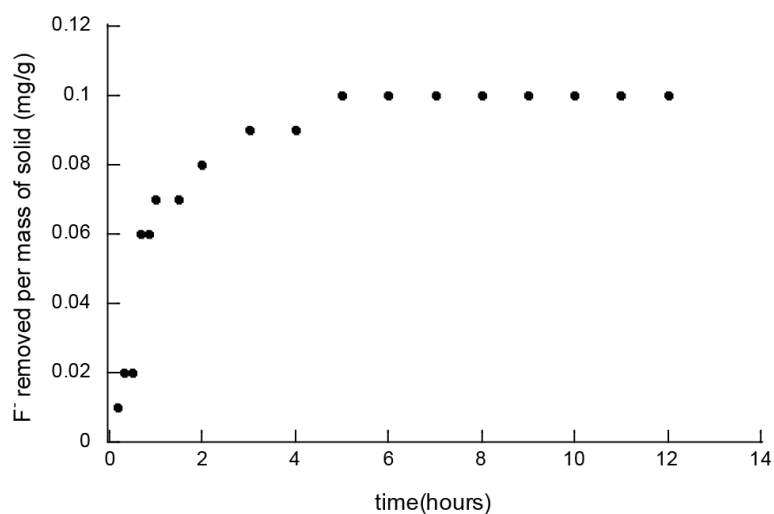
Figure 3.1: The amount of fluoride removed on calcite as a function of time. Initial fluoride concentration is 10 mg/l.

3.4.3. Effect of ionic strength and pH

Figure 3.3 showed the change of the amount of removed fluoride with respect to the concentration of the inert electrolyte. It showed that with an increase in ionic strength, fluoride removal decreased. Such behavior was attributed to outer sphere complexation (Hayes et al., 1988). However, to my knowledge, there has been no study which evidences for outer sphere complexation of fluoride on calcite. Ionic strength elevates the degree of aggregation, which in turn may influence adsorption (Chesne and Kim, 2014). In this study, I used relatively large calcite particles (180 µm), therefore, the effect of aggregation on sorption could be small. The observed effect of ionic strength on sorption has not yet been fully understood in our experimental conditions.

The effect of sorbate-to-sorbent ratio on sorption and precipitation was illustrated using sorption isotherms (Figure 3.4) where fluoride concentrations in solution were plotted against the fluoride removed from the solution per unit mass of calcite. The considered pH range was from 5 to 9 and the fluoride concentration was from 2.5 to 10 mg/l. The sorption isotherms could not be explained by Langmuir type of isotherm. The isotherms showed a convex shape. Removal of fluoride decreased as pH increased from 6 to 9, which is a typical behavior for anion adsorption observed in

many previous studies (So et al., 2008, 2011). Moreover, considering equation (3.1), fluorite precipitation is also dependent on the pH of the solution.
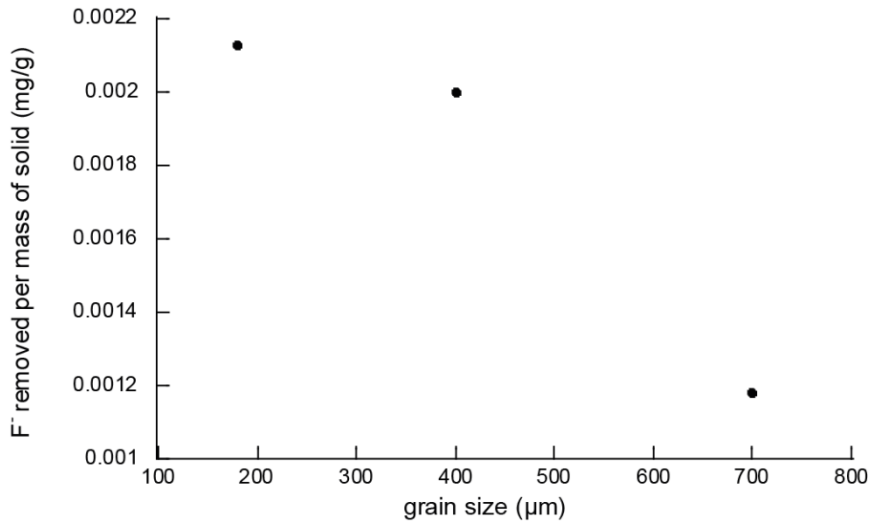
Figure 3.2: Effect of calcite surface area on fluoride removal at 5 mg/l initial fluoride concentration and pH 7.
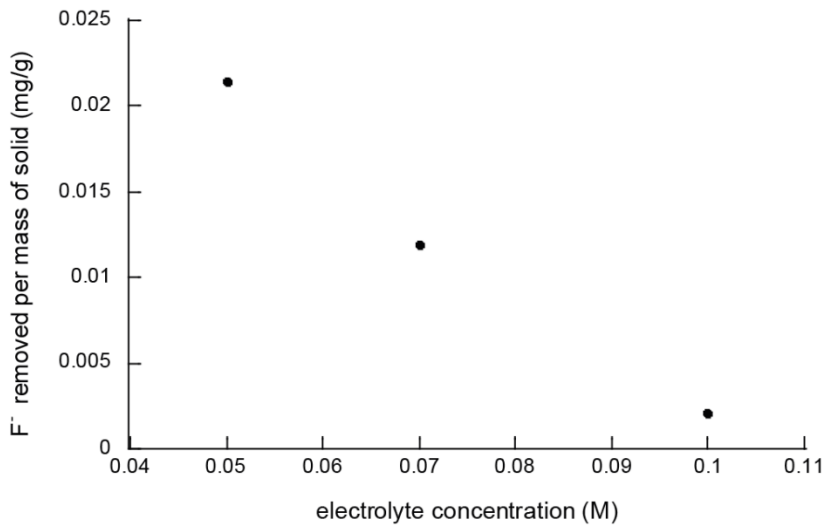
Figure 3.3: Effect of inert electrolyte on fluoride removal at 5 mg/l initial fluoride concentration and pH 7.
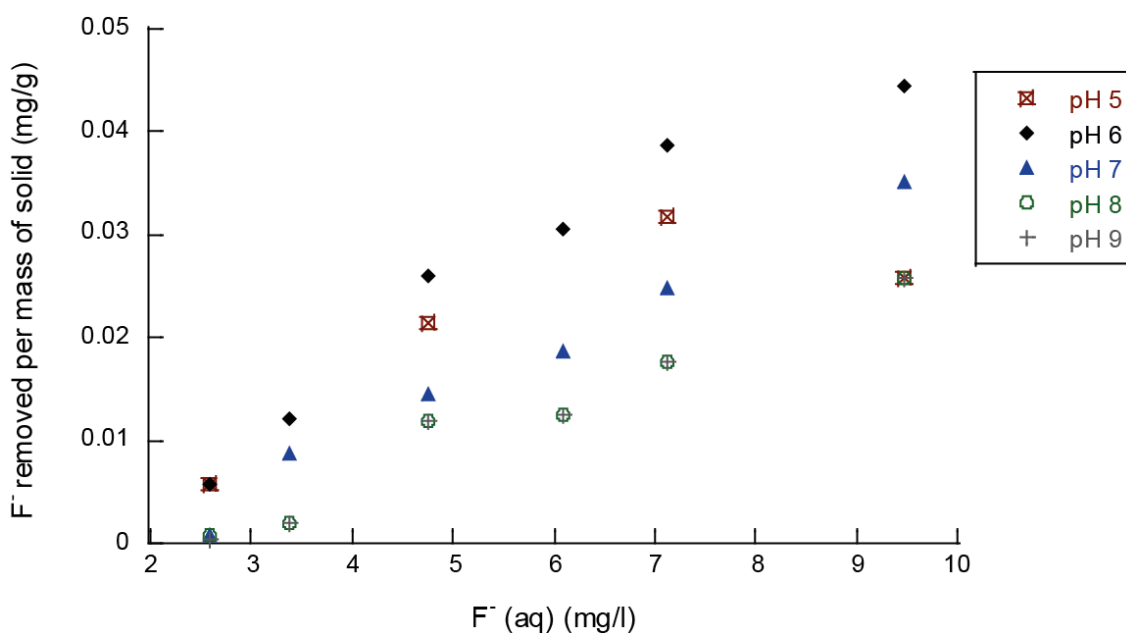
Figure 3.4: Fluoride removal as a function of pH for 2.5 to 10 mg/l initial fluoride concentration. Calcite equilibrated solution was used and the ionic strength was maintained at 0.07M. The error limit considered was 0.1 mg/l fluoride concentration in solution.

Hence, the pH dependency of fluoride removal could be explained by adsorption and precipitation or both. Similar kind of fluoride removal behavior by calcite was observed by Turner et al. (2005) under high initial fluoride concentration and high solid to liquid ratio where no calcite equilibrated solution was used.

The amount of fluoride removed at pH 5 was smaller compared with that at pH 6. This could be related to the less availability of calcite surface for sorption at pH 5 because of the possible calcite dissolution by addition of H_2SO_4 to obtain pH 5 solutions.

3.4.4. Modeling

In this study, Visual Minteq 3.0 (Gustafsson, 2012) was run in three different modes; first for the speciation and $SI_{fluorite}$ calculation of the initial solutions (mode 1), second for predicting pH dependency of fluoride removal by calcite without precipitation (mode 2), and third by allowing precipitation (mode 3). In all the calculations, the default thermodynamic database was used and the Davies equation

(Davies, 1962) was used to calculate the activity coefficients of the aqueous species (it is used for solutions with ionic strength up to 0.1M, Dzombak and Morel, 1990)

3.4.4.1.Aqueous speciation and fluorite saturation calculation

In our preliminary model run (mode 1), speciation calculations for the calcite - Ca^{2+} - CO_3^{2-}- H^+ - F^- system were conducted for all the experimentally conducted fluoride concentrations. The results showed that fluoride was largely dominated by F^- ion in the pH range of 6 to 10 whereas the amount of CaF^+ decreased with the increase in pH (Table 3.2).

Table 3.2: Fluoride speciation in the experimental solutions calculated using the default thermodynamic database of Visual Minteq 3.0 (Gustafsson, 2012) under the condition of 6.5 mg/l initial fluoride concentration.

pH	% of species		
	F-	CaF^+	HF(aq)
6	87.8	12.0	0.1
7	97.5	2.45	0.01
8	99.63	0.3	-
9	99.95	0.04	-
10	99.99	-	-

The $SI_{fluorite}$ for different initial fluoride concentration at a pH range of 6 to 10 was calculated and plotted in Figure 3.5. Fluorite saturation ($SI_{fluorite}>0$) was prominent in the systems with increasing initial fluoride concentration and decreasing pH.

We measured the pH of the solution after each sorption experiment. A mere increase in pH (0.1-0.9 unit) was observed for solutions with initial pH of 6 to 8

whereas no pH increase was observed for initial pH of 9, which might give another evidence for fluorite precipitation at low pH (equation (3.1)).
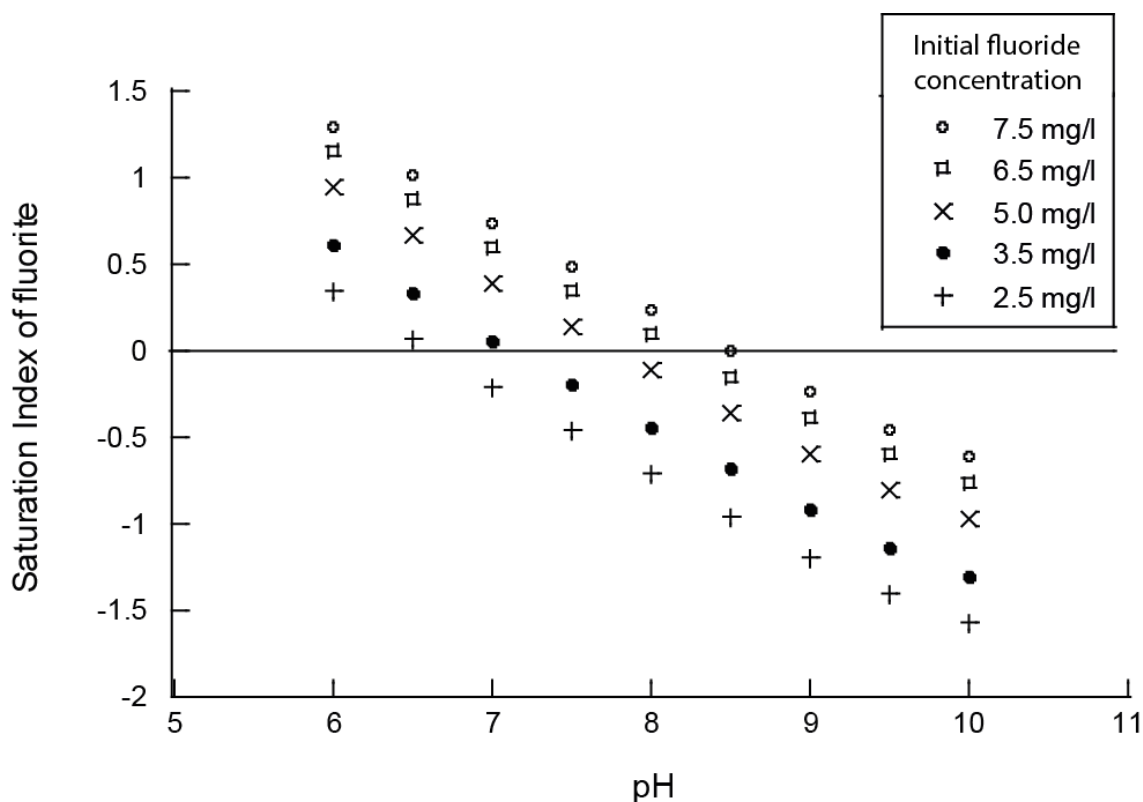
Figure 3.5: Saturation index of fluorite ($SI_{fluorite}$) as a function of pH for different initial fluoride concentration calculated by Visual Minteq 3.0 (Gustafsson, 2012). The SIs were calculated for the calcite - Ca^{2+} - CO_3^{2-} - H^+ - F^- system. The solid line shows the saturation index to be zero. Data of which $SI_{fluorite}$ were greater than 0.5 were not used for calculating the errors

3.4.4.2.Predictive simulations

3.4.4.2.1. Choice of surface complex reactions of fluoride

Surface complexation of fluoride in this study were represented by reactions (3.3) and (3.4) (section 3.2.2). Reaction (3.3) is based on the analogy between surface complexation reactions and solution equilibrium reactions. Although F^- is the major fluoride species in our initial solutions (Table 3.2), adsorption of CaF^+ was included in the model because it improved the model fit. In addition, in our experimental conditions, the pH of the solution after adsorption increased for initial pH of 6 to 8 (ca. 0.9 unit

with pH 6, ca. 0.7 unit with pH 7, and ca. 0.1 unit with pH 8 respectively) while no change in pH was observed for initial pH of 9. Hence, a pH dependent sorption reaction was required to be included in our model to explain the pH dependency of fluoride sorption (Figure 3.4) and pH change enhanced by sorption.

3.4.4.2.2. Parameter optimization

In this study, FITEQL version 4.0 (Herblin and Westall, 1999) was first used to estimate the expected ranges of the intrinsic surface complexation constants ($logK_{int}$) for fluoride sorption reactions. The fluoride sorption data for optimization were selected based on the values of $SI_{fluorite}$. The $SI_{fluorite}$ for some of our initial solutions was greater than zero at high initial fluoride concentration and low pH (Figure 3.5). Paces (1972) suggested that the equilibrium condition may be achieved in the SI range of 0.5 and -0.5. Here, we considered the sorption data with $SI_{fluorite}$ less than 0.5 units for the optimization.

The equilibrium formation constants for the calcite - Ca^{2+} - CO_3^{2-} - H^+ - F^- system (Table 3.1) and the surface complexation constants for calcite surface (Table 3.3) were used in the FITEQL program. A constant capacitance model (CCM) was used to fit the data and to optimize the reaction constants. CCM was chosen in this study because of its simplicity and requirement of less number of parameters. Also, this model successfully described the surface speciation of calcite and cation and anion adsorption at calcite surface (van Cappllen et al., 1993; So et al., 2008). The value of capacitance in the model was not varied; rather it was fixed at a value calculated using the formula $\kappa = I^{1/2}/\alpha$, where κ is the capacitance, α is an empirical parameter equal to 0.006 for calcite and I is the ionic strength (moles/l) (Pokrovsky et al., 2000). The obtained capacitance value was high, but consistent with previous studies using high capacitance values in order to describe divalent metal adsorption at calcite surface (Pokrovsky and Schott, 2002). The overall fit was assessed by an indicator of goodness of fit, i.e., the overall variance defined as Vy=SOS/DF, where SOS is the weighted sum of squares of the residuals and DF is the degrees of freedom. The fit was accepted to be good with values of Vy less than 20 (Herblin and Westall, 1999). The optimization program was run for each initial fluoride concentrations and the optimized $logK_{int}$s obtained ranged from -2.2

to -2.8 for reaction (3.3) and 1.55 to 1.8 for reaction (3.4), respectively. The calculated Vy values ranged from 0.23 to 1.09.

Table 3.3: Surface complexation reactions for surface speciation of calcite and fluoride sorption along with intrinsic surface complexation reactions ($logK_{int}$).

Surface complexation reactions	$logK_{int}$
$>CO_3H^0 = >CO_3^- + H^+$	-5.1[a]
$>CO_3H^0 + Ca^{2+} = >CO_3Ca^+ + H^+$	-1.7[a]
$>CaCO_3^- + H_2O = >CaOH_2^+ + CO_3^{2-}$	-5.25[a]
$>CaCO_3^- + HCO_3^- = >CaHCO_3^0 + CO_3^{2-}$	-3.929[a]
$>CaCO_3^- + F^- = >CaF^0 + CO_3^{-2-}$	-3.2[b]
$>CO_3H^0 + Ca^{2+} + F^- = >CO_3FCa^0 + H^+$	2.2[b]

[a] *Pokrovsky and Schott (2002)*

[b] optimized in this study

Next, to obtain the best $logK_{int}$ values which explain all the measured data, i.e., those obtained by different initial fluoride concentrations, we calculated averaged errors and constructed the contour map showing the errors with variable sets of $logK_{int}$s. The range of $logK_{int}$s considered in the forward modeling was selected based on the optimized $logK_{int}$s obtained by FITEQL 4.0.

The simulations were run in Visual Minteq 3.0 according to the second mode simulation, where precipitation was not included. The pH dependency of fluoride removal was modeled by using a CCM. The sorption database for calcite was created based on the calcite surface reactions and fluoride surface complex formation reactions (Table 3.3) because the database for calcite was not included in the software package. The standard procedure for creating the database was followed (Gustafsson, 2012). The model parameters, e.g., species concentrations (2.5 − 7.5 mg/l), inert electrolyte

concentration (0.07moles/l) and surface site density of 8.22µmoles/l were used in the model. Ca^{2+} and CO_3^{2-} concentrations were the equilibrium concentrations with respect to calcite at the corresponding pH. The ranges of $logK_{int}$ considered for surface complexation reactions are: -1 to -3.3 for reaction (3.3) and 1 to 3 for reaction (3.4).

Fluoride sorption at each pH was compared to the observed value. Then, the weighted mean square error (WMSE) normalized by the calculated value were calculated as follows:

$$WMSE = \frac{1}{n} \sum_{i=1}^{n} \left(\frac{x_i - y_i}{y_i} \right)^2 \qquad (3.5)$$

where n is the number of data points, x_i is the amount of adsorbed fluoride calculated by considering a particular set of $logK_{int}$ values for fluoride sorption at each pH and y_i is the amount of adsorbed fluoride observed in our experiment for fluoride concentrations of 2.5 mg/l, 5.0 mg/l, 6.5 mg/l and 7.5 mg/l at the corresponding pH.
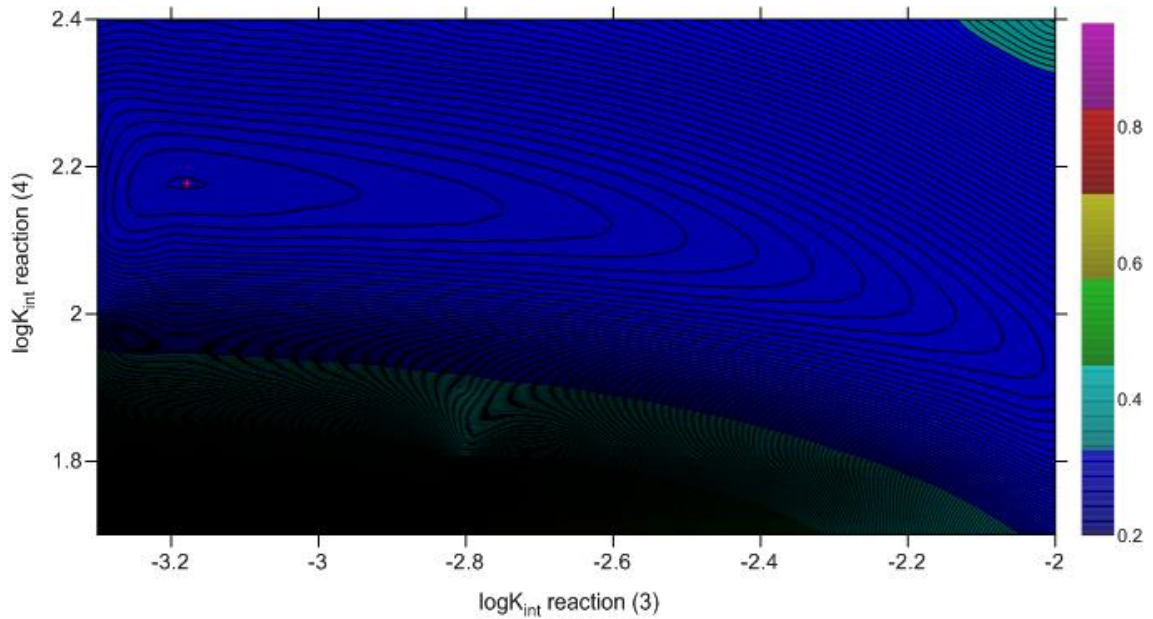
Figure 3.6: Contour map of the average error for initial fluoride concentrations of 2.5 mg/l, 5.0 mg/l, 6.5 mg/l and 7.5 mg/l by choosing different set of $logK_{int}$ values for reactions (3.3) and (3.4).

Observed data with $SI_{fluorite}$ greater than 0.5 were excluded from the error calculation. Figure 3.6 showed the contoured error map for the averaged error (-2 to -3.3 for reaction 3.3 and 1.7 to 2.4 for reaction 3.4) for initial fluoride concentrations of 2.5 mg/l, 5.0 mg/l, 6.5 mg/l and 7.5 mg/l. The averaged error data at other $logK_{int}$s were excluded from the plot because of high value of error. Equilibrium constant for reaction (3.4) was found to be better constrained than that of reaction (3.3) (Figure 3.6).

The $logK_{int}$ values corresponding to the minimum error range, i.e., -3.2 for reaction (3.3) and 2.198 for reaction (3.4) were considered for the subsequent model simulations.

Surface complex formation constants are often correlated with the equilibrium formation constants as evidenced from experimental analysis (Sigg and Stumm, 1981; Schindler et al., 1976). Van Cappellen et al. (1993) formulated the surface complexation reactions of Mn^{2+}, Fe^{2+} and Ca^{2+} at carbonate mineral surface by assuming an analogy between surface equilibria and complexation equilibria in solution. A close relation between formation constants at the surface and solution were observed. Pokrovsky and Schott (2002) derived the surface complex formation constants for carbonate minerals from correlations between surface and homogenous solution equilibria and further refined by fitting experimental electrokinetic data. In the calcite-fluoride system, the surface complex formation reaction (reaction (3.3)) is analogous to the equilibrium reaction in solution:

$$CaCO_3^- + F^- = CaF^+ + CO_3^{2-} \qquad (3.6)$$
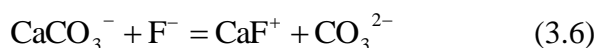
The equilibrium formation constant for reaction (3.6) was calculated to be -2.08 as per the thermodynamic database of Visual Minteq 3.0 (Gustafsson, 2012). The $logK_{int}$ for reaction (3.3) considered in this study was -3.2, and was close to the equilibrium formation constant for reaction (3.6), which might evidence for the reliability of the $logK_{int}$ for reaction (3.3).

3.4.4.2.3. Simulation of pH dependent fluoride removal without fluorite precipitation

The pH dependent fluoride removal according to second simulation mode, i.e., without allowing fluorite precipitation, was set in Visual Minteq 3.0 with $logK_{int}$ values of -3.2 for reaction (3.3) and 2.198 for reaction (3.4), respectively.
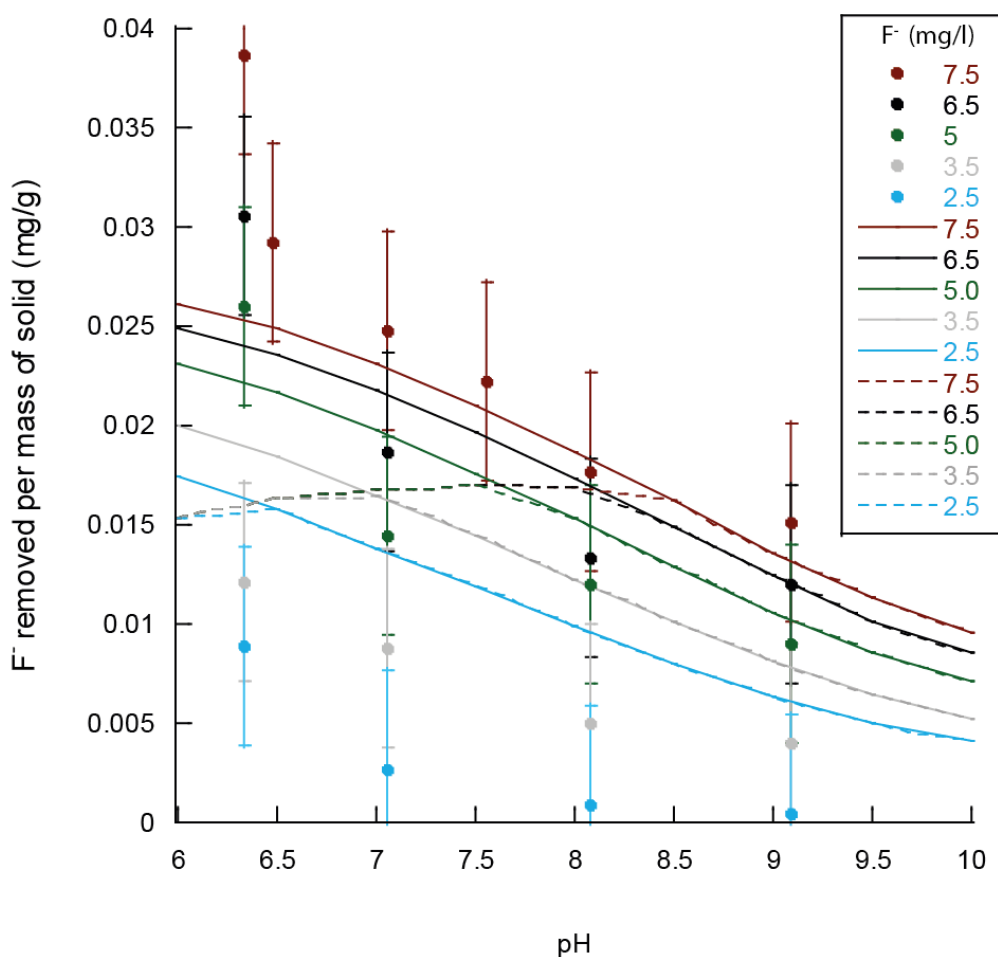
Figure 3.7: Fluoride sorption at varying pH for fluoride concentration from 2.5 mg/l to 7.5 mg/l. The points are measured results. The solid lines are the amount of fluoride removed calculated as per second simulation mode, and dashed lines the amount of fluoride adsorbed calculated as per third simulation mode at the corresponding fluoride concentration. The error bars are for an error estimate of 0.1 mg/l fluoride concentration in solution.

Figure 3.7 shows the results of model calculations along with the experimental data. The curved shape of the isotherm and pH dependency of fluoride removal was reproduced well by the model.

The model calculations for surface species in our experimental conditions for initial fluoride concentration of 6.5 mg/l were shown in Figure 3.8. Note that species distribution at only one concentration was shown here for clarity because the behavior of species distribution at other concentrations was similar.
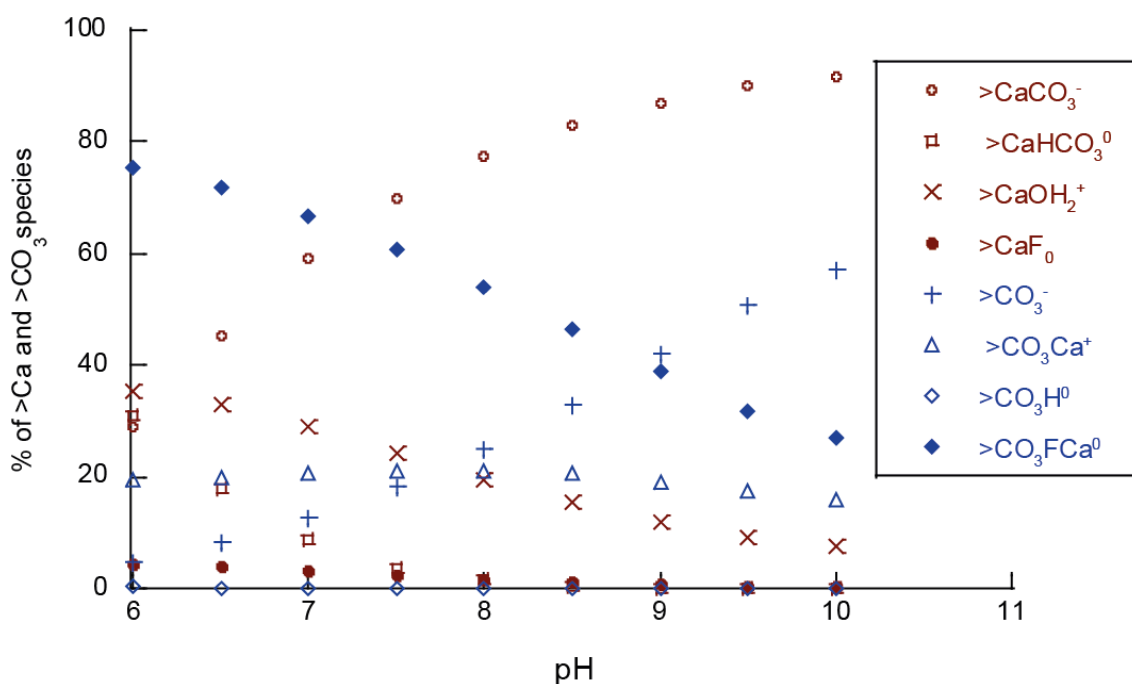
Figure 3.8: Surface species distribution in the calcite-fluoride system as a function of pH at 6.5 mg/l initial fluoride concentration.

In our experimental conditions, F^- was the dominant fluoride species. Thus, reaction (3.3) should be the controlling reaction for fluoride sorption. Considering the speciation of $>Ca$ site, the $>Ca$ site was largely dominated by $>CaCO_3^-$ species and concentration of $>CaCO_3^-$ increased with the increase in pH, thereby decreasing $>CaF^0$. Similarly, in the case where we consider only equation (3.4), fluoride sorption should increase with the increase in pH. However, with the increase in pH, the concentration of CaF^+ decreased remarkably (Table 3.2) and the $>CO_3^-$ species increased (Figure 3.8). In the pH range of 6 to 8, the $>CO_3$ site was represented by $>CO_3FCa^0$, $>CO_3Ca^+$, and $>CO_3^-$ species, whereas in the pH range from 8 to 10, the $>CO_3$ site was dominated by

>CO_3^- species (Figure 3.8). Overall, the combined effect of the surface complexation reactions for calcite surface speciation and fluoride adsorption (Table 3.3) explains the dependencies of pH and initial concentration on fluoride sorption at all pH ranges considered in our model.

Figure 3.7 showed that the offset between the measured data and the model results at pH 6 was larger. This could be explained as follows. The total number of surface sites at calcite surface is 8.22 µmol/m^2, by assuming 1:1 adsorption reaction, the total F$^-$ that could be removed by adsorption alone should be 8.22 µmol/m^2 or 0.031 mg/g. However, the amount of fluoride removed at pH 6 exceeded this value for 7.5 mg/l initial fluoride concentration. Also, the amount of fluoride removed at pH 6, i.e., 0.03 mg/g, with initial fluoride concentration of 6.5 mg/l, was close to this value. Thus, other processes such as precipitation should have played a role in addition to adsorption for these experimental conditions.

At fluoride concentrations when adsorption is the only possible mechanism, only small number of surface sites is accessible for fluoride sorption, which could be attributed to the heterogeneity of the chemical and structural properties of the surface, because reaction sites on the calcite surface are located in kinks and steps on corners, faces, or edges where the crystal ions, i.e., Ca and CO_3 are only partially coordinated (Plummer and Wigley, 1976).

Model calculations except at initial fluoride concentration of 7.5 mg/l over-predicted the data. However, considering an experimental error of 0.1 mg/l in removed fluoride concentrations, the difference between observed and modeled fluoride removal was small. Although there is a mismatch between the calculated adsorption isotherm and the data points, the model adequately described the main features of fluoride sorption including the pH dependency of fluoride sorption on calcite at different initial fluoride concentrations.

Fluoride adsorption in our kinetic adsorption experiments showed a rapid increase followed by a slow increase (Figure 3.1). Adsorption onto strong sites was tested in order to check if it can better explain the observed data. The optimization program did not converge by considering the strong sites. Moreover, by fixing the

number of strong sites (0.23 μmol/m^2) as reported by So et al.(2008), the model result did not improve. Hence, inclusion of strong sites was not considered in this study.

3.4.4.2.4. Model simulation including precipitation

The third mode of simulation includes pH dependent fluoride removal by surface complexation with fluorite precipitation. The simulated adsorbed fluoride amount is plotted along with the observed fluoride removed versus pH in Figure 3.7 as dashed lines. The total amount of fluoride removed by precipitation and adsorption is much larger than that of the total amount of fluoride removed in our experiment (Table 3.4). In the case where there is no fluorite precipitation, the model results were similar to the calculations from simulation mode 2 (Figure 3.7). The model in which precipitation was not allowed well reproduced the main features of the experimental results, although the observed data were slightly over predicted.

Allowing fluorite to precipitate (simulation mode 3) could not explain our data. However, fluorite super-saturation was observed in some of the samples. Surface precipitation is a continuum between surface complexation and bulk solid precipitation, where the surface phase composition varies continuously between that of the original solid and a pure phase precipitate of the sorbing ion (Farley et al., 1985), and surface precipitation occurs at the ion activities lower than those required for precipitation of pure phases. Hence, including surface precipitation in the model may explain the observed data. However, a generally applicable model with intrinsic sorption and surface precipitation constants for calcite is not available. Creating a database for fluoride sorption reactions on calcite including surface precipitation will be interesting to fully explain the observed data.

3.5. Conclusions

The removal of fluoride by calcite was investigated in this study. Under calcite equilibrium conditions, fluorite precipitation affects fluoride sorption at lower initial fluoride concentrations than that of the equilibrium fluoride concentration (7.5 mg/l) with pure water. Adsorption of fluoride decreases as pH increases. Ionic strength also influences fluoride adsorption. Fluoride removal was modeled with a constant

capacitance model with and without precipitation, and the intrinsic surface complexation constants for fluoride sorption were obtained by considering the weighted average minimum error between the observed and modeled sorbed fluoride concentrations. The mechanism of fluoride sorption on calcite was found to be

Table 3.4: The amount of fluorite precipitated and fluoride adsorbed at each pH for initial fluoride concentrations of 2.5 mg/l to 7.5 mg/l, calculated according to third simulation mode with including precipitation.

Amount of Fluorite precipitated in moles for initial fluoride concentrations (mg/l)

pH	7.5	6.5	5.0	3.5	2.5
6	1.45e-4	1.15e-4	7.90e-5	3.76e-5	1.37e-5
7	1.04e-4	7.37e-5	3.84e-5	0	0
8	3.68e-5	7.48e-6	0	0	0
9	0	0	0	0	0
10	0	0	0	0	0

Amount of Fluoride adsorbed in moles/l for initial fluoride concentrations (mg/l)

pH	7.5	6.5	5.0	3.5	2.5
6	1.61e-5	1.61e-5	1.61e-5	1.61e-5	1.61e-5
7	1.77e-5	1.77e-5	1.77e-5	1.74e-5	1.46e-5
8	1.78e-5	1.78e-5	1.61e-5	1.29e-5	1.04e-5
9	1.44e-5	1.30e-5	1.12e-5	8.52e-6	6.7e-6
10	1.00e-5	7.09e-6	7.51e-6	5.56e-6	4.29e-6

adsorption at low fluoride concentrations whereas precipitation plays a role at higher fluoride concentration and lower pH (Padhi and Tokunaga, 2015). Thus, in natural environments, adsorption of fluoride to calcite can influence the mobility of fluoride in soil under suitable conditions where calcite is abundant. Moreover, surface adsorption should also be considered in addition to precipitation in defluoridation methods, which use calcite or limestone as one of the defluoridating agents.

Calcite can be an important adsorbent phase for fluoride in calcareous geochemical systems. Although the number of sorption sites on calcite is less than sorption sites on iron oxides (Goethite -3.0 $*10^{-5}$ mol/m^2; $Fe_2O_3.H_2O(s)$ -1.6$*10^{-5}$ mol/m^2) or on aluminum oxides (α-Al_2O_3 -1.6$*10^{-5}$ mol/m^2), the maximum adsorption density of fluoride on calcite is quite comparable to that of on kaolinite (Weerasooriya, et al., 1998), although much lower to that of goethite or alumina. Thus, in spite of the fact that oxides and clays are expected to be the primary sorbents for fluoride in most situations, calcite may be an important sorbent in calcareous unconsolidated geologic material or limestone-dominated aquifer material.

Chapter 4: Experimental investigations of the mechanism of fluoride sorption in a granitic soil from Tsukuba

4.1. Introduction

In this chapter, fluoride uptake by a natural granitic soil from Tsukuba, Japan, was studied with a combination of macroscopic and spectroscopic techniques. Firstly, the sampling site information is provided. Then, the materials and methods used in the experiments and analysis are elaborated. Next, the theory of fluoride sorption on soil and the modeling approach follows. Finally, the results of experiment, analysis and simulation are interpreted and discussed in detail.

4.2. Sampling site

The sampling site is located near Tsukuba Shrine at the foot of the southern face of Tsukuba Mountain (Figure 4.1). The geology comprises mainly granite and the soil is
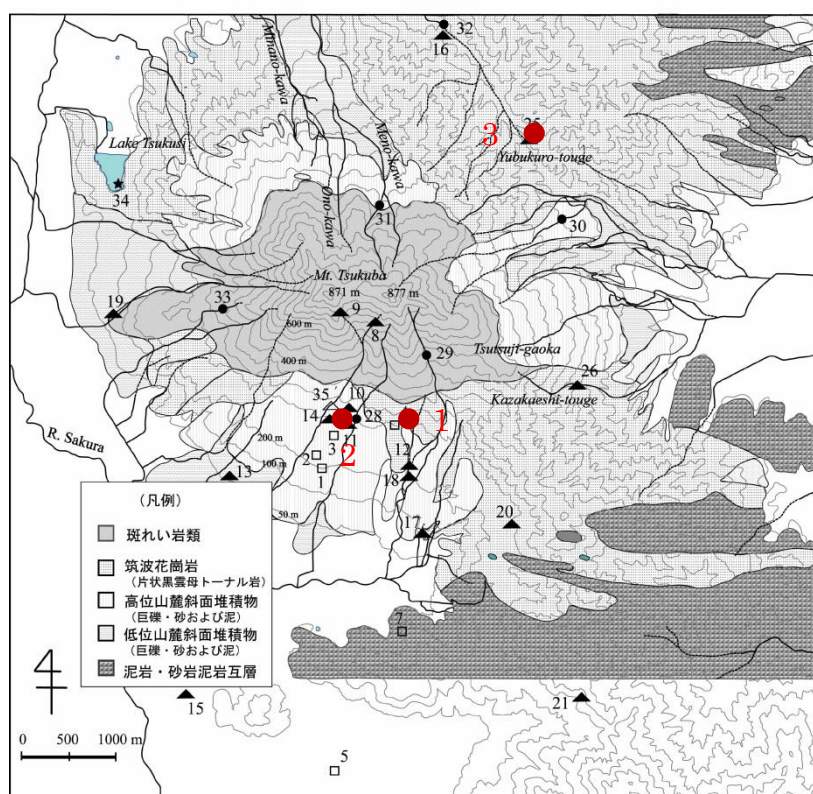
Figure 4.1. Location map of the groundwater, surface water and soil sampling sites modified from Yabusaki et al., (2007).

formed by weathering of the bed rock, and hence, granitic soil. Groundwater samples were collected from sampling sites 1 and 2 and surface water was collected from sampling site no. 3 (Figure 4.1). Soil samples were collected (care was taken to remove the soil organic matter, by removing the upper layer) from sampling sites 1 and 3 (Figure 4.1).Water samples were analyzed for pH and electrical conductivity on-site. These samples were then filtered with 0.45 μm syringe filter and collected in 50 ml acid washed polyethelene bottles for cation and anion analysis separately. Samples for cation analysis were acidified to pH less than 2. The samples were then transferred to the laboratory and stored at 4ºC until analysis. Total alkalinity of the samples was measured within 24 hours in unfiltered samples. Bulk soil samples were collected and characterized as described in Section 4.3. After analyzing the water and soil samples, an acidic granitic soil (sample no. 1, Figure 4.1) was selected for further analysis and to understand the mechanism of fluoride sorption and transport behavior of fluoride in soil (Chapter 5). Granitic soil from the site was chosen in this study to understand fluoride sorption behavior because groundwater and soil fluoride contamination is especially related to granitic terrain. This is because of the relative abundance of fluorine bearing minerals such as biotite, amphibole, apatite and fluorite in granites. Previous studies and field surveys (Section 2.2), also evidence the importance of granitic soil in relation to soil and groundwater fluoride contamination.

4.3. Materials and Methods

4.3.1. *Soil characterization*

The soil sample was oven dried and sieved through a 2 mm mesh prior to characterization and sorption studies. Air dried samples were used for mineralogical and spectroscopic studies. The physical properties of the soil such as soil particle density was determined by pycnometer method, and grain size was determined by sieve test.

Chemical properties of the oven dried sample were analyzed. The soil pH (1:2 aqueous solution and 0.01M $CaCl_2$ solution) was measured by a Sentix 81 pH electrode combined with a inoLab pH 7310 pH meter, leachable ions by IC, total Al and Fe by acid digestion followed by H_2O_2 oxidation, than, the digestate being analyzed by ICP-MS, total fluorine by NaOH fusion (McQuaker and Gurney, 1977), and total

organic carbon by dry combustion.

The mineralogical composition of the bulk soil sample (<2mm, air dried) was identified with XRD. The XRD patterns were also obtained for the clay fraction and ethylene glycol solvated clay fraction. The major oxides in the bulk sample were quantified by XRF.

The details of the analytical procedures followed for the above mentioned soil physical, chemical, mineralogical and elemental properties are discussed in Section 2.1 of Chapter 2.

A spreadsheet program MINSQ (Herrman and Berry, 2002) was used to semi-quantitatively estimate the mineral constituents of soil from mineralogical information and elemental data.

The FTIR spectra of the air dried bulk sample (< 2mm) was obtained with a Jasco FT/IR-670 Plus spectrometer in the region 4000-400 cm^{-1}.

The specific surface area, pore surface area and pore volume were determined by N_2 gas adsorption and desorption process using a surface area and pore size analyzer (NOVA 2200e, Quantachrome). The 10-point Brunauer, Emmett, Teller (BET) method was used to determine specific surface area (Brunauer et al., 1938). Pore area and pore volume was determined by the Barrett, Joyner, Halenda (BJH) adsorption method (Barrett et al., 1951). The t-plot was created from the adsorption/desorption data by plotting the quantity of gas adsorbed as a function of the calculated film thickness, to determine microporosity (Gregg and Sing, 1982). The statistical film thickness was calculated using the Harkins-Jura equation:

$$t\left(A^0\right) = \sqrt{\frac{13.99}{0.034 - \log\left(\dfrac{p}{p^0}\right)}} \qquad (4.1)$$

where, $t(A^o)$ is the statistical film thickness and P/P^0 is the relative pressure.

Micropores and micropore volumes were determined from the curve fits to the linear portion of the plot (Gregg and Sing, 1982; Leofanti et al., 1998; Hay et al., 2011, Craig et al., 2015).

4.3.2. Model approach and data evaluation

4.3.2.1. Isotherm model

The performance of a sorption system can be assessed based on the sorption isotherms. Isotherms deal with the relationship between the activity or equilibrium amount of ion concentration on the solution and on the adsorbent. Langmuir and Freundlich isotherms are the most commonly used nonlinear sorption models (Sparks, 2003). Another isotherm model that is frequently used to determine the possible adsorption mechanism is the Dubinin–Radushkevick (D-R) equation (Romero-Gongalez et al., 2005).

The Langmuir isotherm model assumes that adsorption sites are energetically the same with monolayer formation and independent of surface coverage (Langmuir, 1918), whereas the Freundlich isotherm model proposes a monolayer sorption with a heterogeneous energetic distribution of active sites, accompanied by interaction between adsorbed molecules (Freundlich, 1906).

These isotherm equations can be easily transformed to their respective linear forms, so that the adjustable parameters can be calculated by linear regression.

The Langmuir isotherm is generally expressed as:

$$q_e = \frac{q_m b C_e}{1 + b C_e}, \qquad\qquad (4.2)$$

which can be linearized in many different ways. The commonly used linearized form is:

$$\frac{1}{q_e} = \left(\frac{1}{b q_m}\right)\frac{1}{C_e} + \frac{1}{q_m} \qquad\qquad (4.3)$$

where, C_e is the equilibrium fluoride concentration (mg l^{-1}) in solution, q_e is the equilibrium amount of fluoride sorbed on the sorbent (mg g^{-1}), and q_m (mg g^{-1}) and b (l mg^{-1}) are the Langmuir isotherm constants related to the capacity and the energy, respectively.

Plotting $\dfrac{1}{q_e}$ vs $\dfrac{1}{C_e}$ gives a straight line. q_m and b can be calculated from the slope and intercept respectively.

The Freundlich isotherm is written as:

$$q_e = K_f C_e^{1/nF}, \qquad\qquad (4.4)$$

The linear form of which is as follows:

$$\log(q_e) = \log(K_f) + \frac{1}{nF}\log(C_e) \qquad\qquad (4.5)$$

K_f (l g^{-1}) and $1/n_F$ are Freundlich constants that can be obtained by plotting, $\log(q_e)\, vs\, \log(C_e)$ where these constants signify the capacity and the intensity of sorption respectively.

The D-R isotherm and its linearized form are presented in equations 4.6 and 4.7 respectively.

$$\frac{q_e}{q_m} = \exp\left(-K_E\left(RT\ln\left(1+\frac{1}{C_e}\right)\right)^2\right) \qquad\qquad (4.6) \text{ and}$$

$$\ln q_e = \ln q_m - K_E \varepsilon^{0^2} \qquad\qquad (4.7)$$

where ϵ^{0} is the Polanyi potential, q_m is the monolayer capacity (mg g^{-1}), and K_E is the constant related to sorption energy (mol^2 K J^{-2}). The parameters q_m and K_E can be obtained from the intercept and slope of the linear plot ($\ln q_e\, vs\, \varepsilon^{0^2}$). The D-R equation has the advantage that the mean free energy of sorption, E, can be calculated as:

$$E = (-2K_E)^{-1/2} \qquad\qquad (4.8)$$

4.3.2.2. Surface complexation model

The necessary aspects of developing a SCM are to determine the total number of surface sites, to define the mass action and mass balance equations that describe the equilibria of surface reactions, to determine the conditional equilibrium constants for surface species, and to develop an approach to quantify the Coulombic correction factors (Davis et al., 1998). The SCM development in this study is as follows.

4.3.2.2.1. Total surface site density determination for natural soil

Total site density determination of single mineral phases can be achieved by a variety of methods (Davis and Kent, 1990). For complex mineral assemblage, the most used method is determining the reactive specific surface area of the assemblage, and

then calculating the total reactive surface area from the recommended site density which is 2.31 sites/nm^2 (Davis and Kent, 1990). According to Davis and Kent (1990), the actual site density may vary from 1 to 7 sites/nm^2, however, to encourage the development of a self-consistent thermodynamic database that can be applied easily to soils and sediments, it is important to select one value. The chosen value of 2.31 sites/nm^2 closely approximates the site densities found by adsorption on various minerals and the edge sites of clay minerals.

4.3.2.2.2. Surface complexation reactions

Both constant capacitance model (Stumm et al., 1980) and the generalized two-layer model (Dzombak and Morel, 1990) were fit to the fluoride sorption data in this study, which consider only inner surface complexes. Considering SOH as a functional group of oxide minerals from the clay particle of soil fraction (>SOH), protonation and deprotonation reactions of >SOH are defined as:

$$> SOH + H^+ \Leftrightarrow > SOH_2^+ \qquad\qquad (4.9)$$

$$> SOH \Leftrightarrow > SO^- + H^+ \qquad\qquad (4.10)$$

The surface complexation reactions for fluoride sorption considered in this study are presented in Equations 4.11 to 4.14. These reactions were chosen based on the study by Hao and Huang (1986) for fluoride sorption onto hydrous alumina.

$$> SOH + F^- + H^+ \Leftrightarrow > SF + H_2O \qquad\qquad (4.11)$$

$$> SOH + F^- \Leftrightarrow > SOHF^- \qquad\qquad (4.12)$$

$$> SOH + 2F^- + H^+ \Leftrightarrow > SF_2^- + H_2O \qquad\qquad (4.13)$$

$$> SOH_2^+ + F^- \Leftrightarrow > SF + H_2O \qquad\qquad (4.14)$$
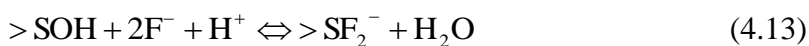
The intrinsic equilibrium constants considered for the aforementioned reactions (Equation 4.11 to 4.14) are represented by equations4.15 to 4.18 respectively.

$$K_F^1(\text{int}) = \frac{[\text{SF}]}{[\text{SOH}]\,[\text{F}^-]\,[\text{H}^+]} \tag{4.15}$$

$$K_F^2(\text{int}) = \frac{[\text{SOHF}^-]}{[\text{SOH}]\,[\text{F}^-]}\exp\left[-F\psi_0/RT\right] \tag{4.16}$$

$$K_F^3(\text{int}) = \frac{[\text{SF}_2^-]}{[\text{SOH}]\,[\text{F}^-]^2\,[\text{H}^+]}\exp\left[-F\psi_0/RT\right] \tag{4.17}$$

$$K_F^4(\text{int}) = \frac{[\text{SF}]}{[\text{SOH}_2^+]\,[\text{F}^-]} \tag{4.18}$$

where F: Faraday constant (C mol^{-1}), R: molar gas constant (J mol^{-1} K^{-1}), int: intrinsic, T: absolute temperature (K), square brackets: concentrations (mol L^{-1}).

The mass balances of the surface functional group >SOH considering the fluoride sorption reactions (Equations 4.11 to 4.14) is

$$[SOH]_T = [SOH] + [SOH_2^+] + [SO^-] + [SF] + [SOHF^-] + [SF_2^-] + [SF] \tag{4.19}$$

The charge balance expression is written as:

$$\sigma_d = [\text{SOH}_2^+] - [\text{SO}^-] - [\text{SOHF}^-] - [\text{SF}_2^-] \tag{4.20}$$

where σ_d is the surface charge (mol L^{-1}).

4.3.2.2.3. Parameter optimization

First, the computer program FITEQL version 4.0 (Herblin and Westall, 1999) was used to fit surface complexation constants to the experimental adsorption data. This program uses a nonlinear least squares optimization routine to fit equilibrium constants to experimental data. The goodness of fit was accessed by WSOS/DF (weighted sum of squares divided by degrees of freedom). When insufficient data were available to extract a surface-complexation constant for a reaction in FITEQL 4.0, or when convergence problems were experienced with FITEQL 4.0 for other reasons, manual adjustments of surface-complexation constants was performed using Visual Minteq (3.0) (Gustafsson, 2012). This kind of methodology was followed in other studies to fit the surface complexation constants, e.g., by Karamalidis and Dzombak (2010).

Next, the software PEST (Doherty, 2004) by coupling with PHREEQC (Parkhrust and Appello, 1999), was used to estimate the surface/sorption constants and the site density parameter from the experimental data. PEST is commonly used with groundwater flow and transport modeling (Doherty, 2004), and coupling PHREEQC with PEST to optimize surface complexation constants has been reported (Appelo et al. 2002; Bachmaf and Merkel, 2011; So et al., 2008). The advantage of using PHREEQC-PEST approach over other codes such as FITEQL 4.0 is that any number and type of parameters can be optimized as long as the number of parameters to be estimated is less or equal to the number of observations.

4.3.3. Adsorption experiments

All chemicals used in the adsorption experiments and soil characterization were reagent grade and used without further purification. Milli-Q water was used to prepare the solutions. Fluoride solutions were prepared by dissolving appropriate amount of analytical grade NaF (Wako Pure Chemicals Industries, Ltd.). The desired fluoride concentration solutions were prepared from the stock solution by dilution. The soil sample used in the batch experiments were the sieved samples to less than 250 µm, unless otherwise stated. The batch experiments were conducted in clean, acid washed polyethylene bottles and the temperature was kept constant at 25°C (+/- 0.5ºC). The shaker bath used to keep the temperature constant and to agitate the samples was set to a agitation speed of 60 rotations per minute (+/-2 rpm).

4.3.3.1. Kinetic uptake experiments

In order to characterize fluoride uptake by soil, kinetic experiments were conducted at a total fluoride concentration of 5 mg/l and solid concentration of 5 g/l. 0.25g of soil was weighed to the bottles and 50 ml of 5 mg/l fluoride solution was added to it. The initial pH of the solution was measured. The bottles were than capped and placed in a shaker water bath. Samples were collected at regular intervals (10, 20, 30 minutes, 1, 1.5, 2, 3, 4, 5, 6, 7, 9, 12, 18, 24, and 30 hours) over a total reaction time of 30 hours. Blank sample with deionized water was run to ensure fluoride release from soil. The pH of the solution after the experiment was measured immediately. The

solution was filtered using 0.45 µm syringe filter, and the fluoride concentration in the filtrate was measured. Amount of sorbed fluoride was calculated from the initial fluoride concentration and the amount of fluoride in solution.

4.3.3.2. Sorption isotherm

Fluoride sorption isotherms were obtained to characterize fluoride uptake by soil as a function of initial fluoride concentration at a pH range of 4 to 9. 0.5g of soil was weighed to the bottles. 0.5 ml of deionized water was added to it, the bottles were than capped and left overnight for soils to equilibrate with the solution. Appropriate amount of 100 mg/l fluoride solution was added in order to produce a total fluoride concentration ranging from 2.5 to 10 mg/l in 50 ml solution. The ionic strength of the solution was kept constant by adding 2.5M KNO_3 solution. The pH of the solution was measured and adjusted by adding 0.01M KOH or 0.01M HNO_3. The total volume was adjusted to 50 ml, and the bottles were capped and placed in the shaker bath for 24 hours. After the experiment was finished, the solutions were measured for pH, than filtered with 0.45µm syringe filter and measured for fluoride concentration in solution. The concentration of adsorbed fluoride was calculated as the difference between amount added and the amount remaining in solution after equilibrium.

4.3.3.3. Adsorption at various ionic strength, solid to solution ratio and grain size

The effect of soil mass loading on fluoride sorption was investigated by varying the solid to solution ratio from 5 g/l to 30 g/l. Fluoride adsorption on soil was also tested at various ionic strengths (e.g., 0 (no electrolyte addition), 0.01, 0.001 M) and different grain size (e.g. >425µm, >250µm, >106µm and <106µm). The experimental procedure and reaction time were the same as that described for the batch pH dependent isotherm experiments.

4.3.4. Analytical methods

The pH of the solutions was measured using an Horiba model pH meter and sensor, calibrated using commercial pH 4.0, 7.0, and 10.0 buffers. Filtered solutions from sorption experiments were analyzed for major anions including fluoride by IC

(Dionex DX120, with Dionex IonPac Column, AS18, 4×250 mm) with an eluent of 23mM KOH and a flow rate of 1 ml/min (Section 2.1.1.3.3. of Chapter 2). However, barring the filtrates from the kinetic experiment and the experiments where the electrolyte is not added, the IC results were erroneous because of high concentration of NO_3^-, as dissolved KNO_3 salts were used as a background electrolyte in the experiments. Hence, the samples were reanalyzed for fluoride with the SPADNS method with a Hach 890 colorimeter (Section 2.1.1.3.2. of Chapter 2). The samples were also analyzed for total metal concentrations by ICP-MS (Section 2.1.1.4. of Chapter 2).

4.4. Results

4.4.1. Physical and chemical properties of soil

4.4.1.1. Physical characteristics

The N_2 gas adsorption/desorption isotherms were used to calculate the surface area of the dried (< 2mm) sample and for the sample after fluoride sorption for sufficient long time (the procedure for obtaining this sample is described in Chapter 5, from the fluoride transport experiment during fluoride sorption) by BET method and pore area and pore volume by the BJH method (Table 4.1).

Table 4.1. The BET surface area, BET c parameter, BJH cumulative pore area and volume using adsorption curve, and the t-plot surface area and micropore volume

Parameter	value	
	Tsukuba sample (<2mm) oven dried	fluoride sorbed Tsukuba sample (<2mm) oven dried
Surface area (m^2/g) (BET)	7.6	5.7
BET c parameter	167	162
Pore area (m^2/g) (BJH)	4.7	3.6
Pore volume (cm^3/g) (BJH)	0.02	0.018
Surface area (m^2/g) (t-plot)	7.18	5.52
Micropore volume (cm^3/g) (t-plot)	$5.4*10^{-4}$	$2.5*10^{-4}$

The adsorption/desorption results for both the samples before and after fluoride sorption show a type IV isotherm with an H3-type hysteresis loop (Figure 4.2 (a) and (b)) (Leofanti et al., 1998; Sing, 1989, Hay et al., 2011, Craig et al., 2015). The BET c parameter was 167 and 162 for samples before and adsorption, respectively, suggesting mesopore dominated samples (Davis and Kent, 1990). The BJH method was also applied to determine the pore area and pore volume, as it is widely used. However, the
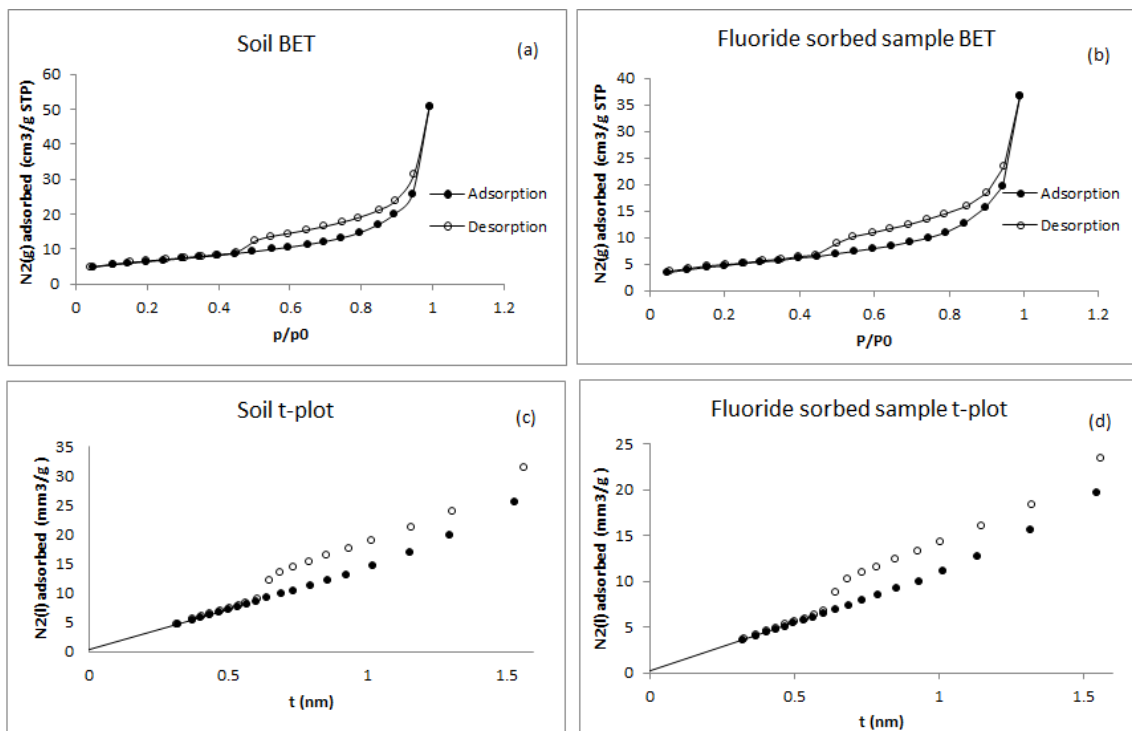
Figure 4.2: BET plot for N_2 gas adsorption and desorption isotherm for (a) the Tsukuba soil (<2mm, oven dried) and (b) fluoride sorbed Tsukuba soil (<2mm, oven dried). The t-plot for Tsukuba soil is represented in (c) and that for fluoride sorbed soil is represented in (d). The lines in the t-plots represent the linear fit to the adsorption data at p/p_0 0.04 to 0.3. In all the plots, solid symbols represent N_2 gas adsorption data and open symbols represent N_2 gas desorption data.

results of BJH analysis are highly unreliable for type IV isotherms with an H3 hysteresis loop (Gregg and Sing, 1982). The t-plot method is quite often used to determine the presence of micropores. The *t*-plots produced using the N_2 adsorption and

desorption isotherms are shown in Figure 4.2 (c) for the soil before sorption experiment and Figure 4.2 (d) for the sample after fluoride sorption. The linear fit for the lowest part of the curve (0.3 to 0.5 nm) (Figure 4.2 (c) and (d)) was used to calculate the surface area from the slope and micropore volume from the intercept (Davis and Kent, 1990). The t-plot surface area is almost equal to the surface area calculated by BET method (Table 4.1). The adsorption and desorption isotherms yield very similar fits in this range and indicate <0.6 nm pore volumes of 0.54 and 0.25 mm^3/g for the samples before and after fluoride sorption, respectively.

4.4.1.2. Grain size distribution

Grain size of the sorbing material is an important parameter considering sorption processes because of change in physical properties and available area for sorption. Figure 4.3 shows particle size distribution for the Tsukuba bulk soil. The distribution of different grains in the sample is also listed in Table 4.2. The soil is largely dominated by larger grain particles.
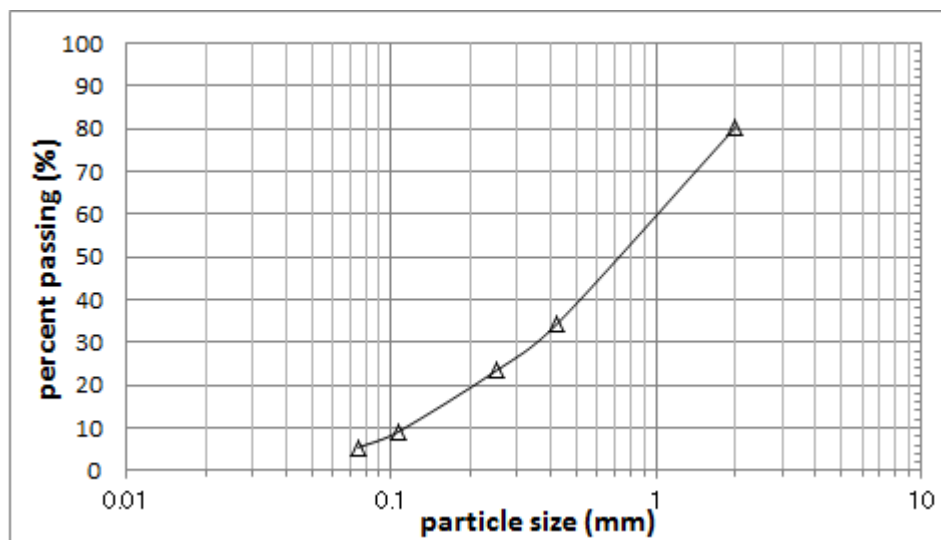
Figure 4.3: Particle size distribution for the Tsukuba bulk soil.

4.4.1.3.Chemical properties:

The dried sample was characterized by physical-chemical analysis, e.g., quantification of chemical constituents and surface characteristics (Table 4.2). The soil is acidic with a

Table 4.2: Physical and chemical properties of the experimental soil

Parameter	Value	Parameter	Value
$pH_w{}^a$	4.41	*Surface area (m^2/g)* [d]	
$pH_{CaCl2}{}^a$	4.01	SA_{BET}-bulk	7.67
particle density (g/cm^3)	2.27	SA_{BET}- >425 μm	3.39
soil leachate concentration		SA_{BET}->250 μm	7.31
F (mg/kg)	0.1	SA_{BET}->106 μm	9.68
SO_4 (mg/kg)	30	SA_{BET}-<106 μm	13.74
Total element concentration [b]		*Pore radius (A^0)* [e]	
Tot. Al (mg/g)	19.5	adsorption	16.89
Tot. Fe (mg/g)	14.9	desorption	19.17
Grainsize distribution		*Mass % of major elements* [f]	
>2mm (%)	19.5	SiO_2	64.44
>425μm (%)	46	Al_2O_3	15.52
>250μm (%)	11	Fe_2O_3	2.85
>106μm (%)	14.4	TiO_2	0.26
>75μm (%)	3.6	MnO	0.09
<75μm (%)	5.4	MgO	0.52
Mineral phase quantification (%) [c]		CaO	1.15
Quartz	29.1	Na_2O	2.15
Feldspar	44.1	K_2O	3.35
Chlorite	4.2	TOC (%)	0.7
Kaolinite	13.6		

[a]: pH_w and pH_{CaCl2}: soil pH measured in deionized water and $CaCl_2$ solution respectively

[b]: total Al and total Fe of soil are obtained by acid digestion method.

[c]: Mineral phase quantification was done as per Herrman and Berry (2002).

[d]: BET surface area of bulk soil sample and sieved samples

[e]: pore radius was calculated from BJH method

[f]: major elements data of soil sample was obtained from XRF spectroscopy

pH$_{(aq)}$ of 4.4. Leachable fluoride for this soil is negligible. Total organic carbon (TOC), as estimated from the dry combustion method, shows that TOC accounts for 0.7 % of the bulk soil before fluoride sorption and 0.66 % of the fluoride sorbed soil. The oxide contents in the soil is presented in Table 4.2 and a comparison between the oxides present in the sample before and after sorption are given in Table 4.3. The soil is silica rich with 15 % Al$_2$O$_3$ and 2.8 % Fe$_2$O$_3$, which are considered to be responsible for fluoride retention. The total Al and Fe is also high. The BET surface area increases with decrease in grain size of the soil fraction, as expected.

Figure 4.4 represents the XRD pattern of the sample before and after sorption. The minerals identified in the bulk sample are: quartz, feldspar, and kaolinite (Figure 4.4(a)). The clay minerals in the bulk sample before sorption are further identified to be kaolinite and chlorite by the analysis of clay fraction and the peaks were differentiated by analysis of the expandable mineral by ethylene glycol solvation treatment (Figure 4.4 (b)).

Table 4.3. Comparison between major oxides for sample before and after fluoride sorption

Oxides (wt %)	Sample before fluoride sorption	Sample after fluoride sorption
SiO$_2$	64.4	61.6
Al$_2$O$_3$	15.5	18.2
Fe$_2$O$_3$	2.8	3.2
TiO$_2$	0.25	0.3
MnO	0.09	0.1
MgO	0.52	0.54
CaO	1.1	1.3
Na$_2$O	2.1	2.6
K$_2$O	3.3	2.9
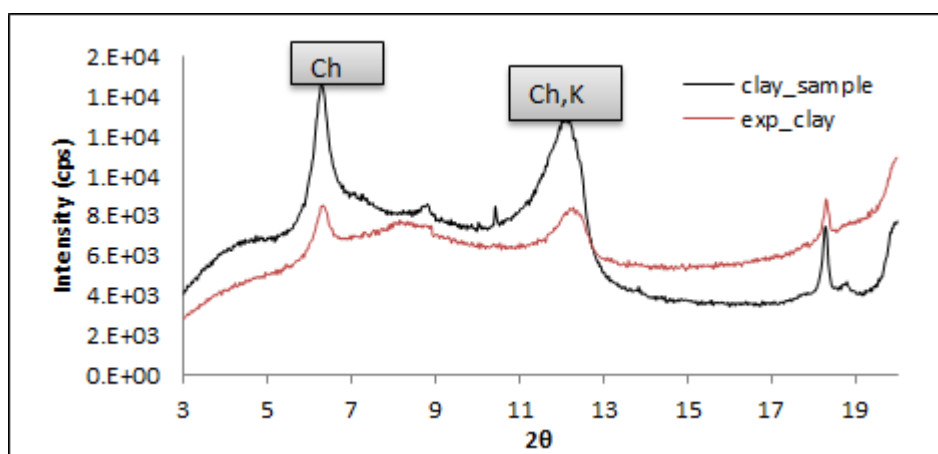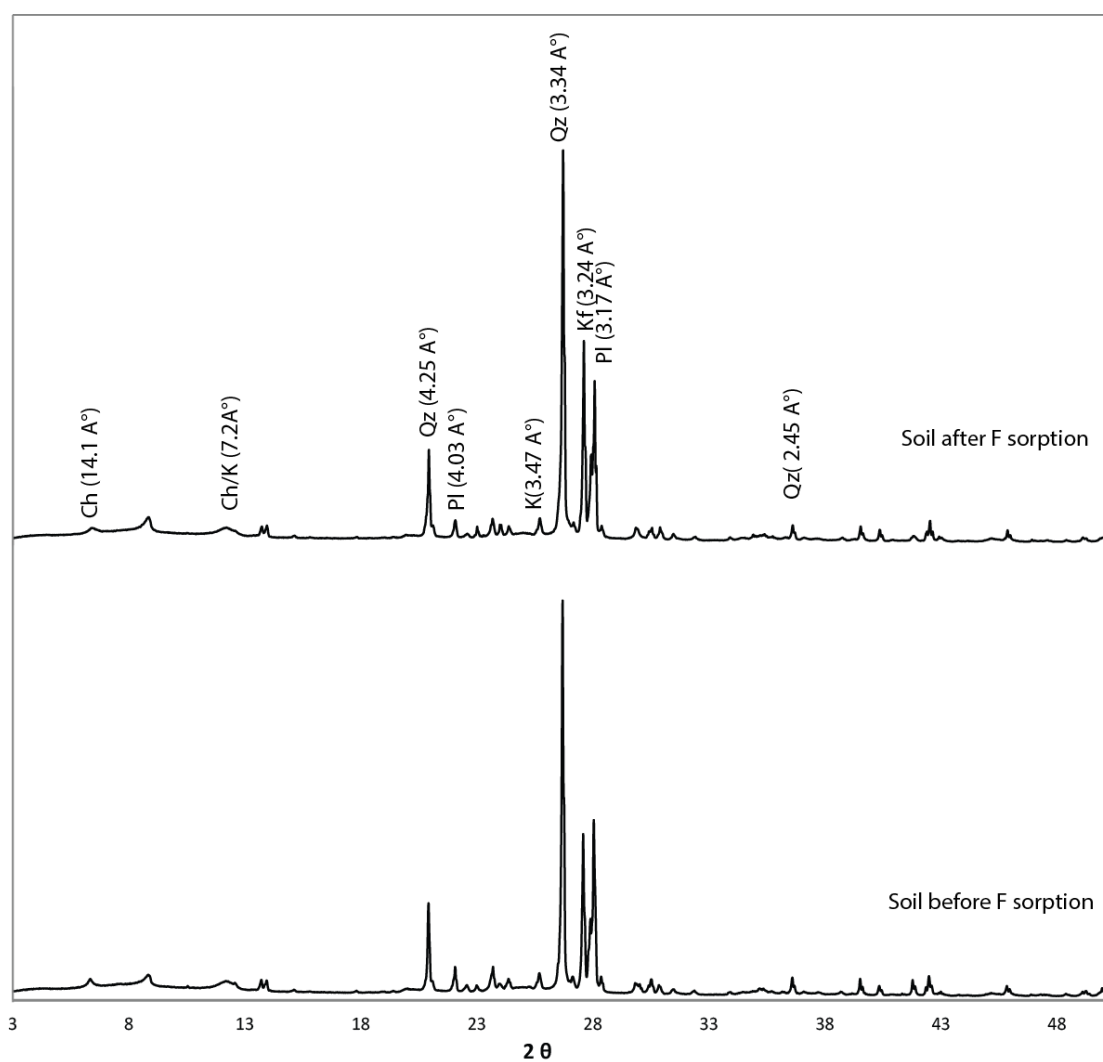
Figure 4.4: (a) XRD pattern of the bulk soil and fluoride sorbed soil. (b) XRD pattern of the clay and ethylene glycol solvated clay from the sample before fluoride sorption.

4.4.1.4. *Semi-quantitative analysis of mineral phases*

Quantification of the mineral phases from major element analysis was carried out with a spreadsheet based program- MINSQ (Hermaan and Berry, 2002). This program adjusts the proportions of all selected phases by iteration to provide a best-fit solution to the composition data. The results of mineral phase quantification for the sample before sorption are presented in Table 4.2. As per the analysis, the soil contains 29 % of quartz, 44% of feldspar and 18 % clay mineral (kaolinite and chlorite).

4.4.1.5. *FTIR spectroscopic analysis*

Spectroscopic techniques are useful in identifying clay minerals and defining sorption mechanism. FTIR spectra have been used for this purpose in previous studies, e.g., Balan et al., (2001) and Madejova and Komadel, (2001) among others for clay mineral analysis, and Arai and Sparks (2001) and Vithanage et al., (2013) for identifying mineral sorption. The FTIR spectra of the bulk soil (< 2mm) before and after fluoride sorption are shown in Figure 4.5, and band assignment to the corresponding
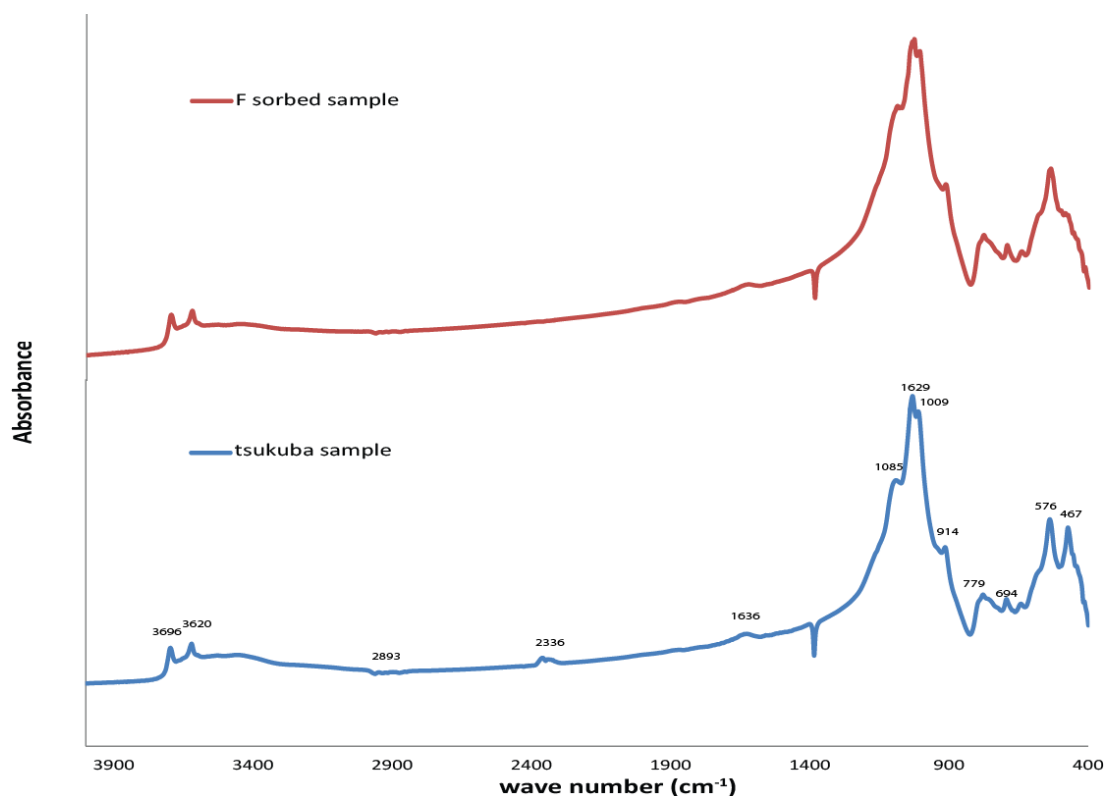
Figure 4.5: FTIR spectra of the bulk soil (<2mm) before and after fluoride sorption.

peak are presented in Table 4.4. The peak at 3463 cm^{-1} (3400~3700) and 1635 cm^{-1} could be assigned to adsorbed water, the former could be due to the stretching modes of OH bands related to free water (surface adsorbed water) and the latter to the bending mode of H-O-H band. After fluoride sorption, some absorbance loss was observed at 564 and 467 cm^{-1}, which could be attributed to structural deformation of the Al-O-Si bond, whereas, the sorption of fluoride could not be confirmed.

Table 4.4. FTIR peak assignment for the bulk soil (Madejova and Komadel, 2001)

Peak position (cm^{-1})	Assignment
~3695	Inner surface hydroxyl group, OH stretching
3620	Inner hydroxyl group, OH group linked to -Si
3463	OH stretching of water
1635	OH deformation of water
1085, 1029	Si-O stretching (or Si-O of quartz)
915	Inner hydroxyl group, OH group linked to -2 Al^{3+}
779	Si-O stretching (or Si-O of quartz)
694	Si-O stretching (or Si-O of quartz)
574	Al-O-Si deformation
467	Si-O-Si deformation

4.4.2. Adsorption experiments

4.4.2.1. Kinetics

Kinetic experiments were conducted in order to get first assessment of how fast the system reaches equilibrium, and based on the results, to determine an appropriate equilibration time for the fluoride sorption experiments. In the kinetic experiments, the

initial fluoride concentration used was 5 mg/l at a solid to solution ratio of 5 g/l. Figure 4.6 shows the data of fluoride sorption as a function of time.

The results of the kinetic experiment showed that 70–80% of the fluoride sorption took place within the first 1.5 hours of interaction. This initial step of rapid sorption was followed by a decreasing rate of fluoride uptake, which continued throughout the time frame of the experiment, i.e., up to 30 hour. The initial rapid uptake indicates surface bound sorption to readily available surface sites whereas the following slow removal is sometimes assumed to represent diffusion to additional less accessible sites in pores and fractures, or adsorption to sites that have a lower reaction rate due to lower affinity (e.g., Davis et al., 1987).
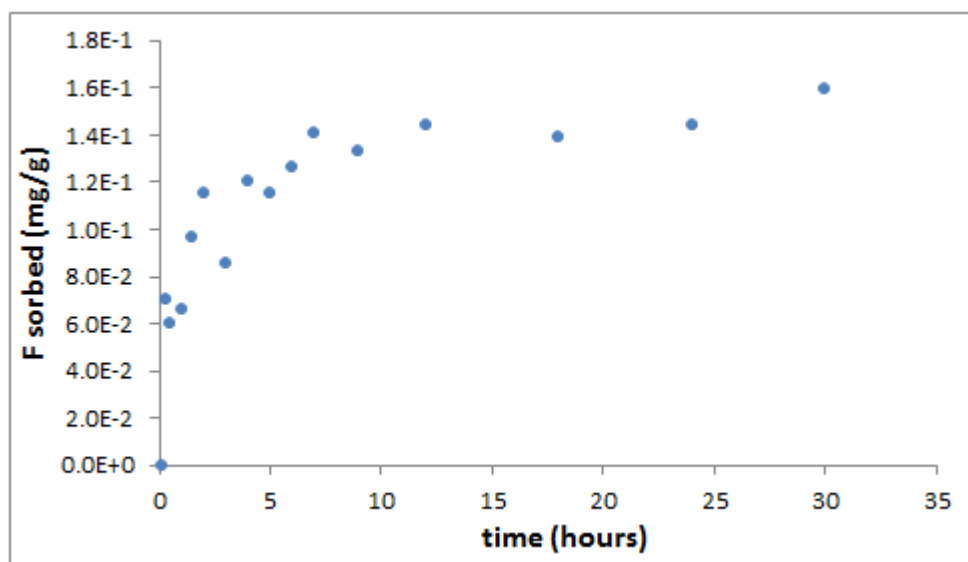
Figure 4.6. Fluoride uptake by soil as a function of time at an initial fluoride concentration of 5 mg/l and solid to solution ration of 5 g/l. The pH of the solution was not controlled during the experiment.

4.4.2.1.1. Kinetic modeling and determination of rate parameters

Various kinetic models have been proposed to throw light on the mechanism of sorption, based on the kinetic sorption data. The most widely used kinetic models in literature related to sorption processes are the Lagergren's pseudo-first order model (Lagergren, 1898; Ho, 2004), Ho's pseudo-second order model (Ho, 2004), intraparticle surface diffusion model by Weber and Morris and the Elovich model. Here, the models

that are applied to the kinetic fluoride sorption data are the Lagergren's pseudo-first order model and the Ho's pseudo-second order model. The applicability of a particular model for kinetic uptake of fluoride by soil was evaluated from the goodness of data fit and regression coefficient value (R^2). The linear fit to these models are presented in Figures 4.7 (a) and (b) respectively.

The Lagergren pseudo-first-order kinetic model is generally expressed as (Lagergren, 1898; Ho, 2004):

$$\frac{dq_t}{dt} = k_1(q_e - q_t) \tag{4.21}$$

Equation 4.21 can be rearranged and integrated with boundary conditions t=0 to $t = \infty$ and q_t =0 to $q_t = q_e$ to give the linearized form as:

$$\ln(q_e - q_t) = \ln q_e - k_1 t \tag{4.22}$$

where q_e and q_t are the amount of fluoride on soil (mg g^{-1}) at equilibrium and at time t, respectively, and ks_1 (min^{-1}) is the first-order rate constant. A linear fit between log(q_e $-q_t$) versus contact time (t) (Figure 4.7 (a)), as indicated by Equation (4.22) imply that the reaction may follow a pseudo-first-order. The R^2 value for the linearized Lagergren model is 0.67. The poor fit to the model indicates that the sorption reaction may not follow the pseudo-first-order kinetics.

The pseudo-second-order chemisorption kinetic rate equation can be expressed as (Ho, 2004):

$$\frac{dq_t}{dt} = k_2(q_e - q_t)^2 \tag{4.23}$$

Equation 4.23 reduces to the linearized form by rearranging and integrating as:

$$\frac{1}{q_e - q_t} = \frac{1}{q_e} + k_2 t \tag{4.24}$$

or

$$\frac{t}{q_t} = \frac{1}{h} + \frac{1}{q_e} t \tag{4.25}$$

where k_2 is the pseudo-second-order rate constant (g mg^{-1} min^{-1}) and h is the initial sorption rate (mg g^{-1} min^{-1}), expressed as:

$$h = k_2 q_e^2 \tag{4.26}$$

where q_e and q_t are the amount of fluoride on soil (mg g^{-1}) at equilibrium and at time t, respectively. The linear fit obtained with Equation 4.25 showed excellent fit with a R^2 value of 0.9949 (Figure 4.7 (b)), showing that the sorption processes follow the second order kinetics.
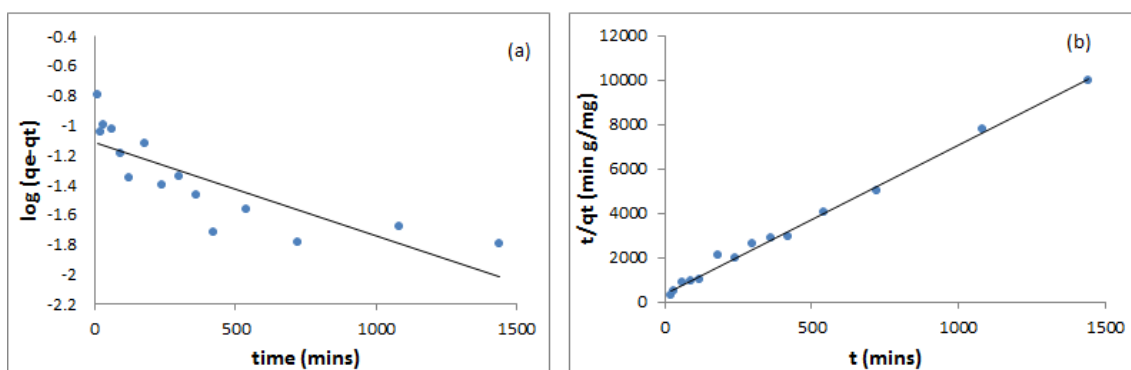
Figure 4.7: (a) Fit to the Linearized Lagergren plot and (b) Linearized Ho's Pseudo second order plot for Kinetic uptake of fluoride on soil

4.4.2.2. Fluoride adsorption isotherm and pH dependent fluoride adsorption

Fluoride adsorption data obtained as a function of pH at initial fluoride concentration of 2.5 and 10.0 mg/l are presented in Figure 4.8.
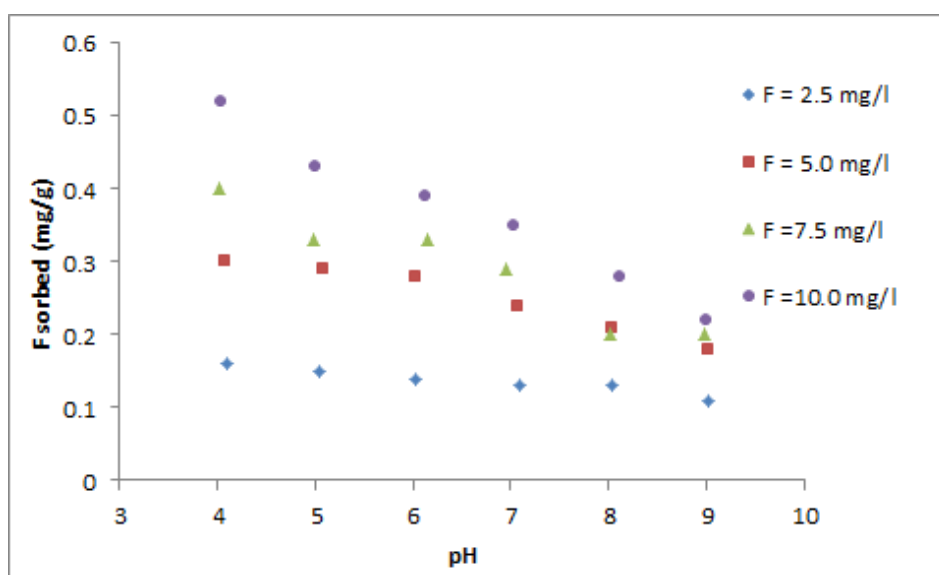
Figure 4.8: pH dependent fluoride sorption on soil at initial fluoride concentration of 2.5 mg/l and 10.0 mg/l at 25ºC. The ionic strength is kept constant at 0.01M.

Amount of fluoride sorption increases with increase in initial fluoride concentration. The data show a decrease in fluoride adsorption with increase in pH, which is a typical behavior for anion adsorption, with a change in adsorption pattern from pH 5 to 7.

The effect of solid concentration, background electrolyte and surface area on fluoride sorption on soil are also evaluated and presented in Figures 4.9 (a-c), respectively.
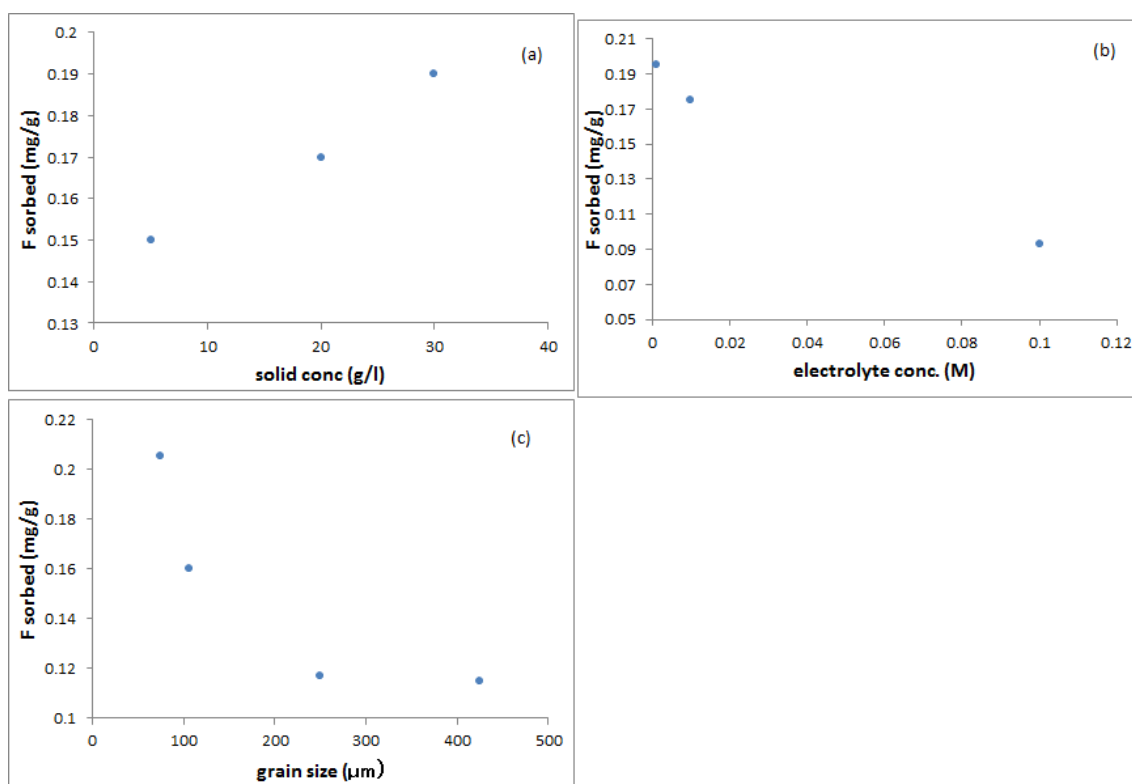
Figure 4.9: Effect of (a) solid concentration, (b) background electrolyte concentration and (c) grain size on fluoride sorption by soil. The experimental conditions are: initial fluoride concentration: 5 mg/l; pH: soil pH, electrolyte concentration: 0.1M; temperature: 25ºC.

Fluoride sorption increased with increase in mass loading in the range of solid concentrations tested (5-30 mg/l) because of increase in available surface sites. Grain size also has similar kind of effect on fluoride sorption, by decrease in sorption with increase in grain size because the surface area decreases with increase in grain size

(Table 4.2). Effect of electrolyte on fluoride sorption is also well pronounced in Figure 4.9 (c). Decrease in fluoride sorption with increase in background electrolyte concentration is due to the fact that increase in electrolyte concentration presses the double layer thickness and reduces the electrostatic repulsion on the surface (Yang et al., 2007).

4.4.2.2.1. Isotherm models

The Freundlich and Langmuir equations are traditionally used to describe an array of reactions on soils and soil components. These models often describe experimental data quite well and can be useful in making comparisons about sorption behavior between soils. The parameters calculated from these equations can be used to get information about the binding sites and strengths and types of sorption mechanisms,
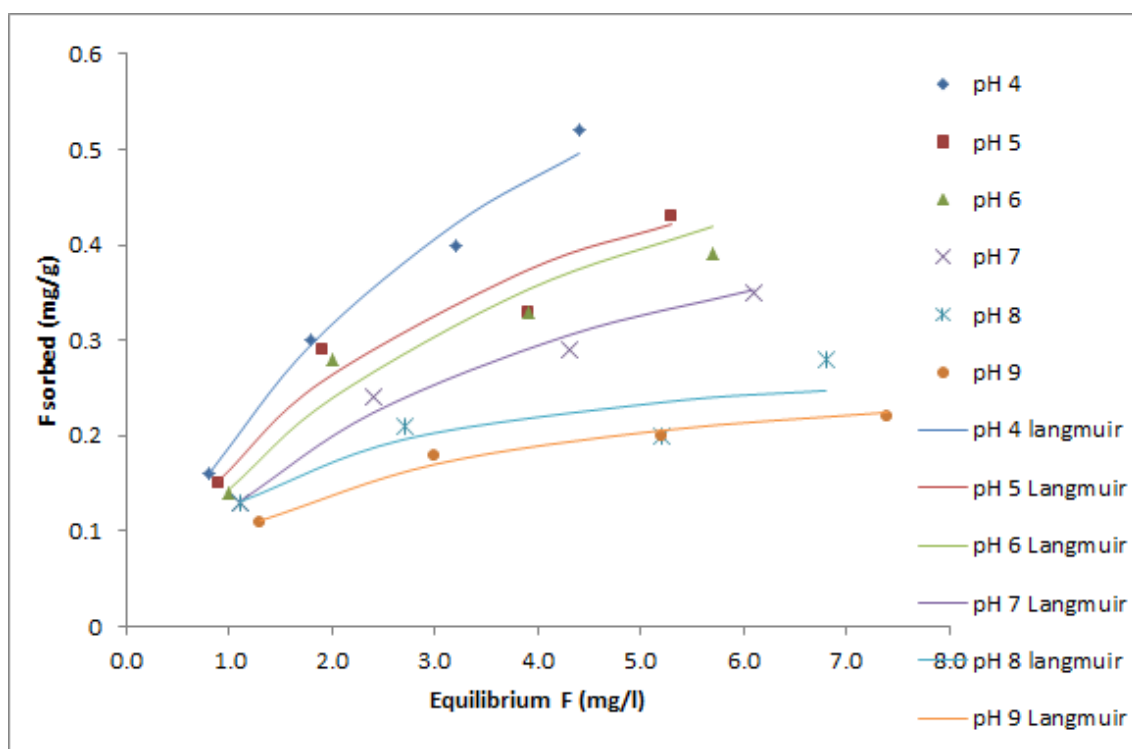
Figure 4.10. Sorption data and Langmuir isotherm for fluoride on soil at different pH. The lines are Langmuir isotherm fitted to the experimental data. The experimental conditions are: initial fluoride concentration: 2.5-10.0 mg/l; electrolyte concentration: 0.01M; temperature: 25°C.

e.g., adsorption, precipitation etc. Fluoride sorption data were investigated by Freundlich and Langmuir isotherm models (Section 4.3.2.1.). The data fit to the Langmuir model at a pH range of 4-9 are shown in Figure 4.10. Fluoride sorption could be well represented by Langmuir equations with high R^2 values for the linear fits at all pH ranges. The data could also be well described by the Freundlich model with lower R^2 values for linear fit than that to the Langmuir model.

The sorption data were also analyzed by the Dubinin–Radushkevick equation, which has been used to determine the possible adsorption mechanism (Section 4.3.2.1). Figure 4.11 shows the fit of fluoride sorption data at pH 4 (data at pH 4 is shown because the maximum sorption occurs at pH 4) to the linearized Dubinin–Radushkevick equation (Section 4.3.2.1). The data fit is quite good with a R^2 value of 0.992.
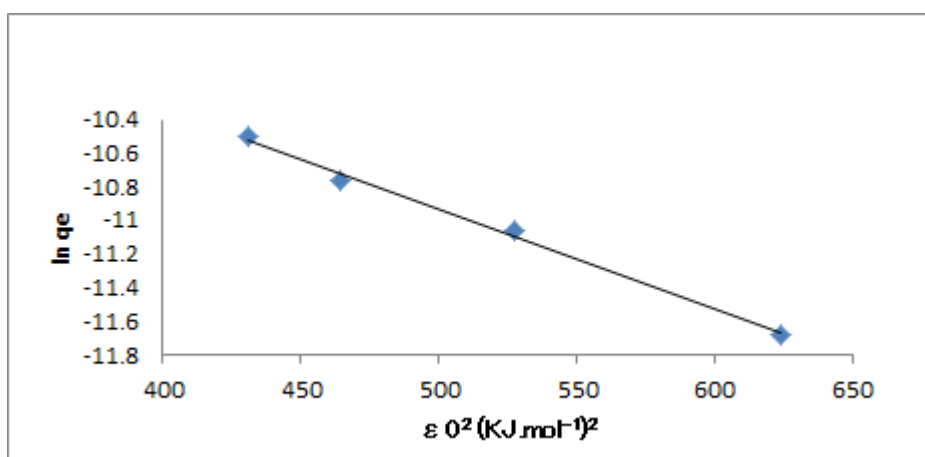
Figure 4.11. Linearized Dubinin-Raduschkevick plot for fluoride sorption on soil at pH 4. Initial fluoride concentration: 2.5-10 mg/l.

4.4.2.2.2. Surface complexation modeling

In the past years, major advances have been made in modeling sorption reactions at the mineral water interface and elucidating the kinetics and mechanisms of sorption desorption phenomena in soils. Empirical models, such as Freundlich and Langmuir, are valid only for the conditions under which the experiment was conducted (Goldberg et

81

al., 2007), for example, adsorption isotherm datasets are typically developed for a single pH value. Hence, most adsorption isotherm models are valid only at the pH it was developed and cannot be used to predict sorption behaviors involving pH variations. This is also clarified in Figure 4.10, where, Langmuir fit at each pH range requires a different data set.

Surface complexation models (SCM) based on a thermodynamic approach are able to describe surface species, mass balance, and chemical reactions and are used to model the effect of pH variation on sorption (Davis and Kent, 1990; Dzombak and Morel, 1990). Application of SCM to single mineral phases is already well known, whereas, application of SCM to mineral assemblage (or soil) is complicated because of the presence of mineral coatings. Two kinds of major approach are suggested for application of SCM to mineral assemblage/soils/sediments: the component additivity (CA) and generalized composite (GC) approaches (Davis et al., 1998). The assumptions, approaches and details of these methods are presented in Table 4.5. Both CA and GC approach have been applied to explain metal and oxy (an)ion sorption to complex mineral assemblage and soil, e.g., Serrano et al. (2009) used the CA approach to explain Pb and Cd sorption on to natural soil, Davis et al. (2004) used the GC approach to explain U(VI) sorption to natural sediments. The advantages and limitations of using CA and GC approach are illustrated well by Davis et al. (1998), Davis et al. (2004) and the references therein. Based on the discussion on both these approaches, the GC approach is chosen to describe the sorption behavior of fluoride in soil. Both constant capacitance model (CCM) and the generalized two layer model are used to explain the sorption data. The SCM framework is explained in (Section 1.2.4.2. of Chapter 1).

4.4.2.2.2.1. Model simulation and parameter optimization using CCM

A constant capacitance model (CCM) was used to describe the fluoride sorption edges in soil and to optimize the reaction constants. CCM was chosen in this study because of its simplicity, requirement of less number of parameters and because it has been successfully applied for contaminant adsorption to heterogeneous soil surface. Fluoride sorption was assumed to take place on a generic surface site (>SOH). This assumption is clearly a gross simplification since soils are complex multisite mixtures

containing many diverse surface sites. The sorption reaction equations that are considered in the model are as explained in Section 4.3.2.2.2 (Equations 4.9 to 4.14).

Table 4.5. The Component additive approach and General composite approach used in surface complexation modeling for ion sorption on mineral assemblage/soil/sediments.

Parameters	CA approach	GC approach
Surface sites	based on mineral composition	Generic surface site
Site concentration	calculated from the concentration of reactive element concentration	a fixed site conc. of 2.31 sites/nm^2 is assumed
Intrinsic surface complexation constants	surface complexation constants of pure minerals	Optimized values
Advantage	no data fitting is Required	Nonelectrostatic model can be used; no. of surface equations can be minimized
Disadvantage	Too simplified	May not perform well when extra-polated beyond the chemical conditions used for calibration
Difficulty	Determining relative abundance of adsorptive phases	---

Moreover, fluoride can effectively facilitate Al dissolution from Al-containing minerals at low pH, which can be increased by increasing fluoride concentration (Haidouti, 1995; Harrington et al., 2003; Zhu et al., 2004). Fluoride induced Al release is observed in our sorption experiments (Figure 4.12). Modeling results for the speciation of Al in solution using Visual Minteq 3.0 (Gustafsson, 2012) shows the predominance of ionic Al as AlF_2^+ at all pH ranges. Figure 4.13 (a) and (b) show the predominance of Al species in solution at pH 4 and 9 for initial fluoride concentration of 5.9 mg/l. The distribution of species at other concentrations was almost similar. Hence, the possibility of fluoride adsorption as AlF_2^+ cannot be ruled out. Fluoride sorption as ionic Al-F complex (AlF_4^-) is suggested by Harrington et al., (2003) because this species was the dominant species in their experimental solutions.
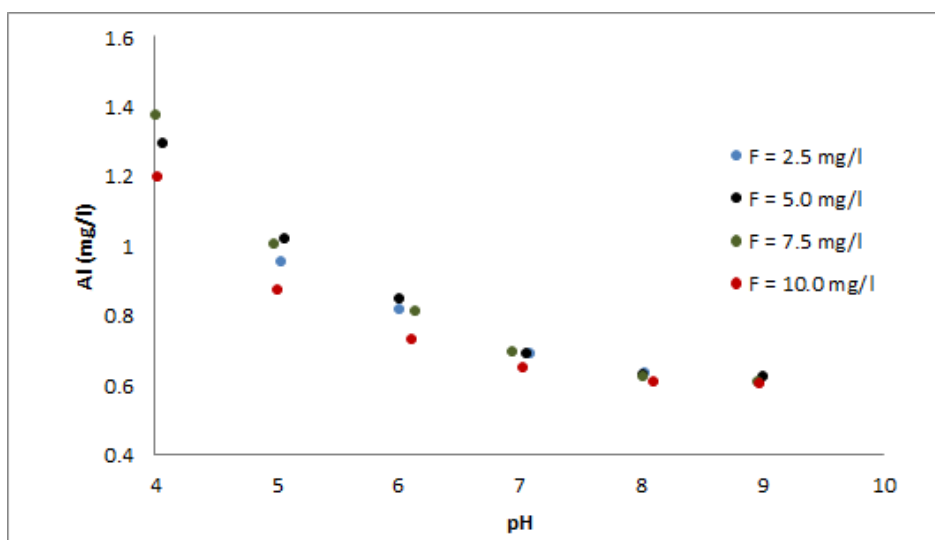
Figure 4.12. Al release during fluoride sorption at varying pH.
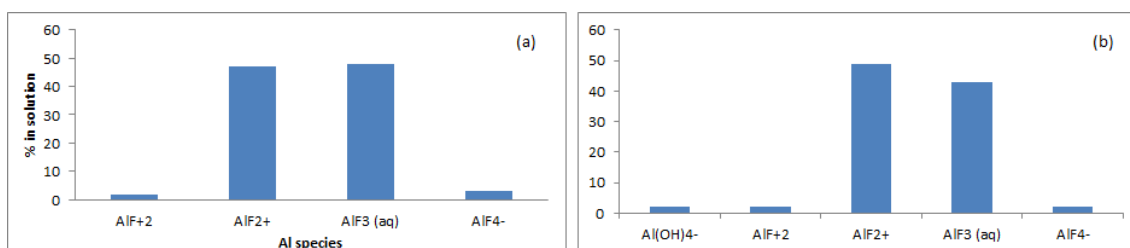
Figure 4.13. Al species distribution in solution after fluoride sorption. (a): at pH 4 and (b) at pH 9.

Hence, model calculations were conducted with and without including dissolved Al and AlF_2^+ sorption.

Reaction equations and the model parameters used in the optimization process and forward modeling are summarized in Table 4.6. The reactive surface hydroxyl groups on oxide minerals and aluminol groups on clay minerals in the soils are represented by >SOH surface site. Some of the model input parameter values were taken from previous studies as an initial guess, such as: the capacitance value C, was chosen to be 1.06 F m^{-2}. This value was chosen because it is considered optimum for Al oxide by Westall and Hohl (1980). The initial guesses for the protonation constant logK$^+_{(int)}$ and deprotonation constant logK$^-_{(int)}$ are 7.35 and -8.95, respectively. These values are average logK$^+_{(int)}$ and logK$^-_{(int)}$ values of a literature compilation for Al and Fe oxides (Goldberg and Sposito, 1984). The number of reactive sites is suggested to be 2.31 sites nm^{-2} (Davis and Kent, 1990).

Table 4.6: Surface complexation reactions for protonation and deprotonation and fluoride sorption along with initial guesses for intrinsic surface complexation reactions (logK$_{int}$) and model parameters.

Surface complexation reactions	logK$_{int}$	Reaction no.
$>SOH + H^+ = >SOH_2^+$	7.35 [a]	4.3
$>SOH = >SO^- + H^+$	-8.95 [a]	4.4
$>SOH + F^- + H^+ = >SF + H_2O$	8.78 [b]	4.5
$>SOH + F^- = >SOHF^-$	1.0 [b]	4.6
$>SOH + 2F^- + H^+ = >SF_2^- + H_2O$	11.94 [b]	4.7
$>SOH + 2F^- + Al^{3+} = >SOAlF_2 + H^+$	10.00 [c]	4.8
Capacitance (F/m^2)	1.06 [d]	
Surface sites density (moles/m^2)	3.84e-6 [e]	
Surface area (m^2/g)	9.68 [c]	

[a] Goldberg and Sposito, 1984; [b]Karamalidis and Dzombak (2010); [c]This study; [d]Westall and Hohl (1980); [e] Davis and Kent (1990).

The C value was found to be not so sensitive to model calculations (Goldberg and Sposito, 1984), hence can be assumed to be constant in the model. Whereas SCMs are highly dependent on the surface site density (Goldberg, 1991) parameter. Surface site density is generally calculated by multiplying number of sites to the surface area. However, for some mineral phases, the surface area determined by BET might be under predicted (Davis et al., 1998). Hence, the surface site density should be estimated for the sorbent considered. Similarly, $logK^+_{(int)}$ and $logK^-_{(int)}$ should also be estimated because surface fluoride sorption reactions and surface protonation/deprotonation reactions are interdependent.

4.4.2.2.2.2. Model simulation parameter optimization using DDL

The optimization process set in PEST and PHREEQC was run for three different cases: Case 1: without adding dissolved Al and Al-F complex sorption to the model; Case 2: with dissolved Al but without Al-F complex sorption and Case 3: with dissolved Al and Al-F complex sorption. The dissolved Al concentration considered was 2.435 mg/kg, which is the exchangeable Al concentration, as explained in section 2.1.2.12. The results of optimization are presented in Table 4.7.

Next, the optimized model parameters were carried to the forward simulation set in PHREEQC using the generalized two layer model. The generalized two layer model in PHREEQC contains the database for sorption to hydrous ferric oxide as per Dzombak and Morel (1990). Hence, the database for fluoride sorption to soil using a generic surface site was created in the PHREEQC format and the pH dependent fluoride sorption in soil were modeled.

The results of simulation for all the three cases are shown in Figures 4.14 (a-c). The modeled data for pH dependent fluoride adsorption at 0.01M ionic strength compare well with the experimental data in case 3, whereas the model with case 1 parameters does not explain pH dependency of fluoride sorption quite well.

Table 4.7: Surface complexation reactions, optimized intrinsic surface complexation reaction constants (logK$_{int}$), and model parameters.

Surface complexation reactions	logK$_{int}$		
	Case 1[a]	Case 2[b]	Case 3[c]
$>SOH + H^+ = >SOH_2^+$	3.0	5.08	4.67
$>SOH = >SO^- + H^+$	-7.02	8.75	-8.26
$>SOH + F^- + H^+ = >SF + H_2O$	6.00	9.28	10.04
$>SOH + F^- = >SOHF^-$	5.89	5.49	5.78
$>SOH + 2F^- + H^+ = >SF_2^- + H_2O$	12.72	11.47	---
$>SOH + 2F^- + Al^{3+} = >SOAlF_2 + H^+$	---	---	10.91
Surface sites density (moles/l)	$4.69*10^{-4}$	$4.58*10^{-4}$	$3.29*10^{-4}$
Surface area (m^2/g)	9.68	9.68	9.68

[a] Case 1: without dissolved Al and Al-F complex sorption; [b] with dissolved Al but without Al-F complex sorption; [c] with dissolved Al and Al-F complex sorption.

The weighted mean square error (WMSE) normalized by the model calculated value were calculated for different cases of fluoride sorption simulation as follows:

$$WMSE = \frac{1}{n}\sum_{i=1}^{n}\left(\frac{x_i - y_i}{y_i}\right)^2$$

where n is the number of data points, x_i is the amount of adsorbed fluoride calculated by considering different sets of fluoride sorption reactions at each pH and y_i is the amount of adsorbed fluoride observed in our experiment for fluoride concentrations of 2.5 mg/l, 5.0 mg/l, 7.5 mg/l and 10.0 mg/l at the corresponding pH. Table 4.8 shows the calculated WMSE for models Case 1 and Case 3.
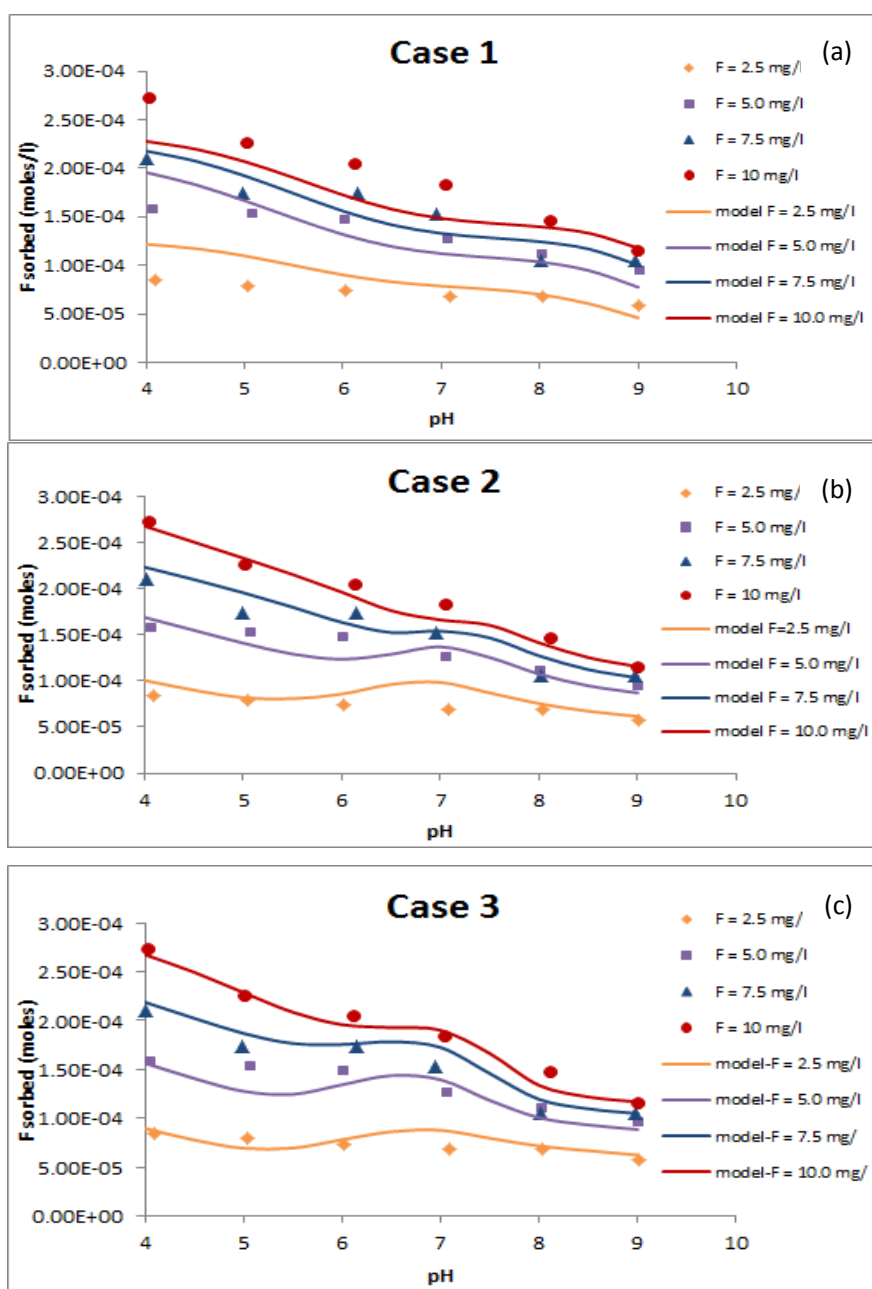
Figure 4.14. Amount of fluoride sorbed with increase in pH for different fluoride concentration. (a) model calculations, where neither dissolved Al or Al-F complex sorption were considered, (b) model calculations, where dissolved Al was included in the model without Al-F complex sorption, (c) model calculations, both dissolved Al and Al-F complex sorption were considered. The symbols represent experimentally observed amount of fluoride sorption and lines represent model calculations. The symbol and line definitions in Figure (a) also indicate the symbols and lines in Figure (b) and (c).

Table 4.8: WMSE by considering different sets of fluoride sorption reactions for different fluoride concentrations.

Initial fluoride concentration	WMSE	
	Case 1[a]	Case 3[a]
2.5 (mg/l)	0.05	0.01
5.0 (mg/l)	0.02	0.01
7.5 (mg/l)	0.01	0.005
10.0 (mg/l)	0.02	0.002

[a] Conditions for Model cases Case 1 and Case 3 are as represented in Table 4.7.

4.5.Discussion

4.5.1. Physical and chemical properties that effect fluoride sorption

4.5.1.1. Surface area and porosity:

The micropore size distribution analysis with t-plot method gives valuable information regarding sorption processes. The results of Figure 4.2 and Table 4.1 show that the sample contains both micro-pores and meso-pores. The t-plot calculated surface area is almost identical to the BET surface area suggesting lesser micro-pores. The micropore-volume as calculated by the t-plot method for the sample after fluoride sorption is reduced by 50% of micro-pore volume of the sample before fluoride sorption, which suggests that not all the micropores are filled even after fluoride sorption for long duration. Although there is a decrease in surface area (BET and t-plot) (Table 4.1) after fluoride sorption, the decrease is not much pronounced.

Another discussion that could be made from the N_2 gas sorption/ desorption isotherm is from the hysteresis loop. The hysteresis loop for the samples analyzed closed at p/p^o of about 0.45 (Figure 4.2 (a) and (b)), which corresponds to a Kelvin radius for capillary condensation (Hay et al., 2011), and to a pore width of about 2.4 nm for parallel sheets and 3.6 nm for cylindrical pores (Gregg and Sing, 1982, Craig et al., 2015). This kind of desorption isotherm suggests that many of the pores are controlled by pore necks that are narrower than the above Kelvin radius (Hay et al., 2011). Considering the hydrated ionic radii of fluoride to be 0.34 nm (the ionic radii is 0.13

nm), this kind of discussion could be useful, which is beyond the scope of this study. Also, diffusion to the intragranular region is a slow process, which could affect the sorption processes.

The discussion above shows that pore structure, size, and shape can greatly impact the adsorption processes, which should be studied in sorption process evaluation.

4.5.1.2.   Chemical properties:

Fluoride sorption in soil is negatively correlated with soil pH, and CaO, but positively correlated with Al_2O_3 and Fe_2O_3 and organic matter content (Wang et al., 2002). Considering the chemical properties (Table 4.2), fluoride sorption is favored for this soil sample concerned. Since the total organic carbon for the sample is low, effect of organic carbon on fluoride sorption is not considered in this study.

The semi-quantitative mineralogical estimation shows that the soil consists of 29% silica, mostly as quartz, which is a very poor sorbent for fluoride (Fan et al., 2002) and the major clay minerals are kaolinite and chlorite, which can adsorb fluoride. Although, the Al oxides found might be occupied in the feldspars, the sorption behavior shows that some sorption occurs to Al-oxides (Figure 4.8) because of the change in sorption pattern at 6-7. Fluoride sorption to alumina shows the sorption maximum at neutral pH range (pH 6.5-7.5) (Ghorai and Pant, 2005).

Also, the XRD patterns of the samples before and after fluoride sorption are quite similar and no new mineral phase could be identified due to fluoride sorption.

4.5.2.   Spectroscopic evidence for fluoride sorption on soil

The results and details of spectroscopic analysis by FTIR are discussed in Section 4.4.1.5. The FTIR spectra are shown in Figure 4.5 and the assignments of the bands are given in Table 4.4. The sharp doublet at 3696 and 3620 cm^{-1} is characteristic for the kaolin group in general, which arise from the internal surface OH groups (Balan, 2001). The OH deformation bands of kaolinite are situated at 938 and 913 cm^{-1}. Supporting bands at 794 (Si-O) and 698 cm^{-1} (Si-O) are diagnostic for kaolinite, too. The peak at 3463 cm^{-1} (3400~3700) and 1635 cm^{-1} could be assigned to adsorbed water, the former could be due to the stretching modes of OH bands related to free water

(surface adsorbed water) and the latter to the bending mode of H-O-H band. After fluoride sorption, some absorbance loss was observed at 564 and 467 cm^{-1}, which could be attributed to structural deformation of the Al-O-Si bond, whereas, the sorption of fluoride could not be confirmed.

4.5.3. *Fluoride sorption kinetics and sorption isotherm*

The behavior of fluoride sorption kinetics and kinetic modeling are discussed in section 4.4.2.1 and 4.4.2.2. The model results show that the data fits well to the Ho's pseudo second order model, which implies that chemisorption processes are governing sorption and the low value of the second order rate constant k_2 (0.098 g mg^{-1} min^{-1}) indicates that the rate of fluoride sorption process is fast.

The sorption data modeled for Langmuir, Freundlich and Dubinin-Raduschvick equations are discussed in section 4.4.2.2.1. The maximum sorption density calculated according to the Langmuir equation at pH 4 is 0.93 mg/g. This value decreases with increase in pH, as expected. The observed maximum sorption at pH 4 for initial fluoride concentration of 10.0 mg/l is 0.52 mg/g; which shows that fluoride occupies ~55% of the available sites. Isotherm models cannot give molecular description of sorption; nevertheless, these models can be used to derive important thermodynamic parameters.

For example, the Gibb's free energy change (ΔG^0) can be calculated from the Langmuir constant "*b*" (Section 4.3.2.1.). ΔG^0 calculated at pH 4 is -21.08 KJ/mol; which indicates that the sorption is feasible under the conditions considered. ΔG^0 at other pH is also similar to this value.

Similarly, the adsorption intensity (R$_L$) can be calculated from the Langmuir "*b*" value as: $R_L = 1/(1+bC_0)$, where C_0 (mol/l) is the initial fluoride concentration (Romero-Gonzalez et al., 2005). A R_L value in the range of 0 to 1 indicates favorable sorption. The R$_L$ values calculated at pH 4 for all the fluoride concentrations are in the range of 0.28 to 0.61 suggesting favorable adsorption. At other pH ranges also the R_L value is in the range of 0 to 1.

Another important information regarding sorption that can be derived from the Dubinin-Raduschvick equation is the mean free energy of sorption (E) (Equation 4.8).

The E values are useful in estimating the type of sorption reaction, e.g., if the E value is in the range of 8-16 kJ/ mol, this indicates an ion-exchange reaction (Helfferich, 1962). The E values at pH ranges 4-9 are calculated to be in the range of 9.2-12.3 kJ/mol, which suggests that ion exchange is occurring in the system.

4.5.4. *Surface complexation modeling*

Fluoride sorption in soil is described by the generalized two-layer surface complexation model (Dzombak and Morel, 1990). Fluoride sorption in the model is described by the sorption reactions as represented in Table 4.7. Reaction 4.5 represents the ion exchange processes, which can explain the change in pH of the solution after sorption. Also, mean energy of sorption as calculated by the Dubinin-Raduschvick equation reveals that ion exchange is occurring in the system. Hence, the ion exchange reaction (Reaction 4.5) was included in the final model. Similarly, Reaction 4.6 represents the sorption processes and Reaction 4.8 represents Al-F complex sorption on the surface. The final model (Case 3; Table 4.7 and Figure 4.14 (c)) could explain quite fairly the observed fluoride sorption at all pH. In order to better explain the modeled results, the species distribution was calculated. Figure 4.15 shows the fluoride surface species distribution at all pH for initial fluoride concentration of 10.0 mg/l.

Ion exchange between the fluoride ion in solution and OH$^-$ at the surface (Reaction 4.5) dominates the sorption processes (blue line in Figure 4.15) in addition to surface processes (Reaction 4.6). With increase in pH, (neutral to alkaline conditions), the ion exchange processes almost ceases because of greater competition between OH$^-$ ions in solution and fluoride ion.

Our experimental data suggests fluoride sorption even at high pH (e.g., pH 8 and 9). Hence other processes need to be examined to explain fluoride sorption at this pH. Reaction 4.6 explains the observed fluoride sorption at higher pH. In order to explain the fluoride sorption behavior at pH range of 6-7, the discussion of fluoride surface distribution is necessary. Figure 4.15 represents the distribution of fluoride surface when the sorption data were modeled without including Al-F complex sorption and dissolved Al (Case 1, Table 4.7, Figure 4.14 (a)) and by including Al-F complex sorption and dissolved Al (Case 3, Table 4.7, Figure 4.14 (c)).

In the case of the model with Case 1, fluoride sorption is almost represented by the sorption reaction, Reaction 4.6 with formation of $>SOHF^-$ species (red line in Figure 4.15 (a)), whereas the contribution of sorbed complex $>SF$ in fluoride sorption is negligible (blue line in Figure 4.15 (a)). Some contribution of the species $>SF_2^-$ is observed at a narrow pH range of 4-5. However, isotherm analysis for thermodynamic properties reveals that ion exchange might be occurring in the fluoride-soil system in the experimental conditions of this study (Section 4.5.3). Hence the model calculations with Case 1 may not be practical to implement in fluoride-soil system.
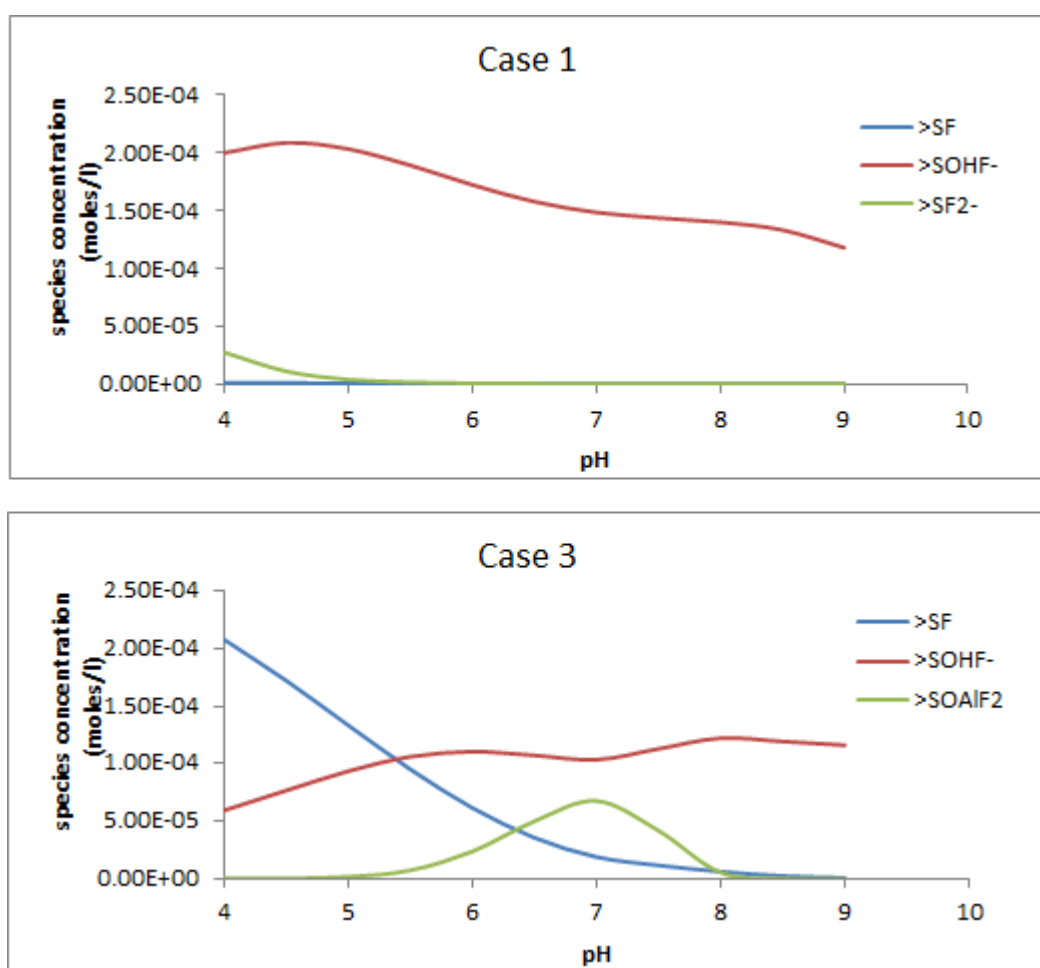
Figure 4.15: Fluoride surface species distribution for initial fluoride concentration of 10.0 mg/l as calculated with the generalized two layer model with model parameters given in Table 4.7, case 3.

Surface speciation calculation with model Case 3 shows that ion exchange contributes to fluoride sorption in the pH range of 4-8, although the effect of ion exchange decreases with increase in pH (blue line in Figure 4.15 (b)). The behavior of fluoride sorption in the range of pH 6-7 can be explained by the behavior of the surface species >SOAlF$_2$ (green line in Figure 4.15 (b)), because the contribution of >SOAlF$_2$ at this pH range is maximum, whereas at other pH ranges, the effect is marginal. Including Al-F sorption and dissolved Al in the model yielded best results (Figure 4.14 (c) and Figure 4.15 (b)), which is also evidenced from the minimization of error between the observed and model calculated fluoride sorption (Table 4.8). The model results strongly evidence the effect of Al on fluoride speciation and sorption on soil.

4.6.   Conclusions

The mechanism of fluoride sorption on a granitic soil from Tsukuba was studied through a series of batch experiments, surface complexation modeling and FTIR spectroscopy. Adsorption processes of fluoride are fast and regulated by chemisorption processes. Fluoride sorption was pH dependent, increase in sorption with decreasing pH, the dependency being non-linear. The amount of fluoride sorbed depends on the surface area and background electrolyte concentration, possibly due to electrostatic effect. Fluoride occupies ~55% of total surface sites. The sorption data were well explained by a generalized two layer model that considers inner sphere complexation. The protonation/deprotonation constants, fluoride sorption constants and site density parameter were optimized instead of using literature cited values. The modeled results are quite different when dissolved Al was not included in the model, suggesting the importance of dissolved Al on fluoride sorption. This study introduced Al-F complex sorption to the model to explain fluoride sorption behavior at pH range of 6-7 which is first of its kind. The results reveal that fluoride may be released into the environment under alkaline conditions because of the weak binding and no precipitation, although acidic pH (pH 4) may help in binding fluoride in soil. The results also encourage to investigate fluoride sorption under different environmental conditions (e.g., high fluoride concentration and low pH, keeping in mind fluoride contamination from industrial waste).

Chapter 5: Flow through experiments for fluoride sorption and desorption in a disturbed soil from Tsukuba, Japan

5.1. Introduction

In this chapter, fluoride desorption from a saturated fluoride-sorbed column was investigated by flow through experiments. Flow interruption with variable stop flow durations was applied to investigate non-equilibrium behavior during fluoride transport. The transport properties of the soil were independently measured by fitting the breakthrough curves of stable isotopes of oxygen (^{18}O) and deuterium (^{2}H), used as tracers to the standard advection dispersion equation (ADE) and to the equation considering the two domain (mobile-immobile zone) concept. Reactive transport models that integrated the physical transport properties and geochemical processes were used to evaluate the kinetics of fluoride desorption from the column.

5.2. Materials and methods

The soil sample chosen for studying fluoride transport behavior is from Tsukuba, Japan (sample no. 1, Figure 4.1). The site at Tsukuba was selected because it is granitic terrain. Our field survey results from granitic terrains in India show high leachable fluoride and possible relation between leachable fluoride and groundwater fluoride, whereas that from Nakatsugawa, Japan has negligible leachable fluoride (Section 2.2). Batch experiment results for fluoride sorption in the granitic soil from Tsukuba found that the sorption capacity of the soil was high (Chapter 4). Hence, the soil from Tsukuba was selected to further understand transport behavior of fluoride in the environment.

5.2.1. Sample characterization

The bulk soil collected from Tsukuba, Japan (the details are explained in Section 4.2.) contained ~20% of > 2mm granules (Table 4.3). The sample used in the column experiment was sieved to < 2mm. The sieved sample was dominated by > 425µm grain

Figure 5.1.: Column experiment set up in the laboratory.

diameter particles (~55%) whereas the finer particles ($< 106\mu m$) constitute ~10% of the total volume. Before the experiment, the bulk soil was subjected to analysis for physical-chemical properties such as pH, particle density, surface area, grain-size distribution, soil leachable ion concentration, mineralogical analysis, elemental analysis and spectroscopic analysis.

5.2.2. Column experiment for fluoride transport during sorption

First, column experiments for fluoride sorption were conducted under saturated conditions at the laboratory. The experimental set up is shown in Figure 5.1. Acrylic resin column (30 cm long and 6.4cm inner diameter) was used in all the experiments.

First, the column was secured to a stand, 100 ml of degassed deionized water was added to the column and 200 g of field moist soil was slowly added to it. Deionized water and soil were added in succession to the column. Following each soil addition, the column was gently tapped on the outside with a rubber mallet to bring the soil to the appropriate volume and to make sure the column is well packed. By adding soil to water this way, fully saturated conditions in the column was ensured. At each end of the column, rubber sheets were used to stop leakage and large diameter filter papers are used to prevent passing of soil particles. The porosity was calculated from the column volume and soil volume. The column was then left overnight to allow equilibrium

before fluoride sorption experiment. Two columns were prepared for the experiments. 50 mg/l of fluoride stock solution was then pumped from the bottom of the column at a flow rate of 3.6 ml/min by a TRIS peristaltic pump with 1/8 inch tubing. For the first column, fluoride was injected for 5.74 pore volumes (PV) and then flow was stopped for 12 hours. Flow was resumed again and continued for another 5.75 PV. Stop flow was applied again for 84 hours and fluoride injection was resumed until breakthrough was obtained (for a total of 17 pore volumes). The effluent was collected with a CHF10 automatic fraction collector. The effluent samples were measured immediately for pH, filtered with a 0.45μm syringe filter and stored for fluoride measurement. An aliquot was removed from the filtered sample, acidified and stored at 4ºC for cation analysis. After the sorption experiment, the column was rested and the fluoride-sorbed sample was analyzed for further physico-chemical analysis.

Fluoride sorption in the second column follows the same procedure as that of the first column, except that in the second column the first stop flow was applied after 13.6 PV and stopped for 15 hours, injected with fluoride solution for another 13.6 PV. The second column was rested for few days and fluoride desorption experiment was conducted, as described below.

5.2.3. *Column experiment for fluoride transport during desorption*

Fluoride desorption kinetics from the fluoride-sorbed column was studied. The flushing solution was ICEFIELD pure and natural Canadian water. ICEFIELD water solution was used because it has a distinct stable $\delta^{18}O$ and δ^2H values than that of the MilliQ water used in the fluoride sorption experiment for saturation and of stock fluoride solution preparation, and could be used as a tracer. Also, the ion concentrations of this water are low (Na$^+$ 0.86 mg/l, Ca^{2+} 8.6 mg/l; Mg^{2+} 1.5 mg/l, Ref: http://www.icefield.jp/index_en.html) to affect fluoride behavior in the column anyway and has a neutral pH (pH 7.0), similar to that of the MilliQ water. Stop flow events were applied at regular intervals. The flushing solution was switched to MilliQ water to obtain the tracer breakthrough data. All the injecting solutions were passed through a degasser before the experiment. The history of the desorption experiment run was presented in Table 5.1. The effluent was collected at regular intervals with a fraction

collector and samples were analyzed for pH. Filtered samples were analyzed for fluoride, major anions and filtered and acidified samples were analyzed for cation. $\delta^{18}O$ and δ^2H values were analyzed for selected samples.

5.2.4. Chemical analysis

The detailed procedure for analysis of soil pH, particle density, surface area, grain size distribution, soil leachable ion concentration, effluent concentration, mineralogical composition, elemental concentration, and FTIR spectra are described in Section 2.1.

Stable isotopes, $\delta^{18}O$ and δ^2H were analyzed with a PICARRO L2130-I δD and $\delta^{18}O$ High-Precision Isotopic Water Analyzer, with guaranteed precision of < 0.025 ‰ for $\delta^{18}O$ and < 0.1 ‰ for δ^2H.

Table 5.1: Fluoride desorption experiment history

Experiment run history	PV/time	Injecting solution
First run	7.7	ICEFIELD water
First stop flow	9.4hours	-
Second run	7.11	ICEFIELD water
Second stop flow	12.4hours	-
Third run	5.9	ICEFIELD water
Third stop flow	37.0hours	-
Fourth run	5.90	ICEFIELD water
Fourth stop flow	85.4hours	-
Fifth run	7.1	DI water

5.3. Parameter optimization and numerical modeling

5.3.1. Estimation of transport parameters using CXTFIT

Stable isotopes of ^{18}O and δ^2H were used as tracers in the column during fluoride desorption to determine the dispersion coefficient and other mass transfer properties. The program named CXTFIT 2.0 (Toride et al., 1995) was used to describe tracer

transport.

CXTFIT 2.0 (Toride et al., 1995) is a computer program for estimating solute transport parameters using a nonlinear least-squares parameter optimization method. In this program, the advection-dispersion equation (ADE) was used to solve the inverse problem by fitting mathematical solutions of theoretical transport models to experimental results. Equation 5.1 represents the generic form of the ADE for a sorbing solute assuming one-dimensional steady flow in a homogenous, isotropic porous medium:

$$\theta \frac{\partial C}{\partial t} + \rho_b \frac{\partial q_e}{\partial t} = \theta D_L \frac{\partial^2 C}{\partial x^2} - \theta v_x \frac{\partial C}{\partial x} \qquad (5.1)$$

where, C: concentration in liquid phase (ML^{-3}), x: distance (L), t: time (T), v_x: average linear velocity in the x direction (LT^{-1}), D_L: coefficient of longitudinal hydrodynamic dispersion (L^2/T), θ: volumetric water content ($L^3 L^{-3}$), ρ_b: dry soil bulk density (ML^{-3}) and q_e: sorbed concentration (MM^{-1}). In the case of linear sorption, the relation between the sorbed concentration and solution concentration can be defined by equation (5.2) as:

$$q_e = K_d C \qquad (5.2)$$

where K_d is an empirical distribution coefficient ($L^3 M^{-1}$). The term retardation factor (R) is defined as:

$$R = 1 + \frac{\rho_b K_d}{\theta} \qquad (5.3)$$

Equations (5.4) and (5.5) below represent the dimensionless physical non-equilibrium ADE (PNADE). The model is based on the assumption that the aqueous phase can be partitioned into mobile and immobile regions.

$$\beta R \frac{\partial C_m}{\partial T} + (1 - \beta) R \frac{\partial C_{im}}{\partial T} = \frac{1}{P_e} \frac{\partial^2 C_m}{\partial X^2} - \frac{\partial C_m}{\partial X} \qquad (5.4)$$

$$(1 - \beta) R \frac{\partial C_{im}}{\partial T} = \omega (C_m - C_{im}) \qquad (5.5)$$

where, $\omega = \frac{\alpha L}{\theta v}$, $\beta = \frac{\theta_m + f \rho_b K_d}{\theta + \rho_b K_d}$ and $P_e = \frac{vL}{D_L} \qquad (5.6)$

where $T = vt/L$ and $X = x/L$ are dimensionless representations of time and distance along the column, and subscripts m and im indicate the mobile and immobilize zones

99

respectively; α is the first-order mass transfer coefficient (T^{-1}), β represents the fraction of mobile water in the case of a nonreactive solute, f is the fraction of adsorption sites that equilibrates with the mobile liquid phase.

$\delta^{18}O$, and δ^2H breakthrough during injection and washout processes were used to estimate various transport parameters using the CXTFIT program. Both equilibrium and non-equilibrium models were used to estimate the model parameters by fitting the experimental results.

Stable isotopes, $\delta^{18}O$ and δ^2H are considered non-reactive, hence, their R values were set to 1 in the fitting program. Effluent δ^2H data were fit to determine D_L value in the equilibrium model, and Peclet number (P_e), mobile water fraction (β), mass transfer coefficient (α) in the non-equilibrium model. Fluoride retardation factor (R) was optimized by both the equilibrium and non-equilibrium models using the optimized parameters from the δ^2H tracer data.

5.3.2. *Geochemical transport code PHREEQC*

There are several public-domain geochemical models that can be used to model transport in addition to geochemical reactions. The geochemical computer model PHREEQC (Parkhrust and Appello, 1999) can be used to model solute transport in one dimension by considering aqueous complexation, precipitation and dissolution of minerals, adsorption, ion-exchange, and oxidation-reduction reactions.

PHREEQC uses a mixing-cell approach to simulate advection. The equilibrium aqueous and solid phase compositions are computed for each cell at the beginning of a transport simulation, then, transport is simulated by shifting the aqueous content of each cell to the adjacent downstream cell and the water is equilibrated with the solid-phase component again. The sequence of shifting, mixing, and equilibration is repeated for each cell until the total number of shifts are completed. By this approach, advective transport and chemical equilibrium are computed separately.

The PHREEQC dual-porosity (mobile-immobile) transport formulation involves a single row of mobile cells adjacent to an array of immobile cells (Parkhrust and Appello, 1999). One dimensional groundwater flow and solute transport occur in the mobile zone via advection, dispersion, diffusion, and solute water-matrix interactions.

Exchange of water and solutes between the two parts, i.e., mobile zone and immobile zone is allowed through diffusion. A first order exchange approximation for diffusion in the immobile zone is generally used in PHREEQC (Parkhrust and Appello, 1999). Mixing factors are used to approximate the diffusive transport of solutes between the mobile and immobile zones and within the immobile zone.

In this study, PHREEQC is used for simulating reactive transport of fluoride in the column during desorption by considering fluoride sorption to soil surface by surface complexation.

5.3.3. Geochemical transport code TOUGHREACT

TOUGHREACT (Xu et al., 2012) is a numerical simulation program for chemically reactive nonisothermal flows of multiphase fluids in porous and fractured media, written in Fortran 77. The program can consider a number of subsurface thermo-physical-chemical processes under various thermos hydrological and geochemical conditions. The code can accommodate any number of chemical species present in liquid, gas and solid phases and can handle physical and chemical heterogeneity present in the porous media effectively.

TOUGHREACT was also used in this study to explain fluoride transport behavior.

5.4. Results and discussion
5.4.1. Soil characteristics

The physical and chemical properties of the experimental soil are listed in Table 4.3 and are discussed in detail in section 4.4.1. A short summary of the results is as follows: the soil is acidic with an aqueous pH of 4.1 and the leachable fluoride from the soil is negligible (0.1 mg/kg). Mineralogical analysis indicated that the soil is dominated by quartz and feldspars. The clay size fraction consisted of mainly kaolinite and chlorite. The elemental analysis indicated that the soil is rich in Si, Al and Fe. Chemical extraction with acid digestion followed by H_2O_2 oxidation showed that the total Al concentration is ~19.5 mg/kg and total Fe concentration is 14.9 mg/kg. Analysis of the

N_2 gas sorption/desorption isotherm of soil indicates that the soil is dominated by meso-pores with small amount of microporosity (Table 4.2).

5.4.2. *Major chemical composition during fluoride desorption*

The composition of the effluent from the column during fluoride desorption was dominated by Na, K, Ca, Mg, Al and Fe (for these elements, the total concentration was measured by ICPMS, Section 2.1.1.4), Cl^-, SO_4^{2-} and NO_3^-. Figure 5.2 shows the effluent concentrations of Na, Ca, Al and Fe during fluoride desorption from the column.

Effluent concentration of Na decreased with time to follow the advective trends (Figure 5.2 (a)). This high Na in solution is because of the injection of fluoride as NaF during
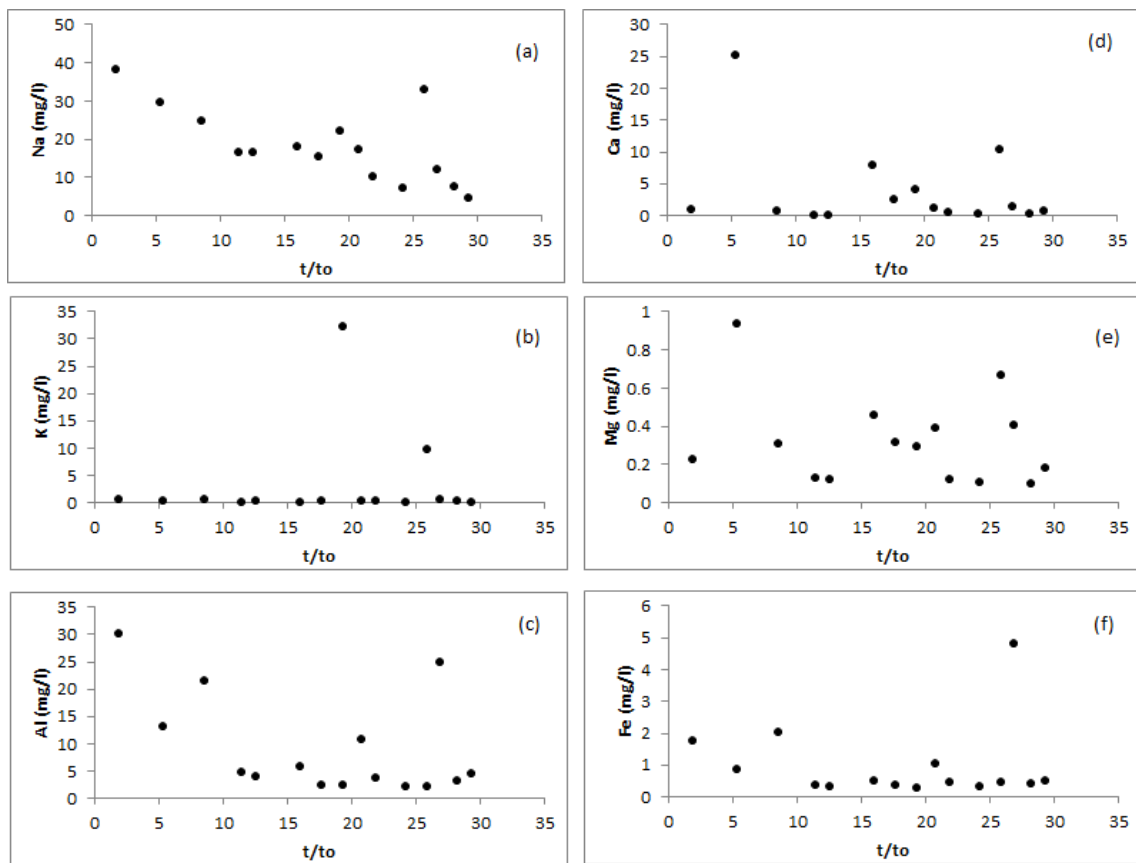
Figure 5.2: Temporal evolution of aqueous solution concentrations (a) Na, (b) Ca, (c) K, (d) Mg, (e) Al and (f) Fe in the effluent solutions during fluoride desorption from the column. The X-axis represents number of pore volumes.

fluoride sorption experiment. Ca in the effluent first increased abruptly after 5 pore volumes and then decreased towards the infiltrating solution (Figure 5.2 (b)). Effluent concentration of K remained constant except after 19.4 and 25.9 pore volume (Figure 5.2 (c)). Concentration of Mg in effluent does not change drastically, however, the concentration profile is similar in behavior to that of Ca (Figure 5.2 (d)).

Al in solution during fluoride desorption decreases with time, with an abrupt increase after MilliQ water injection (Table 5.1 and Figure 5.2 (c)). Because the infiltrating solution does not contain Al and the leachable Al from the original soil is low (0.25 mg/l), such high Al in the effluent is considered to be due to fluoride-induced Al release. Al dissolution from Al-containing minerals at low pH and high fluoride concentration can effectively be facilitated by fluoride (Haidouti, 1995; Harrington et al., 2003; Zhu et al., 2004). According to Polomski et al. (1982) and Nordin et al. (1999), fluoride ions replace –OH/-OH$_2^+$ groups bound to surficial Al atoms via ligand exchange, loosen other Al–OH bonds, and facilitate Al release.

5.4.3. *Fluoride sorption kinetics and pH change during fluoride sorption experiment*

Interrupted flow experiments were performed in order to discriminate between dispersion and non-equilibrium effects. During flow interruption, solute transport proceeds only by diffusion. These methods can be used to discriminate between various sets of processes, such as rate-limited vs. nonlinear sorption and physical nonequilibrium vs. heterogeneity (Brusseau et al., 1997).

5.4.3.1. *pH change during sorption*

Since pH is an important factor in adsorption and desorption of fluoride (Wang et al., 2002; Padhi and Muralidharan, 2012), pH change may cause re-dissolving of solid phase fluoride into the solution phase. Hence, the effluent pH was routinely checked for any change in pH, and is represented in Figure 5.3. The pH values in the effluent increased gradually with time, requiring 17 pore volumes to reach the influent pH value. Stop-flow (SF) events led to an increase in the effluent pH (~0.04 pH unit) immediately after the SF events. However, this small change in pH may not be unanimously attributed to the effect of change in flow conditions. These results

collectively indicate that the hydroxyl ion release from soil was a kinetic process that could be due to the pH buffering reactions and/ or ion exchange processes.
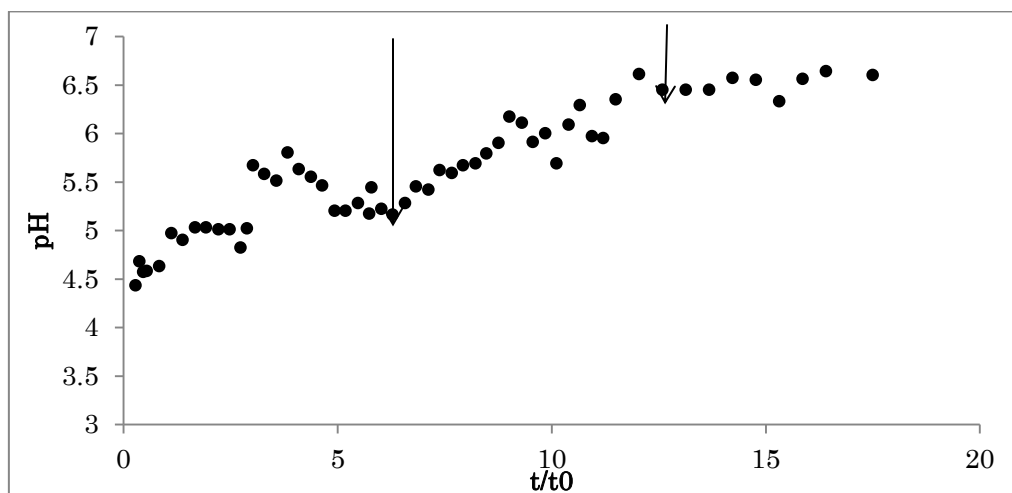
Figure 5.3. pH change during fluoride sorption in the column. The arrows show the points when stop flow events are applied. The horizontal axis represents number of pore volumes

5.4.3.2. Fluoride concentration profile during sorption flow through experiment

At the initial stage of the experiment, fluoride sorbed quite effectively in the soil column. Fluoride starts to appear in the effluent after 6.5 pore volumes (Figure 5.4), which shows high sorption capacity of soil. The effluent fluoride concentration increased with time and reached the infiltrating fluoride concentration after 17 pore volumes. The characteristics of fluoride sorption breakthrough curve is similar to that of the effluent pH break through curve (Figure 5.3), i.e., the effluent concentration reached the infiltrating solution concentration after 17 pore volumes. After the stop flow events, the effluent fluoride concentration was decreased, which shows the kinetic behavior of fluoride sorption, because it provides more time for fluoride sorption (Figure 5.4).
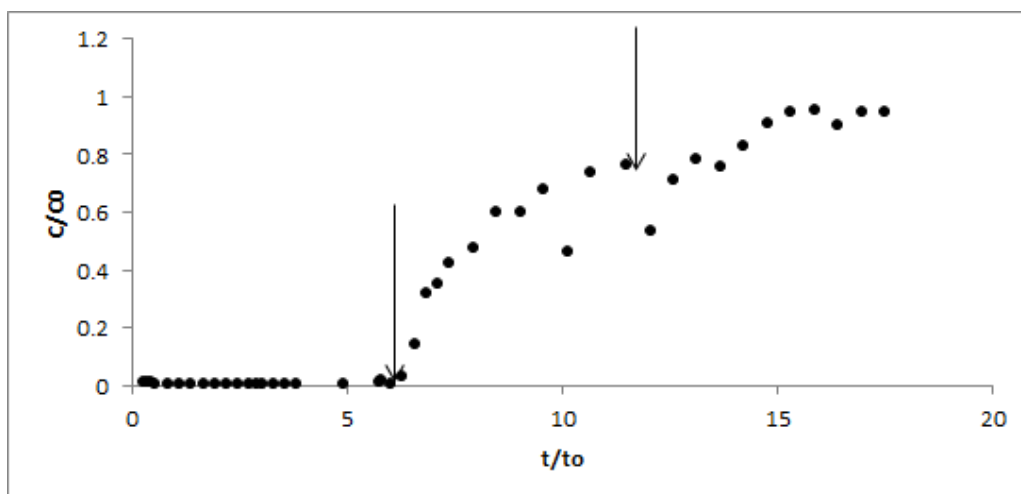
Figure 5.4. Breakthrough curve of fluoride sorption in the column. Two stop flow events are also included. The horizontal axis represents number of pore volumes

5.4.4. *Fluoride desorption kinetics and pH change during fluoride desorption experiment*

5.4.4.1. *pH change during desorption*

The effluent pH immediately after the fluoride sorption experiment was 6.5 (Figure 5.5). Effluent pH during fluoride desorption for the first pore volume was less than 6.5 (Figure 5.5), although the infiltrating solution has a pH of 7.0, which could be due to the change in pH of the pore-water during the resting time (time allowed between end of fluoride sorption experiment and start of fluoride desorption experiment) or the pH buffering capacity of the sediment, such as ion exchange reactions of major cations that released H^+. The effluent pH changed slightly (6.5 to 7.1) with time during fluoride desorption until the flow was interrupted for the second time (~ 15 pore volume). pH change of the effluent after second stop flow event was abrupt, which could not be explained. Effluent pH also changed slightly before and after the SF events, e.g., pH decreased from 6.98 to 6.77 after first SF event and from 7.03 to 6.81 after second SF event. A pH increase was observed after third and fourth SF events with a pH increase from 6.9 to 7.0 in the case of third stop flow and 7.0 to 7.3 in the case of fourth.
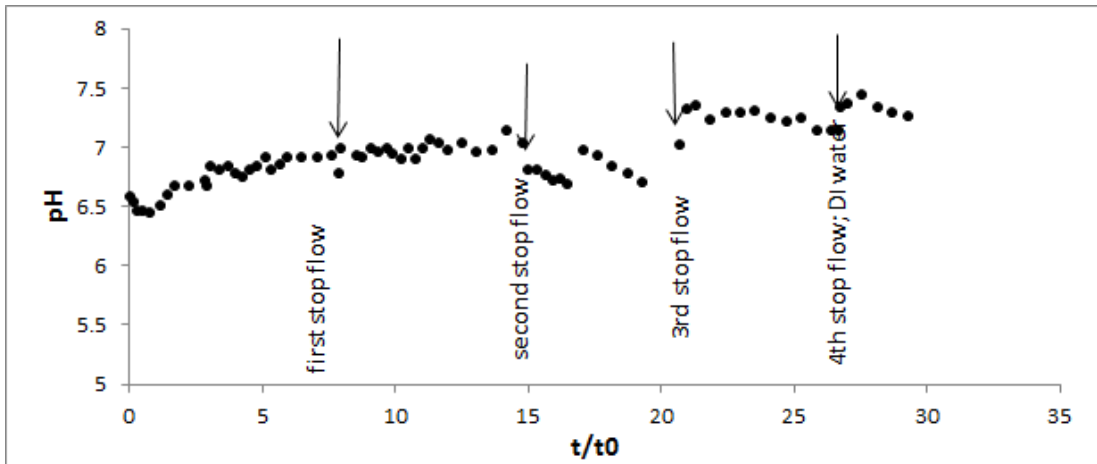
Figure 5.5. pH change during fluoride desorption in the column with number of pore volumes. The arrows show the points when stop flow events are applied.
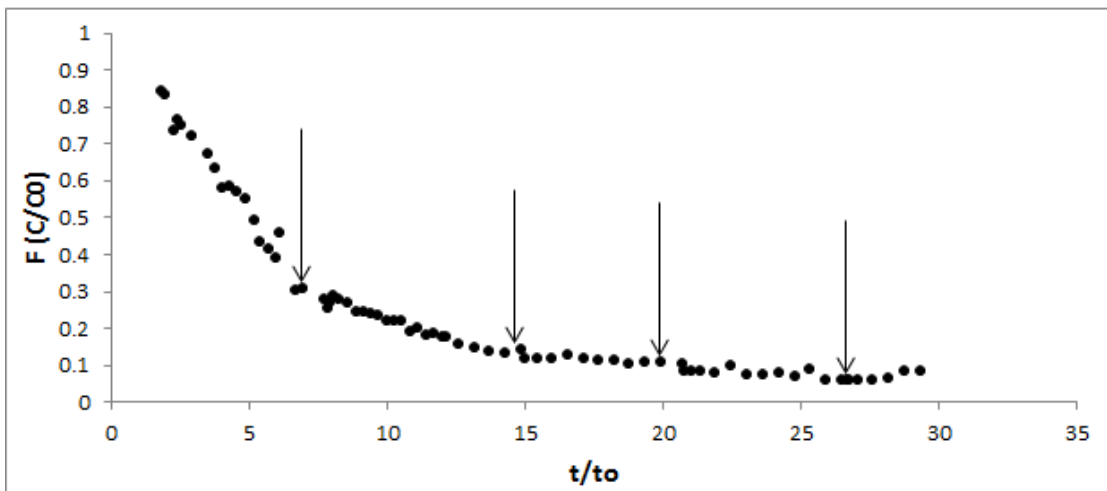
Figure 5.6. Breakthrough curve of fluoride desorption in the column with number of pore volumes. Four stop flow events are also included

5.4.4.2. Fluoride concentration profile during desorption flow through experiment

The effluent fluoride concentration decreased gradually until the first stop flow event (about 7th pore volume) with the continuous flush of fluoride-free influent (Figure 5.6). After 7th pore volume, the effluent fluoride concentration decreased more slowly, which suggests that fluoride was sorbed to sites with a range in kinetic and/or thermodynamic properties (Liu et al., 2008). After the first SF event, there is a decrease in fluoride effluent concentration, which recovered after 1 pore volume. No measurable

change in aqueous concentration of fluoride was observed after second, third or fourth stop flow events. A rise in effluent concentration following a no-flow period has been reported, which could be interpreted as desorption being kinetically controlled (Liu et al., 2008; Tran et al., 1998). Our experiments were conducted in a constant laboratory temperature of 25.0ºC, hence, effect of change in temperature on fluoride desorption may be negligible.

The effluent fluoride concentration gradually decreased with time, reflecting the slow depletion of sorbed-fluoride in the soil column. Moreover, the column was not completely flushed with in the experiment time (~30 pore volumes) with the continuous flush of fluoride free solution.

5.4.5. *Tracer breakthrough curve*

The breakthrough curves for the water isotopes $\delta^{18}O$ and δ^2H in the column are shown in Figure 5.7. The breakthrough curves are symmetric for both $\delta^{18}O$ and δ^2H. As expected, for a non-reactive solute, $\delta^{18}O$ and δ^2H transports were not retarded through the column and their R value can be set to be 1.0. The data for δ^2H were used to calculate the dispersion coefficient (D_L), α and β from the fit to the equilibrium and non-equilibrium ADE (Figure 5.8). The measured porosity (θ), bulk density (ρ_b), and pore velocity (v) values (Table 5.2) were used.

Figure (5.8) shows the results of optimization for the δ^2H breakthrough curve using the ADE and PNADE models. However, the fitted parameters are highly dependent on the initial values if all the three parameters (D_L, α and β) are optimized in the PNADE model. Table (5.3) represents the effect of initial values on the fitted parameters. When the D_L value is fixed at $8.9*10^{-7}$ m^2/s and α and β were optimized, the results were quite similar to that of ADE, suggesting that physical nonequilibrium is not having significant contribution on the tracer breakthrough data (Figure 5.8). The goodness of fit can be estimated from the mean square error parameter.

Moreover, considering a D_L value of $8.9*10^{-7}$ m^2/s, as calculated from the ADE fit to the δ^2H breakthrough data, the Peclet number ($v*L/D_L$) is calculated to be 15.75, which indicates that the flow regime within the column was dominated by advection (Fetter, 1999) which may allow to neglect dispersion effects in the modeling of BTCs of

chemically reactive fluoride. Furthermore, immobile or stagnant regions within the columns, if present at all, may not be significant for the transport of the conservative tracer, which could be confirmed from the fact that, no measurable changes in δ^2H was observed during the stop flow events.
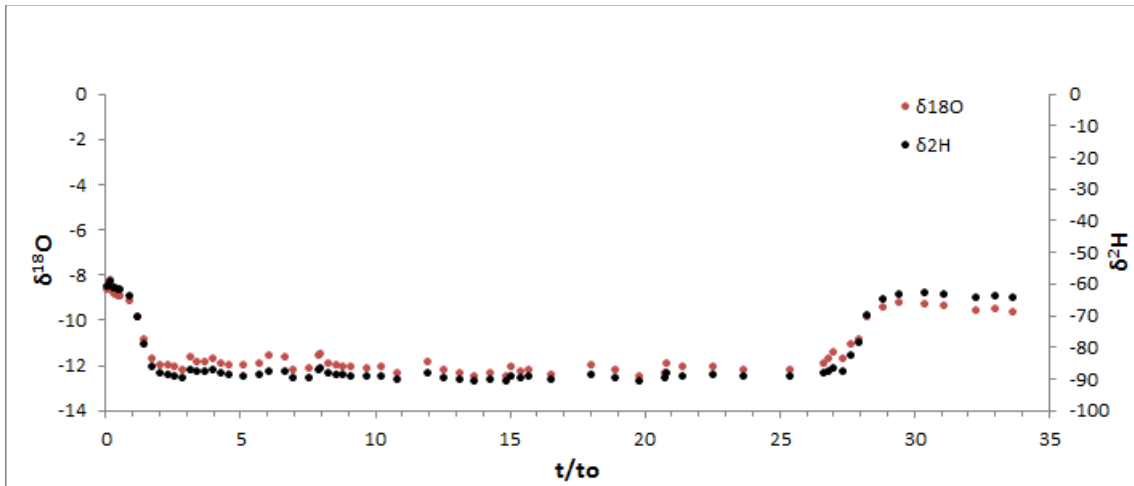
Figure 5.7: Breakthrough curves for $\delta^{18}O$ and δ^2H during fluoride desorption. The arrows indicate stop flow events. The x-axis indicates number of pore volumes.
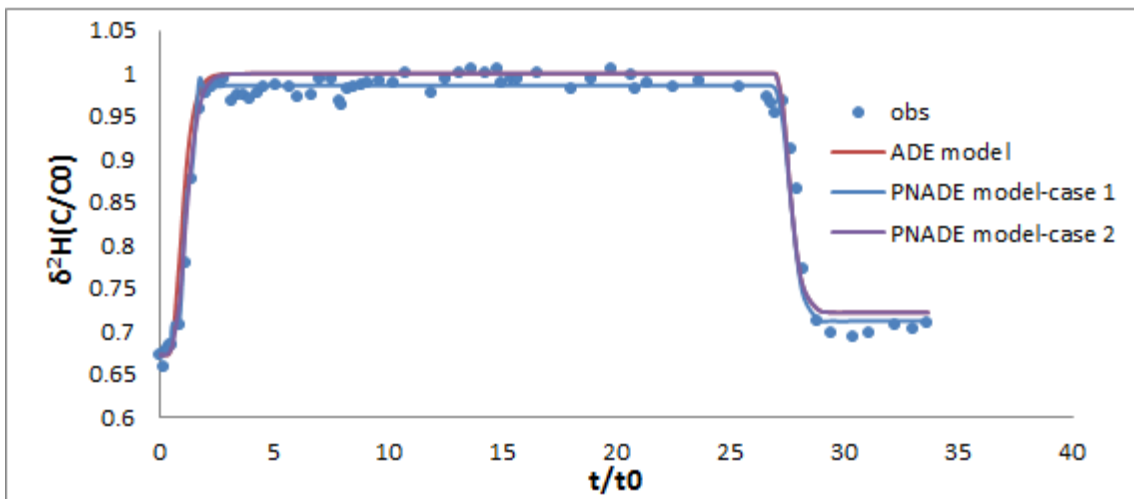
Figure 5.8. δ^2H breakthrough curve. The points are the observed values. Red line represents the model calculations from the ADE model, blue line and violet line represent model calculations from the PNADE model, where in case 1, all the three parameters (D_L, β and ω, Table 5.3) were optimized and in case 2 the D_L value was kept constant at $8.9*10^{-7}$ m²/s and β and ω were optimized.

Table 5.2. Parameters used in the modeling

Parameters	Symbol	Unit	value
Column length	L	cm	30
Pore velocity	v	m/s	$4.55*10^{-5}$
[a]Dispersion coefficient	D_L	m^2/s	$8.9*10^{-7}$
Total porosity	θ	…	0.39
[b]Retardation coefficient	R	…	9.63
[c]Retardation coefficient	R	…	5.16

[a]Dispersion coefficient was optimized from fitting the δ^2H breakthrough curve to the ADE

[b]Retardation factor for fluoride was calculated by fitting fluoride breakthrough curve during sorption to the ADE.

[c]Retardation factor for fluoride was calculated by fitting fluoride breakthrough curve during desorption to the ADE.

5.4.6. *Modeling fluoride sorption and desorption behavior*

A literature search revealed that only a few studies focused on the kinetics of fluoride retention and release during transport in soils. For example, Johannes et al. (1996) and Usunoff et al. (2009) studied fluoride transport in a quartz-sand packed column and Begin et al. (2003) studied fluoride transport in an unsaturated soil, using the linear *Kd* model. Kinetic adsorption data have the advantage that they can account for the non-equilibrium sorption behavior, which may result from the heterogeneities of sorption sites and diffusion processes in the interface between the liquid phase and the soil matrix.

This study simulates the fluoride desorption behavior in a soil column, set in the PHREEQC 1-D transport program. The simple linear *Kd* model and the two domain model were applied to the fluoride desorption concentration data. Fluoride sorption in the soil used in the column experiment was found to be explained by surface complexation reactions (Chapter 4). Surface complexation (SC) model has an advantage over the linear *Kd* model because the SC model with surface reactions with the same reaction constants can be used to describe the fluoride sorption under variable

Table 5.3: Estimates of fitted parameters and coefficient of determination (Mean Square Error) for the optimization of δ^2H Breakthrough curve (during injection) for different sets of initial values

Case	v	D	R	β	ω	r^2	MSE
1. Two parameter (β, ω) estimation							
Initial values	393.1	765.3	1	0.9	10	-	-
Final values	Fixed	Fixed	Fixed	2.57e-3	68.2	0.985	2.74e-4
Initial values	393.1	385.3	1	0.9	10	-	-
Final values	Fixed	Fixed	Fixed	4.42e-3	100	0.979	3.89e-4
Initial values	393.1	100	1	0.9	10	-	-
Final values	Fixed	Fixed	Fixed	7.74e-3	15.72	0.942	1.1e-3
Initial values	393.1	765.3	1	0.1	10	-	-
Final values	Fixed	Fixed	Fixed	4.3e-3	98	0.984	2.9e-4
2. Three parameter (D, β, ω) estimation							
Initial values	393.1	765.3	1	0.9	10	-	-
Final values	Fixed	2.27e-2	Fixed	8.13e-3	14.21	0.986	2.64e-3
Initial values	393.1	385.3	1	0.9	10	-	-
Final values	Fixed	2.27e-2	Fixed	4.6e-2	11.4	0.974	5.05e-3
Initial values	393.1	100	1	0.9	10	-	-
Final values	Fixed	775.3	Fixed	0.999	1.2e-3	0.933	1.33e-3
Initial values	393.1	765.3	1	0.1	10	-	-
Final values	Fixed	1.49e-2	Fixed	1.78e-2	19.4	0.985	2.84e-4

solution compositions such as pH and ionic strength. Whereas, the *Kd* values have to be varied to describe fluoride adsorption and desorption under different solution compositions (Chapter 4). For reactive systems, the traditional ADE with reaction has been shown to give inaccurate predictions of experimental results (Gramling et al., 2002; Kapoor et al., 1997). This is because geochemical reactions occur locally at the pore scale where the ADE assumes complete mixing of the concentrations.

5.4.6.1. Linear Kd model

First, the linear Kd model was used to explain fluoride sorption and desorption data. The model parameters that are used are listed in Table 5.2. The retardation factor, calculated during fluoride sorption by fitting fluoride sorption data in the CXTFIT program was 9.26 and that for fluoride desorption was 5.16. As discussed above, different *Kd* values are required to explain model calculations with change in pH and solution concentrations. These values were then used in the forward simulation to explain fluoride sorption and desorption kinetics.

In PHREEQC, there is no way to strictly implement a linear *Kd* model. By specifying an imaginary surface with a very large number of binding sites, the model could behave linearly as long as the soil chemistry stays within reasonable limits. Nevertheless, it is obvious that this approach is not realistic because the number of binding sites in the model actually should represent the reality (Jaremalm et al., 2013). Hence, TOUGHREACT was used to simulate fluoride desorption processes by linear *Kd* model.

Figure 5.9 shows the calculated results from the linear *Kd* model during fluoride desorption, by using *R* value of 5.16, that was estimated from the fit to fluoride desorption breakthrough. The model poorly fit the observed data, especially the tailing part of desorption could not be observed.

A range of retardation factors (4.1 to 138) are reported by Begin et al., (2003), which was attributed to the differences in the soil properties. For example, highly acidic soils (pH of 3.9 to 4.1) and alkaline soils (pH 8.0) had low retardation factor which could be explained by the formation of soluble fluoride complexes at this pH. A *R* value

of 9.6 was estimated from the model fit to fluoride sorption data. The linear model was also tested with a *R* value of 9.6 to explain fluoride desorption behavior, however, the model fit was not improved.
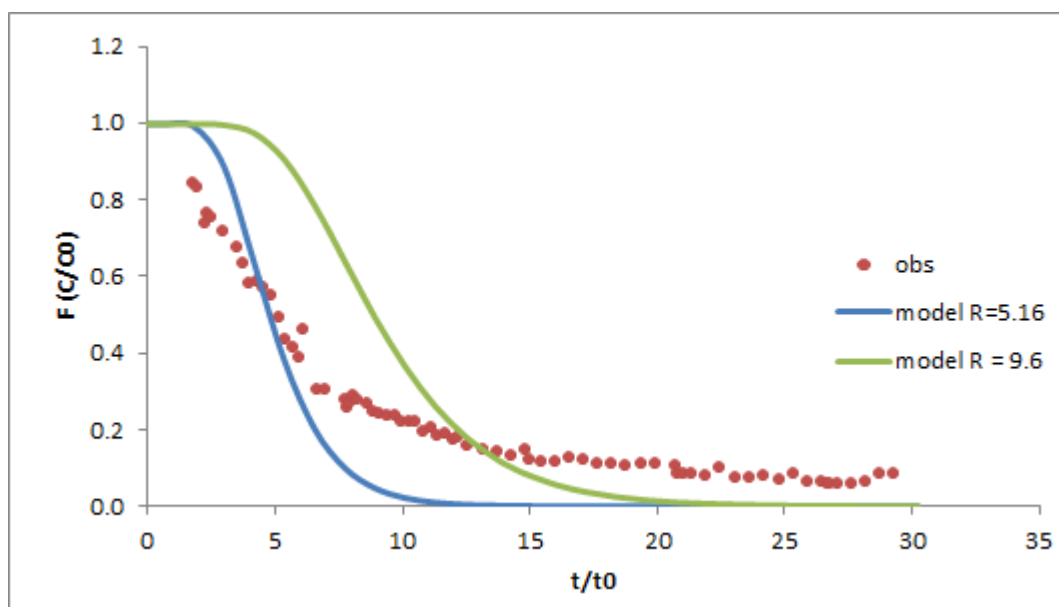
Figure 5.9. Model results for fluoride desorption from the column. The x-axis represents number of pore volumes. The points are the observed data and the lines are simulated results with linear *Kd* model (blue line: with a retardation factor of 5.16 and green line: with a retardation factor of 9.6).

5.4.6.2. Model including surface complexation

5.4.6.2.1.   Scaling of model parameters

Scaling of the parameters is necessary to model contaminant transport using geochemical coupled transport codes because the surface complexation constants strongly depend on the value of the surface site density (Davis and Kent, 1990). According to Davis and Kent (1990), the constants derived using a known surface site density value for a given system may not be directly used for predicting adsorption in another system that has a different surface site density value. Sverjensky (2003) proposed a correction for this purpose.

Equilibrium constants of soil surface reactions were taken from Chapter 4. The transport model used in this chapter involves different solid concentration, although the

site density was the same. Hence, the traditional molar-based constants (K^0) were converted into intrinsic equilibrium constants (K^θ) using the corrections established by Sverjensky (2003).

For example, for the reaction

$$>SOH + H^+ = >SOH_2^+,$$
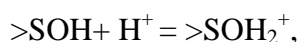
K^θ can be calculated as:

$$K^\theta = K^0 \left(\frac{NA}{N^*A^*} \right) \qquad (5.7)$$

and for the reaction

$$>SOH = >SO^- + H^+,$$
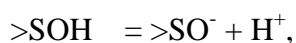
$$K^\theta = K^0 \left(\frac{NA}{N^*A^*} \right)^{-1} \qquad (5.8)$$

where, N and A are site density (sites/nm^2) and specific surface area (m^2/g) of the sample and N* = 10 sites/nm^2 and A* = 10 m^2/g are the selected reference site density and specific surface area.

K^θ can also be calculated for other reactions in the similar way as that of reactions (5.7) and (5.8). The new molar-based constants can be calculated from these intrinsic equilibrium constants.

Following Chapter 4 for the fluoride sorption to the soil, the surface complexation reactions considered are shown in Table 5.4. Table 5.4 also lists the reaction constants after correction for solid concentration and surface area as per Sverjensky (2003), as described before.

The surface area of the soil, 7.67 m^2/g, was as listed in Table 4.2. Site density parameter is $9.356*10^{-2}$ moles/l (optimized site density corrected for solid concentration and surface area).

Table 5.4: Surface complexation reactions, optimized intrinsic surface complexation reaction constants (logK$_{int}$), and model parameters.

Surface complexation reactions		logK$_{int}$	
	Reaction number	Table 4.7 (Chapter 4)	corrected[a]
$>SOH + H^+ = >SOH_2^+$	4.3	4.67	5.9
$>SOH = >SO^- + H^+$	4.4	-8.26	-10.42
$>SOH + F^- + H^+ = >SF + H_2O$	4.5	10.04	12.67
$>SOH + F^- = >SOHF^-$	4.6	5.78	7.3
$>SOH + 2F^- + Al^{3+} = >SOAlF_2 + H^+$	4.8	10.91	13.77
Surface sites density (moles/l)		$3.29*10^{-4}$	$9.3*10^{-2}$
Surface area (m^2/g)		9.68	7.67

[a] logK$_{int}$ values are corrected as per Sverjensky (2003)

5.4.6.2.2.   Transport model including surface complexation

Fluoride sorption was described by a diffuse double layer model (Dzombak and Morel, 1990). The initial soluble ion and mineral concentrations are as listed in Table 4.3.

Modeling fluoride sorption was difficult because of the application of stop flow events before the breakthrough (Figure 5.4) and unavailability of other geochemical parameters. Thus, in this study, only desorption experimental results were used for detailed analysis.

Model 1

Fluoride desorption kinetics was modeled for the second column after the fluoride sorption experiment. First, a 1-D reactive transport model was considered accounting for fluoride sorption represented by fluoride sorption reactions (Table 5.4) with corrected equilibrium constants and site density. However, the model predicted

high fluoride sorption with the calculated site density. Consequently, the site density parameter was decreased by trial and error to fit the fluoride effluent data. The site density considered in the final model is $3.356*10^{-2}$ moles/l. This variation could be due to the variation in the soil properties, e.g., the batch experiments of Chapter 4 used < 250 μm grain sized soil, whereas the column considered for fluoride transport consists of soil with < 2mm grain diameter. This kind of corrections were already adapted by Liu et al., (2008), e.g., for corrections of $logK_{int}$ of U(VI) sorption reactions. The simulated results from the final model were shown in Figure 5.10. The model well predicted fluoride desorption from the column. Stop flow events were not included in the final model (Figure 5.10), as the effect of stop flow on fluoride desorption was negligible (Figure 5.6) and the model including stop flow events where flow interruptions were defined by diffusive flow only, did not produce any change in concentration during fluoride desorption. The final set of flow and transport parameters and geochemical parameters are presented in Table 5.5.

Model 2: The two domain model coupled with surface complexation reaction:

The concept of a two-domain model for solute transport in soil was presented by Coats and Smith (1964). This model has been proven to be a versatile and popular method for analyzing solute breakthrough curves (BTCs). The final set of model parameters considered in the PNADE model is presented in Table 5.5. The porosity (θ) and velocity (v) were the measured values, while the dispersion coefficient was determined by fitting the δ^2H breakthrough curve to the ADE (Figure 5.8). The mass transfer coefficient (α) and mobile water fraction β values are adjusted by trial and error and considered to be $1.32*10^{-3}$ s^{-1} and 0.73, respectively. The simulated results from the PNADE model are quite similar to that of the results from ADE model (Figure 5.10). The agreement of the predicted values for fluoride desorption data with these two different models demonstrates that physical nonequilibrium may not be important in the conditions simulated in this study.

Numerical oscillation could not be eliminated in both the model calculations (ADE and PNADE model), which resulted in overshooting in the fluoride breakthrough

curve during early part of the simulation calculations, however, the tailing was not affected.

Table 5.5: Parameters considered in the final model

Parameters	ADE model	PNADE model
Column length (cm)	30	30
Pore velocity (m/s)	$4.55*10^{-5}$	$4.55*10^{-5}$
[a]Dispersion coefficient (m^2/s)	$8.9*10^{-7}$	$8.9*10^{-7}$
Total porosity	0.39	0.39
Mas transfer coeff. (sec^{-1})	--	$1.32*10^{-3}$
Mobile water fraction	--	0.76
logK for reactions		
4.3	5.9	5.9
4.4	-10.42	-10.42
4.5	12.67	12.67
4.6	7.3	7.3
4.8	13.77	13.77
Sites density (moles/l)	$3.356*10^{-2}$	$3.356*10^{-2}$
Surface area (m^2/g)	7.67	7.67
Influent water	Fluoride free water with pH 7 in both the model	
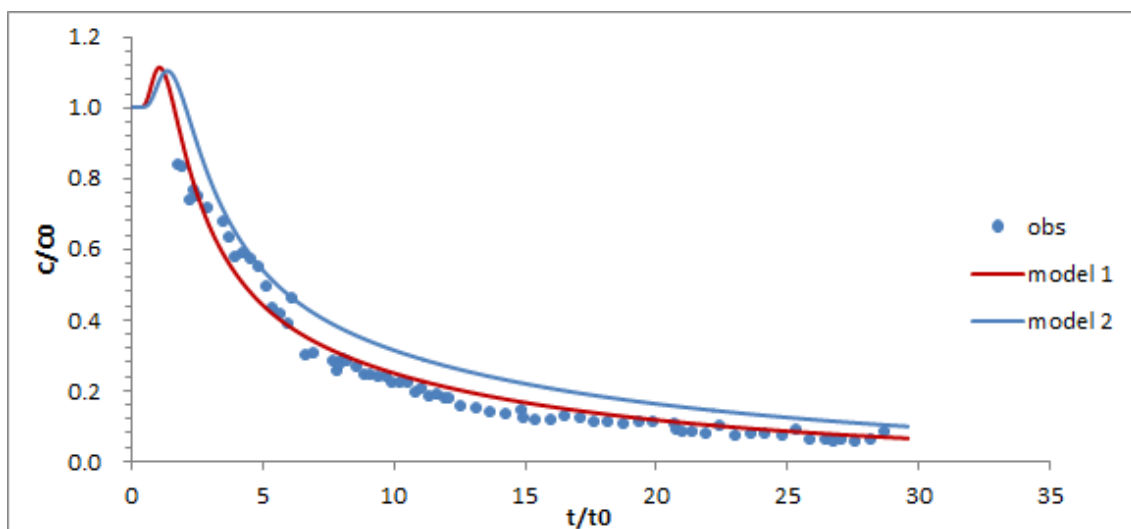
Figure 5.10: Fluoride desorption from the soil column. Symbols are the experimental data, and lines are model-calculations. Model 1 represents model calculations, where fluoride sorption was described by surface complexation and the surface complexation constants were corrected. Model 2 represents model calculations with the two-domain model coupled with surface complexation reactions, with the two-domain model parameters estimated from δ^2H breakthrough data and corrected to fit the observed fluoride desorption data.

A drop in effluent concentration immediately after the resumption of flow indicates nonequilibrium behavior (Brusseau et al., 1989). In this study, a small drop in effluent fluoride concentration was observed after the first stop flow event, which may suggest nonequilibrium, however, stop flows after the first stop flow does not have significant effect.

The Damkohler number (DaI) (DaI = $\alpha L/v$) can indicate whether reaction rates should be considered in analyzing sorption/desorption processes. For example, if DaI$\gg$1, then the solid phase concentration is considered to be in equilibrium with the solution phase concentration for the time scale of the experiment (Barry and Li, 1994). In this experiment, the combination of DaI value of 8.7 and β value of 0.73 may suggest equilibrium conditions.

Considering the multitude of processes and scales that may contribute to rate limited mass transfer, e.g., when fluoride will exist as adsorbed phase that could be associated with mineral surfaces, dispersed in grain coating materials, and/or distributed

117

within intra-aggregates, the multisite kinetic processes should be considered (Haggerty and Gorelick, 1995). The multirate mass transfer models have already been developed and applied for contaminant release, e.g., U(VI) release from sediment by accounting for the surface processes of U(VI) sorption to the sediment (Liu et al., 2009). In addition, the mixing model approach of PHREEQC has been questionable by many researchers to predict effluent release from soil/sediment in comparison to the sequential iteration approach. Hence, the model can be considerably improved by considering a multi-site and multirate mass transfer processes.

5.5. Conclusions

Potential applications of the two-region model for predicting fluoride transport under conditions of chemical and physical nonequilibrium were demonstrated in this chapter. The inclusion of surface complexation of fluoride on the soil surface improved the description of effluent data. The results from the PHREEQC dual-porosity transport model that uses a finite-difference approach showed good agreement with the observed data.

The fate and transport of fluoride in the geo-environment is important considering possible contamination of groundwater and plant availability. Sorption of fluoride in a soil column during fluoride transport in a soil column showed that the sorption is high and could be explained by surface complex formation on the soil surface.

Stable isotopes of water (δO^{18} and $\delta^2 H$) are found to be useful tracers for column experiments in laboratory scale.

Chapter 6: Summary, Implications and Recommendations

6.1. Summary

The results of this thesis can be summarized as follows:

Leachable fluoride from soil can contaminate the shallow groundwater under suitable conditions. Hence, it is necessary to decipher fluoride transport processes in soil. Studying contaminant transport in the laboratory scale gives an idea to scale the geochemical reactions and kinetics into reactive transport models for large-scale porous media containing multiple flow domains (e.g., mobile and stagnant zones). The overall objectives of this study were (1) to identify the mechanism of fluoride sorption/desorption in a granitic soil under wide range of environmental conditions, (2) to develop a fluoride reactive transport model describing the physical and chemical non-equilibrium processes observed in laboratory scale.

First, areas with fluoride contamination of groundwater in India (e.g. Rangareddy, Telengana) and Japan (Nishinomiya, Japan) were selected and investigated to understand the behavior of fluoride in groundwater and soil system. Granitic soils from Nakatsugawa (Japan) and Tsukuba (Japan) were also investigated to understand the geochemical factors responsible for fluoride mobilization in the soil system. The leachable fluoride in Rangareddy, India is comparatively high (1.2-30 mg/kg) and corresponds to the occurrence of dissolved fluoride in groundwater in the respective area (2.0-2.3 mg/l). Fluoride in groundwater and soil leachate is negligible in Nakatsugawa (Japan) and Tsukuba (Japan). In Nishinomiya (Japan), soil leachable fluoride is in lower range although shallow groundwater is contaminated with fluoride. Soil pH, mineral constituents and infiltrating solutions were found to be correlated to soil leachable fluoride. From the field observations, it can also be inferred that in areas with heavy rainfall, the leachable fluoride is negligible whereas in arid/semi-arid areas, the leachable fluoride is rather high, which may suggest secondary enrichment of fluoride in soil.

Next, fluoride sorption to calcite was studied because calcite is a major soil constituent in calcareous soil and fluorite precipitation was reported to be the mechanism of fluoride removal from aqueous solution. The batch experiment results and surface complexation modeling suggest that at low fluoride concentration, surface adsorption could be the governing mechanism. Fluoride adsorption was described by the formation of two surface complexes, $>CaF^0$ and $>CO_3FCa^0$ on the calcite surface. The database for fluoride sorption on calcite was created which can be used in other studies for fluoride interaction with calcite. The importance of this part of research lies in the understanding of the confirmation of fluoride interaction with calcite at lower fluoride concentrations, where fluorite precipitation does not occur, by surface complexation modeling approach.

Next, fluoride sorption to a granitic soil was investigated. The results from batch experiment, surface complexation modeling, pore structure analysis and spectroscopic investigation suggest strong fluoride retention in soil. The characteristics of pH dependent fluoride sorption were well understood by surface complexation modeling with general composite approach. Fluoride sorption was considered by the formation of $>SF$, $>SOHF$ and $>SOAlF_2$ complexes. The intrinsic surface complexation constants for fluoride sorption reactions and site protonation reaction along with surface site density were optimized. The results demonstrate the importance of including dissolved Al and Al-F complex sorption in the model, despite the fact that dissolved Al and Al-F complex sorption were neglected in previous studies.

Finally, kinetic transport of fluoride in a granitic soil was investigated in the laboratory during fluoride sorption and desorption. Sorption capacity of the soil is high with breakthrough occurring after 17 pore volumes of fluoride injection. Fluoride desorption was comparatively fast, and desorption was slow after 10 pore volumes of flushing with long tailing. No considerable effect of flow interruption on the effluent data during desorption was found, which is reasonable considering the high peclet number considered.

The linear Kd model was first used to explain fluoride desorption data. The transport parameters were optimized from the tracer data (stable isotope of water, $\delta^{18}O$

and δ^2H). The linear model could not explain fluoride desorption, especially the tailing during desorption. Hence, a geochemical model considering fluoride sorption in soil by surface complexation was developed and used to explain fluoride transport during desorption in the column. Both the single domain and two domain models were used to explain the observed data. Fluoride sorption was described by sorption to a generic surface site, and the intrinsic surface complexation constants for fluoride sorption reactions and surface site protonation and deprotonation reactions were corrected from that of the optimized results from batch experiments, in order to account for the site concentration. The results show that the model, where fluoride sorption was described by surface complexation could explain fluoride desorption observed data quite satisfactorily. The results from the two domain model does not vary much from that of the single domain model, which shows that in the experimental conditions, mass transfer to the immobile zones may not be important as that of considering fluoride sorption by surface processes.

The results of this thesis show that fluoride desorption is highly affected by pH and the interfering ions and presence of dissolved Al effects the model calculations. Long tailing was observed during fluoride desorption, which needs attention while designing remediation measures. Both of the two-domain model and single domain model produced almost similar breakthrough curves. Moreover, inclusion of fluoride sorption as surface complexation resulted good fit to the observation. Fluoride induced Al release from soil was observed which needs attention as the toxicity of Al-F complexes is controversial.

6.2. Implications

1. The results of this study show that the transport of fluoride is dependent on the geochemical factors. In highly contaminated soils, the slow and gradual release of fluoride can be of significant concern, under favorable conditions.

2. Dissolved Al is important to be considered in model applications considering fluoride sorption in presence of Al.

3. SCMs could successfully describe fluoride sorption behavior in contrast to the classic isotherm models.

4. Mobility of fluoride also depends on the complex form of fluoride (e.g., precipitate, surface bound or co-precipitate).

5. Since experimental and numerical investigation of kinetic behavior of fluoride in natural soil is first of its kind, the transport model can be used for further laboratory investigations and can be tested in the field by scaling up the parameters.

6. Stable isotope of $\delta^{18}O$ and $\delta^{2}H$ could be used as tracers in laboratory experiments without affecting the contaminant of concern.

7. The observations from this study also show fluoride induced Al release, which is another potentially toxic element, which warrants further investigation.

6.3. Recommendations

1. Fluoride measurement in soil solution:

   This study used colorimetric, ionmetric and chromatographic methods for fluoride analysis. The analytical results from batch experiments show that with increase in ionic strength of solution, Al release from soil increases. All of the methods used in this thesis for fluoride analysis are affected by Al in solution in addition to other parameters. Although different methods exist to diminish the effect of Al on fluoride measurement, attention should be paid to the methods used for removing Al interference. Also, during batch experiments relating soil and fluoride, ionic strength should be checked for possible Al release from soil in addition to fluoride.

2. Surface complexation modeling

   Dissolved Al and Al-F complex should not be neglected in the model, when Al is present in solution.

3. Fluoride desorption processes should be studied in more detail, e.g., under different flow conditions, under the influence of competing ions and different pH conditions. The two-domain model should be improved to account for the sorption to multi-sites at different rate of mass transfer processes.

4. Soil fluoride leaching could be an important contributor to groundwater fluoride contamination in suitable conditions (change in pH, change in flow field and change in environmental conditions). This could also enhance plant fluoride and Al uptake. Hence, the transport behavior of fluoride in soil should be investigated in areas rich in leachable soil fluoride.

References

Abdelgawad, A. M.; Watanabe, K.; Takeuchi, S.; Mizuno, T. The origin of fluoride-rich groundwater in Mizunami area, Japan-Mineralogy and geochemistry implications. Eng. Geol., 2009, 108, 76 - 85.

Abugri, D. A.; Pelig-Ba, K. B. Assessment of fluoride content in tropical surface soils used for crop cultivation. Afr. J. Environ. Sci. Technol., 2011, 5(9), 653 - 660.

Adachi, A.; Akamatsu, N.; Iwaisako, A.; Senkoku, M.; Kobayashi, T. Fluoride levels in tap and underground water samples from Kinki area in Japan. Bull. Environ. Contam. Toxicol., 1991, 46, 677 - 680.

Amalraj, A; Pius, A. Health risk from fluoride exposure of a population in selected areas of Tamil Nadu South India. Food. Sci. Human. Wellness., 2013, 2, 75 - 86.

Amini, M.; Muller, K.; Abbaspour, K.C.; Rosenberg, T.; Afyuni, M.; Moller, K.N.; Sarr, M.; Johnson, C.A. Statistical modeling of global geogenic fluoride contamination in ground waters. Environ. Sci. Technol. 2008, 3662 - 3668.

Apambire, W. B.; Boyle, D. R.; Michel, F. A. Geochemistry, genesis, and health implications of fluoriferous groundwaters in the upper regions of Ghana. Environ. Geol. 1997, 33 (1): 13 - 24.

Arai, Y.; Sparks, D.L. ATR–FTIR Spectroscopic Investigation on Phosphate Adsorption Mechanisms at the Ferrihydrite–Water Interface. Jour. Colloid. Inter. Sci., 2001, 241, 317 - 326.

Arnesen, A. K. M.; Krogstad, T. A. Sorption and desorption of fluoride in soil polluted from the aluminium smelter at Ardal in Western Norway. Water. Air. Soil. Pollut., 1998, 103, 357 - 373.

Ayoob, S.; Gupta, A. K. Fluoride in drinking waters: a review on the status and stress effects. Crit. Rev. Environ. Sci. Technol., 2006, 36, 433 - 487.

Ayoob, S.; Gupta, A. K.; Bhat, V. T. A. Conceptual overview on sustainable technologies for the defluoridation of drinking water. Crit. Rev. Environ. Sci. Technol., 2008, 38, 401 - 470.

BIS, Indian Standard for Drinking Water – Specification. 1991, IS 10500.

Bachmaf, S.; Merkel, B.J. Sorption of Uranium (VI) at the clay mineral-water interface. Environ. Earth. Sci., 2011, 63(5), 925- 934.

Balan, E.; Saitta, A.M.; Mauri, F.; Calas, G. First-principles modeling of the infrared spectrum of kaolinite. Am. Mineral., 2001, 86, 1321 - 1330.

Barrett, E.P.; Joyner, L.G.; Halenda, P.P. The determination of pore volume and area distributions in porous substances. I. Computations from nitrogen isotherms. J. Am. Chem. Soc., 1951, 73, 373 - 380.

Barrow, N.J. Testing a mechanical model. 1. The effects of time and temperature on the reaction of fluoride and molybdate with a soil. J. Soil. Sci., 1986, 37, 267 - 275.

Barry, D.A.; Li, L. Physical basis of nonequilibrium solute transport in soil. 15th International Congress of Soil Science Transactions, Acapulco, Mexico, July 10–16. International Society of Soil Science and Mexico Society of Soil Science, 1994, 2, 86 - 105.

Begin, L.; Fortin, J.; Caron, J. Evaluation of the fluoride retardation factor in unsaturated and undisturbed soil columns. Soil. Sci. Soc. Am. J., 2003, 67, 1635 -1646.

Borr'ero, C.; Pena, F.; Torrent, J. Phosphate Sorption by Calcium Carbonate in Some Soils of the Mediterranean Part of Spain. Geoderma. 1988, 42, 261 - 269.

Brunauer, S.; Emmett, P.H.; Teller, E. Adsorption of gases in multi-molecular layers. J. Am. Chem. Soc., 1938, 60, 309 - 319.

Brusseau, M.L.; Hu, Q.; Srivastava, R. Using flow interruption to identify factors causing nonideal contaminant transport. J. Cont. Hydrol., 1997, 24, 205 - 219.

Brusseau, M.L.; Rao, P.S.C.; Jessup, R.E.; Davidson, J.M. Flow interruption: A method for investigating sorption nonequilibrium. J. Cont. Hydrol., 1989, 2, 223 - 240.

CGWB. Groundwater brochure, Rangareddy district, Andhra Pradesh, Southern Region, Hyderabad. Central Groundwater Research Board, Ministry of Water Resources, Govt. of India. 2013.

Chaudhary, V.; Sharma, M.; Yadav, B. S. Elevated fluoride in canal catchment soils of northwest Rajasthan, India. Fluoride 2009, 42 (1), 46 - 49.

Chesne, R.B.; Kim, C.S. Zn(II) and Cu(II) adsorption and retention onto iron oxyhydroxide nanoparticles: effects of particle aggregation and salinity. Chesne and Kim Geochemical Transactions., 2014, 15 (6).

Coats, K. H.; Smith, B. D. Dead-end pore volume and dispersion in porous media. SPE Journal., 1964, 4 (1), 73 - 84, doi: 0.2118/647-PA.

Cochiara, S.G. Solid-state NMR investigation of dissolved fluoride uptake by minerals. PhD thesis. 2009, Stony Brook University.

Craig, L.; Stillings, L.L.; Decker, D.L.; Thomas, J.M. Comparing activated alumina with indigenous laterite and bauxite as potential sorbents for removing fluoride from drinking water in Ghana. Appl. Geochem., 2015, 56, 50 - 66.

Cronin, S. J.; Manoharan, V.; Hedley, M. J.; Loganathan, P. Fluoride: a review of its fate, bioavailability, and risks of fluorosis in grazed-pasture systems in New Zealand. New. Zeal. J. Agr. Res., 2000, 43, 295 - 321.

DWQS. Drinking Water Quality Standards in Japan. 2010, http://www.mhlw.go.jp/english/policy/health/water_supply/4.html.

Davies, C W. Ion association. Butterworths, Washington DC, 1962.

Davis, J.A., and J.O. Leckie. Surface ionization and complexation at the oxide/water interface. II. Surface properties of amorphous iron oxyhydroxide and adsorption of metal ions. J. Colloid. Inter. Sci., 1978, 67, 90 - 107.

Davis, J.A.; Coston, J.A.; Kent, D.B.; Fuller, C.C. Application of the surface complexation concept to complex mineral assemblages. Environ. Sci. Technol. 1998, 32 (19), 2820 - 2828.

Davis, J.A.; Fuller, C.C.; Cook, A.D. A model for trace metal sorption processes at the calcite surface: Adsorption of Cd^{2+} and subsequent solid solution formation. Geochim. Cosmochim. Acta., 1987, 51, 1477 - 1490.

Davis, J.A.; Kent, D.B. Surface complexation modeling inaqueous geochemistry. In Mineral-Water Interface Geochemistry, Mineralogical Society of America, 1990, 23, 177 - 260. (eds. M. F. HochellaJr. and A. F. White).

Davis, J.A.; Meece, D.E.; Kohler, M.; Curtis, G.P. Approaches to surface complexation modeling of Uranium(VI) adsorption on aquifer sediments. Geochim. Cosmochim. Acta., 2004, 68 (18), 3621 - 3641.

Dey, U.; Mondal, N. K.; Das, K.; Datta, J. K. Dual effects of fluoride and calcium on the uptake of fluoride, growth physiology, pigmentation, and biochemistry of Bengal gram seedlings. Fluoride 2012, 45(4), 349 - 353.

Doherty, J. PEST Model-Independent Parameter Estimation. User Manual (5th ed). Corinda, Australia: Watermark Numerical Computing, 2004.

Du, J.; Wu, D.; Xiao, H.; Li, Ping. Adsorption of fluoride on clay minerals and their mechanisms using X-ray photoelectron spectroscopy. Front. Environ. Sci. Engin. China., 2011, 5(2), 212 - 226.

Dudley, L.M.; McLean, J.E.; Sims, R.C.; Jurinak, J.J. Sorption of copper and cadmium from the water soluble fraction of an acid mine waste by two calcareous soils. Soil. Sci., 1988, 45, 207 - 214.

Dzombak, D.A.; Morel, F.M.M. Surface complexation modeling- Hydrous Ferric Oxide; Wiley: New York, 1990.

Edmunds, M.; Smedley, P. Fluoride in natural waters. In Essentials of Medical Geology, Impacts of Natural Environment on Public Health; Selinus, et al., Eds.; Elsevier Academic Press: London, 2005, 301 - 329.

Elloumi, N.; Abdallah, F. B.; Mezghani, I.; Rhouma, A.; Makki, B. Effect of fluoride on almond seedlings in culture solution. Fluoride., 2005, 38 (3), 193 - 198.

Fan, X.; Parker, D. J.; Smith, M. D. Adsorption kinetics of fluoride on low cost materials. Water. Res., 2003, 37, 4929 - 4937.

Farley, K.J.; Dzombak, D.A.; Morel, F.M.M. A Surface precipitation model for the sorption of cations on metal oxides. J. Coll. Inter. Sci., 1985, 106 (1), 226 - 242.

Farrah, H.; Slavek, J.; Pickering, W. F. Fluoride sorption by soil components: calcium carbonate, humic acid, manganese dioxide and silica. Aust. J. Soil. Res., 1985, 23, 429 - 439.

Fetter, C. W. Contaminant Hydrogeology. Prentice Hall, Upper Saddle River, N.J., 1999, 500 pp.

Foxnall, T., Peterson, G.C., Rendall H.M., and Smith A.L. Charge determination at calcium salt/aqueous solution interface. J. Chem. Soc. Faraday Trans. 1979, 75, 1034 - 1039.

Freundlich, H. M. F. Uber die adsorption in losungen, Z. Phys. Chem., 1906, 57A, 385 − 470.

Fuge, R.; Andrews, M. J. Fluorine in the UK environment. Environ. Geochem. Health., 1988, 10, 96 - 104.

Fukushi, K.; Sverjensky, D. A. A surface complexation model for sulfate and selenate on iron oxides consistent with spectroscopic and theoretical molecular evidence. Geochim. Cosmochim. Acta., 2007, 71 (1), 1 - 24.

Gago, C.; Fernández Marcos, M. L.; Álvarez, E. Aqueous aluminum species in forest soils affected by fluoride emissions from an aluminum smelter in NW Spain. Fluoride, 2002, 35, 110 - 121.

Gautam, R; Bhardwaj, N; Saini, Y. Fluoride accumulation by vegetables and crops grown in Nawa tehsil of Nagaur district (Rajasthan, India). J. Phytol., 2010, 2(2), 80 - 85.

Ghorai S; Pant K. K. Equilibrium, kinetics and breakthrough studies for adsorption of fluoride on activated alumina. Sep. Purif. Technol., 2005, 42, 265 - 271.

Gitonga J. N.; Nair K. R.; Manji, F. Occurrence and distribution of fluoride in water in Kenya. East. Afri. Med. J., 1984, 61, 503 -512.

Goldberg, S. Use of surface complexation models in soil chemical systems. Adv. Agron., 1992, 47, 233 - 329.

Goldberg, S., Sposito, G. A chemical model of phosphate adsorption by soils: 1. Reference oxide minerals. Soil. Sci. Soc. Am. J., 1984, 48, 772 - 778.

Goldberg, S.; Glaubig, R. A. Anion sorption on a calcareous, montmorillonitic soil-Selenium. Soil. Sci. Soc. Am. J., 1988a, 52, 954 - 958.

Goldberg, S.; Glaubig, R. A. Anion Sorption on a calcareous, montmorillonitic soil-Arsenic. Soil. Sci. Soc. Am. J., 1988b, 52, 1297 - 1300.

Goldberg, S.; Lesch, S.M.; Suarez, D.L. Predicting selenite adsorption by soils using soil chemical parameters in the constant capacitance model. Geochim. Cosmochim. Acta., 2007, 71, 5750 - 5762.

Gramling, C. M.; Harvey, C. F.; Meigs, L. C. Reactive transport in porous media: a comparison of model prediction with laboratory visualization. Environ. Sci. Technol., 2002, 36 (11), 2508 - 2514.

Gregg, S. J.; Sing, K. S. Adsorption, surface Area, and porosity. Academic Press, London, 1982.

Gustafsson, J. P.; Visual MINTEQ, 3.0. Royal Institute of Technology, KTH, Stockholm, Sweden, 2012.

Haggerty, R.; Gorelick, S. M. Multiple-rate mass transfer for modeling diffusion and surface reactions in media with pore-scale heterogeneity. Wat. Res. Res., 31(10), 383 - 2400.

Haidouti, C. Effects of fluoride pollution on the mobilization and leaching of aluminum in soils. Sci. Total. Environ., 1995, 166, 157 - 160.

Handa, B. K. Geochemistry and genesis of fluoride containing ground waters in India. Ground Water. 1975, 13, 275 - 281.

Hao, O. J.; Huang, M. Asorption characteristics of fluoride onto hydrous alumina. J. Environ. Eng., 1986, 112, 1054 - 1069.

Harrington, L. F.; Cooper, E. M.; Vasudevan, D. Fluoride sorption and associated aluminum release in variable charge soils. Jour. Colloid. Inter. Sci., 2003, 267, 302 - 313.

Hay, M. B.; Stoliker, D. L.; Davis, J. A.; Zachara, J. M. Characterization of the intra-granular water regime within subsurface sediments: pore volume, surface area, and mass transfer limitations. Wat. Res.. Res., 2011, 47, 1 - 19.

Hayes, K.F.; Papelis, Ch.; Leckie, J. O. Modeling ionic strength effects on anion adsorption at hydrous oxide/solution interfaces. J. Colloid. Inter. Sci., 1988, 125, 717 - 726.

Helfferich, F. G. Ion Exchange. McGraw-Hill, New York, 1962.

Herbelin, A. L.; Westall, J. C. FITEQL4.0: A computer program for the determination of chemical equilibrium constants from experimental data; Report 99-01; Oregon State University: Corvallis, OR, 1999.

Hermaan, W.; Berry, R. F. MINSQ – a least squares spreadsheet method for calculating mineral proportions from whole rock major element analyses. Geochem. Explor. Environ. Anal., 2002, 2, 361 - 368.

Ho, Y. S. Citation review of Lagergren kinetic rate equation on adsorption reactions. Scientometrics, 2004, 59, 171 - 177.

Huang, C. P.; Stumm, W. Specific adsorption of cations on hydrous γ-Al_2O_3. J. Colloid. Inter. Sci., 1973, 43, 409 - 420.

IGCAR. Report no. SP 2004-2. 2004.

Jacks, G.; Bhattacharya, P.; Chaudhary, V.; Singh, K. P. Controls on the genesis of some high-fluoride groundwaters in India. Appl. Geochem., 2005, 20, 221 - 228.

Jaremalm, M.; Kohler, S; Lidman, F. Precipitation of barite in the biosphere and its consequences for the mobility of Ra in Forsmark and Simpevarp. Technical Report, TR-13-28. Svensk Kärnbränslehantering AB Swedish Nuclear Fuel and Waste Management Co. 2013.

Jayawardana, D. T.; Pitawala, H. M. T. G. A.; Ishiga, H. Geochemical assessment of soils in districts of fluoride-rich and fluoride-poor groundwater, north-central Sri Lanka. Jour. Geochem. Explor., 2012, 114, 118 - 125.

Jianhui, Z. Geochemixtry of fluorine in shallow groundwater- A case study in the Xingtai Piedmont Plain, Hebei, China. Proc. 30th Intl. Geol. Cong., 1997, 2-3, 67 - 82. Zhang et al.,(Eds).

Johannes, C. L.; Meeussen, A. S.; Himestra, T.; Riemsdijk, W. H. V.; Borkovec, M. Predicting multicomponent adsorption and transport of fluoride at variable pH in a Goethite-Silica sand system. Environ. Sci. Technol. 1996, 30, 481 - 488.

Kabata-Pendias, A.; Pendias, H. Trace elements in soils and plants. 2nd edition, 1992, CRC Press, London.

Kapoor, V.; Gelhar, L.W.; Miralles-Wilhelm, F. Bimolecular second-order reactions in spatially varying flows: segregation induced scale-dependent transformation rates. Wat. Res. Res., 1997, 33 (4), 527 - 536.

Karamalidis, A. K.; Dzombak, D. A.; Surface complexation modeling: Gibbsite. 2010, ISBN: 978-0-470-58768-3.

Kau, P. M. H.; Smith, D. W.; Binning P. Experimental sorption of fluoride by Kaolinite and Bentonite. Geoderma, 1998, 84, 89 -108.

Lagergren, S. About the theory of so-called adsorption of soluble substances, Kungliga Svenska Vetenskapsakademiens, Handlingar, 1898, 24, 1 - 39.

Lakshtanov, L. Z.; Stipp, S. L. S. Experimental study of nickel (II) interaction with calcite: Adsorption and coprecipitation. Geochim. Cosmochim. Acta., 2007, 71, 3686 - 3697.

Langmuir, I. The constitution and fundamental properties of solids and liquids, J. Am. Chem. Soc. 1916, 38 (11), 2221 - 2295.

Leij, F. J.; Bradford, S. A. Combined physical and chemical nonequilibrium transport model: Analytical solution, moments, and application to colloids. J. Contam. Hydrol. 2009, 110, 87 - 99.

Leofanti, G.; Padovan, M.; Tozzola, G.; Venturelli, B. Surface area and pore texture of catalysts. Catal. Today., 1998, 41, 207 - 219.

Lin, R.; Srinivasan, K.; Divan, K.; Pohl, C. Analysis of fluoride in drinking water in the presence of interfering metal ions such as iron and aluminum. Dionex Corporation, Sunnyvale, CA, USA, 2009..

Liu, C.; Shi, Z.; Zachara, Z. M. Kinetics of Uranium(VI) desorption from contaminated sediments: effect of geochemical conditions and model evaluation. Environ. Sci. Technol., 2009, 43, 6560 - 6566.

Liu, C.; Zachara, Z. M.; Quafoku, N. P.; Wang, A. Scale-dependent desorption of uranium from contaminated subsurface sediments. Wat. Res. Res., 2008, 44, W08413, doi:10.1029/2007WR006478.

Liu, S.; Lu, Y.; Sun, Z.; Wu, L.; Lu, W.; Wang, S.; Yan, S. Report on the intellectual ability of children living in high fluoride areas. Fluoride, 2008, 41(2), 144 - 147.

Loganathan, P.; Hedley, M. J.; Wallace, G. C.; Roberts, A. H. C. Fluoride accumulation in pasture forages and soils following long term applications of phosphorus fertilizers. Environ. Pollut., 2001, 115, 275 - 282.

Madejova, J.; Komadel, P. Baseline studies of the clay minerals society source clays: Infrared methods. Clay. Clay. Miner., 2001, 49, 410 - 432.

Madhavan, N.; Subramanian, V. Fluoride in fractionated soil samples of Ajmer district, Rajasthan. J. Environ. Monit., 2002, 4, 821 - 822.

Mahramanlioglu, M.; Kizilcikli, I.; Bicer, I. O. Adsorption of fluoride from aqueous solution by acid treated spent bleaching earth. J. Fluorine. Chem., 2002, 115, 41 - 47.

McQuaker, R. N.; Gurney, M. Determination of total fluoride in soil and vegetation using an alkali fusion selective ion electrode technique. Anal. Chem., 1977, 49, 53 - 56.

Meenakshi.; Garg, V. K.; Kavita.; Renuka.; Malik, A. Ground water quality in some villages of Haryana, India: focus on fluoride and fluorosis, J. Hazard. Mater., 2004, B106, 85 - 97.

Mohapatra, M.; Routa, K.; Singh, P.; Anand, S.; Layek, S.; Verma, H. C.; Mishra, B. K. Fluoride adsorption studies on mixed-phase nano iron oxides prepared by surfactant mediation-precipitation technique. J. Hazard. Mater., 2011, 186, 1751 – 1757.

Murakami, H.; Isihara, S. REE mineralization of weathered crust and clay sediment on granitic rocks in the Sanyo Belt, SW Japan and the southern Jiangxi Province, China Res. Geol., 2008, 58 (4), 373 - 401.

Murray, F. Fluoride retention by sandy soils. Water. Air. Soil. Pollut., 1983, 20, 361 - 367.

Nasr, A. B.; Walha, K.; Puel, F.; Mangin, D.; Amar, R. B.; Charcosset, C. Precipitation and adsorption during fluoride removal from water by calcite in the presence of acetic acid. Desalination.Water.Treat., 2014, 52 (10-12), 2231 - 2240, DOI: 10.1080/19443994.2013.799441.

Neal, R. H.; Sposito, G.; Holtzclaw, K. M.; Traina, S. J. Selenite adsorption on alluvial aoils: I. Soil composition and pH effects. Soil. Sci. Soc. Am. J., 1987, 51 (5), I161 - 1165.

Nielsen, D. R.; van Genuchten, M. T.; Biggar, J. W. Water flow and solute transport processes in the unsaturated zone. Wat. Res. Res., 1986, 22(9), 89 - 108.

Nordin, J. P.; Sullivan, D. J.; Phillips, B. L.; Casey, W. H. Mechanisms for fluoride-promoted dissolution of bayerite [β-Al(OH)$_3$(s)] and boehmite [γ-AlOOH]: ^{19}F-NMR spectroscopy and aqueous surface chemistry. Geochim. Cosmochim. Acta., 1999, 63 (21), 3513 - 3524.

Nordstrom, D. K.; Jenne, A. J. Fluorite solubility equilibria in selected geothermal waters. Geochim. Cosmochim. Acta., 1977, 41, 175 - 188.

Omueti, J. A. I.; Jones, R. L. Fluoride adsorption by Illinois soil. J. Soil. Sci., 1977, 28, 564 - 572.

Otsuka, M.; Terakado, Y. Rare earth element abundances in high phosphorus and low iron groundwaters from the Nishinomiya district, Japan: Variations in Ce anomaly, redox state and heavy rare earth enrichment Geochem. J., 2003, 37,: 1 - 19.

Paces, T. Chemical characteristics and equilibrium in natural water-felsic rock-CO$_2$ systems. Geochim. Cosmochim. Acta., 1972, 36, 217 - 240.

Padhi, S.; Muralidharan, D. Fluoride occurrence and mobilization in geo-environment of semi-arid Granite watershed in southern peninsular India. Environ. Earth. Sci., 2012, 66, 471 - 479.

Padhi, S.; Tokunaga, T. Surface complexation modeling of fluoride sorption onto calcite. J. Environ. Chem. Eng., 2015, 3, 1892 - 1900.

Parkhurst, D. L.; Appelo, C. A. J. User's Guide to PHREEQC (version 2). A Computer Program for speciation, Batch-Reaction, One-Dimensional Transport, and Inverse

Geochemical Calculation. U.S.G.S., Water Resources Investigation Report, 1999, 99-4259.

Peek, D. C.; Volk, V. V. Fluoride sorption and desorption in soils. Soil. Sci. Soc. Am. J. 1985, 49 (3), 583 - 586.

Pickering, W. The mobility of soluble fluoride in soils. Environ. Pollut. (B), 1985, 9, 281 - 308.

Plummer, L. N.; Wigley, T. M. L. The dissolution of calcite in CO_2 saturated solutions at 25ºC and 1 atmosphere total pressure. Geochim. Cosmochim. Acta., 1976, 40, 191 - 202.

Pokrovsky, O. S.; Mielczarski, J. A.; Barres, O.; Schott, J. Surface speciation models of calcite and dolomite/aqueous solution interfaces and their spectroscopic evaluation. Langmuir, 2000, 16, 2677 - 2688.

Pokrovsky, O. S.; Pokrovski, G. S.; Schott, J. Gallium (III) adsorption on carbonates and oxides: X-ray adsorption fine structure spectroscopy study and surface complexation modeling. J. Colloid. Inter. Sci., 2004, 279, 314 - 325.

Pokrovsky, O. S.; Schott, J. Surface chemistry and dissolution kinetics of divalent metal carbonates. Environ. Sci. Technol., 2002, 36, 426 - 432.

Polomski, J.; Fluhler, H.; Blaser, P. Accumulation of airborne fluoride in soils. J. Environ. Qual., 1982, 11, 457 - 461.

Reardon, E. J.; Wang, Y. A limestone reactor for fluoride removal from wastewater, Environ. Sci. Technol., 2000, 34, 3247 - 3253.

Burt, R. Soil Survey Laboratory Methods Manual. Soil Survey Investigations Report No. 42, Version 4.0, November 2004. United States Department of Agriculture Natural Resources Conservation Service.

Sarkar, M.; Banerjee, A.; Pramanick, P. P. Kinetics and mechanism of Fluoride removal using Laterite. Ind. Eng. Chem. Res., 2006, 45, 5920 - 5927.

Saxena, S.; Rani, A. Fluoride ion leaching kinetics for alkaline soils of Indian origin. J. Sci. Res. Reports., 2012, 1(1), 29 - 40, Article No. JSRR.2012.003.

Scanlon, B. R.; Stonestrom, D. A.; Reedy, R. C.; Leaney, F. W.; Gates, J.; Cresswel, R. G. Inventories and mobilization of unsaturated zone sulfate, fluoride, and chloride related to land use change in semiarid regions, southwestern United States and Australia. Wat. Res. Res., 2009, 45, W00A18, doi:10.1029/2008WR006963.

Schindler, P. W.; First, B.; Dick, R.; Wolf, P. U. Ligand properties of surface silanol groups. I. Surface complex formation with Fe^{3+}, Cu^+, Cd^{2+} and Pb^{2+}. J. Colloid. Inter. Sci., 1976, 55, 469 - 475.

Serrano, S.; O'Day, P. A.; Vlassopoulos, D.; Garcıa-Gonzalez, M. T.; Garrido, F. A. Surface complexation and ion exchange model of Pb and Cd competitive sorption on natural soils. Geochim. Cosmochim. Acta., 2009, 73, 543 - 558.

Sigg, L.; Stumm, W. The interaction of anions and weak acids with the hydrous goethite (α-FeOOH) surface. Colloids. Surf., 1981, 2 (2), 101 - 117.

Simunek, J.; van Genuchten, M. T. Contaminant transport in the unsaturated zone Theory and Modeling. The Handbook of Groundwater Engineering. 2006, JACQ: "4316_c022", 1 - 46.

So, H. U.; Postma, D.; Jakobsen, R.; Larsen, F. Sorption and desorption of arsenate and arsenite on calcite. Geochim. Cosmochim. Acta., 2008, 72, 5871 - 5884.

So, H.U.; Postma, D.; Jakobsen, R.; Larsen, F. Sorption of phosphate onto calcite; results from batch experiments and surface complexation modeling. Geochim. Cosmochim. Acta., 2011, 75, 2911 - 2923.

Somsundaran, P.; Agar, G. E. The zero point of charge of calcite. J. Colloid. Inter. Sci., 1967, 24, 433 - 440.

Sparks, D. L. Environmental Soil Chemistry. Second edition, 2003, Academic Press.

Sposito, G. The surface chemistry of soils. 1984, Oxford Univ. Press, Oxford, England.

Steefel, C. I.; DePaolo, D. J.; Lichtner, P. C. Reactive transport modeling: An essential tool and a new research approach for the earth sciences. Earth. Planet. Sci. Lett., 2005, 240, 539 - 558.

Stumm, W.; Huang, C. P.; Jenkins, S.R. Specific chemical interaction affecting the stability of dispersed systems. Croat. Chem. Acta., 1970, 42, 223 - 245.

Stumm, W.; Kummert, R.; Sigg, L. A ligand exchange model for the adsorption of inorganic and organic ligands at hydrous oxide interfaces. Croat. Chem. Acta., 1980, 53, 291 - 312.

Sumikawa, K. On the groundwater of Nishinomiya District, Kinki, Japan-with special reference to the characteristics of permeability of the aquifer and chemical composition of the Miyamizu. J. Sci. Hiroshima Univ. Ser. C, 1990, 9 (2), 361 - 376.

Susheela, A. K. A treatise on Fluorosis, 2nd ed., Fluorosis Research and Rural Development Foundation, New Delhi, India, 2003.

Sverjensky, D. A.; Standard states for the activities of mineral surface sites and species. Geochim. Cosmochim. Acta, 67(1), 17 - 28.

Thompson, D. W.; Pownall, P. W. Surface electrical properties of calcite. J. Colloid. Inter. Sci. 1989, 131, 74 - 82.

Toride, N.; Leij, F. J.; van Genuchten, M. Th. The CXTFIT code for estimating transport parameters from laboratory or field tracer experiments. Research Report No. 137, 1995, USSL, Agricultural research service, US DAE, Riverside, California.

Tran, Y.; Bajracharya, K.; Barry, D.A. Anomalous cadmium adsorption in flow interruption experiments. Geoderma, 1998, 84, 169 – 184.

Tsurumaki, M.; Sakuramoto, Y. Origin of high fluoride groundwaters in Kinki district. J. Japanese Assoc. Groundwater. Hydrol., 1985, 27(1), 1 - 16.

Turner, B. D.; Binning, P.; and Stipp, S. L. S. Fluoride removal by calcite: Evidence for fluorite precipitation and surface adsorption. Environ. Sci. Technol., 2005, 39, 9561 - 9568.

Usunoff, E.; Weinzettel, P.; Dietrich, S. Fluoride retardation from quartz sand-packed column tests. Geoacta, 2009, 34, 27 - 34.

Van Cappellen, P.; Charlet, L.; Stumm, W.; Wersin, P. A surface complexation model of the carbonate mineral-aqueous solution interface. Geochim.Cosmochim. Acta., 1993, 57, 3505 - 3518.

Vithanage, M.; Rajapaksha, A. U.; Dou, X.; Bolan, N. S.; Yang, J. E.; Ok, Y. S. Surface complexation modeling and spectroscopic evidence of antimony adsorption on iron-oxide-rich red earth soils. J. Colloid. Inter. Sci., 2013, 406, 217 - 224.

141

WHO, Guidelines for Drinking-Water Quality, Fourth Edition. World Health Organization, 2011 Geneva, ISBN 9789241548151.

WHO. Guidelines for Drinking-Water quality. World Health Organization, Geneva, 2004, Third Edition, 212 pp.

Wang, W.; Li, R.; Tan, J.; Luo, K; Yang, L; Li, H; Li, Y. Adsorption and leaching of fluoride in soils of china. Fluoride, 2002, 35(2), 122 - 129

Weerasooriya, R.; Wickramarathne, H. U. S. Modeling Anion Adsorption on Kaolinite. J. Colloid. Inter.Sci., 1999, 213, 395 - 399.

Weerasooriya, R.; Wickramarathne, H. U. S.; Dharmagunawardhane, H. A. Surface complexation modeling of fluoride adsorption onto kaolinite. Colloids. Surfaces A: Physicochemical and Engineering Aspects, 1998, 144, 267 - 273.

Wenzel, W. W.; Blum, W. E. H. Fluorine speciation and mobility in F-contaminated soil. Soil. Sci., 1992, 153 (5), 357 - 364.

Westall, J.; Hohl, H. A comparison of electrostatic models for the oxide/solution interface. Adv. Colloid. Inter. Sci., 1980, 12, 265 - 294.
Westall, J.C. Reactions at the oxide-solution interface: Chemical and electrostatic models. Am. Chem. Soc. Symp. Ser., 1986, 323, 54 - 78.

Xu, T.; Spycher, N.; Sonnenthal, E.; Zheng, L.; Pruess, K. TOUGHREACT User's Guide: A Simulation program for non-isothermal multiphase reactive transport in variably saturated geologic media, version 2.0. 2012. Earth Sciences Division, Lawrence Berkeley National Laboratory University of California, Berkeley, CA 94720.

Yabusaki, S.; Tase, N.; Tsujimura, M.; Hayashi, Y. Visit to valuable water springs (77). Valuable water springs in Mt.Tsukuba. Groundwater. J., 2007, 49 (2), 153 - 168.

Yang, M.; Hashimoto, T.; Hoshi, N.; Myoga, H. Fluoride removal in a fixed bed packed with granular calcite. Water. Res., 1999, 33, 3395 - 3402.

Yang, X.; Sun, Z.; Wang, D.; Forsling, W. Surface acid–base properties and hydration/dehydration mechanisms of aluminum (hydr)oxides. J. Colloid. Inter. Sci., 2007, 308, 395 – 404.

Zachara, J. M.; Cowan, C. E.; Resch, C. T. Sorption of divalent metals on calcite. Geochim. Cosmochim. Acta., 1991, 55, 1549 - 1562.

Zhu, L.; Zhang, H. H.; Xia, B.; Xu, D. R. Total fluoride in Guangdong soil profiles, China: Spatial distribution and vertical variation. Environ. Int., 2007, 33, 302 - 308.

Zhu, M. X.; Jiang, X.; Ji, G. L. Interactions between variable-charge soils and acidic solutions containing fluoride: an investigation using repetitive extractions. J. Colloid. Inter. Sci., 2004, 276, 159 - 166.

Zhu, S.; Zhang, J.; Dong, T. Removal of fluorine from contaminated field soil by anolyte enhanced electrokinetic remediation. Environ. Earth. Sci., 2009, 59, 379 - 384.

van Genuchten, M. T.; Wagenet, R. J. Two-Site/Two-Region models for pesticide transport and degradation: Theoretical development and analytical solutions. Soil. Sci. Soc. Am. J., 1989, 53, 1303 - 1310.

van Genuchten, M. T.; Wierenga, P. J. Mass transfer studies in sorbing porous media I. analytical solutions. Soil. Sci. Soc. Am. J., 1976, 40(4), 473 - 480.